DISSERTATION

ENRICHMENT OF ORGANIC MATTER AND MICROORGANISMS IN THE SEA SURFACE MICROLAYER OF TEMPERATE COASTAL WATERS AND ITS ROLES IN AIR-SEA GAS EXCHANGE

March 2019

SOKA UNIVERSITY

GRADUATE SCHOOL OF ENGINEERING

YOUTA SUGAI

ENRICHMENT OF ORGANIC MATTER AND MICROORGANISMS IN THE SEA SURFACE MICROLAYER OF TEMPERATE COASTAL WATERS AND ITS ROLES IN AIR-SEA GAS EXCHANGE

MARCH 2019

YOUTA SUGAI

SOKA UNIVERSITY

Author:	Youta Sugai
Title:	Enrichment of organic matter and microorganisms in the sea surface microlayer of temperate coastal waters and its roles in air-sea gas exchange
Department:	Environmental Engineering for Symbiosis
Faculty:	Engineering
Degree:	Ph. D.
Convocation:	March 2019

We certify that we have read this dissertation and that, in our opinion, it is satisfactory in scope and quality as a dissertation for the degree of Doctor of Philosophy in Engineering.

March 2019

DISSERTATION COMMITTEE

Prof. Dr. Tatsuki Toda

Prof. Dr. Ken Furuya

Prof. Dr. Koji Hamasaki

CONTENTS

ACKNOWLEDGEMENTS

I express my sincere appreciation to my supervisor, Prof. Dr. Tatsuki Toda, for all of his support, guidance, and encouragement throughout my student life.

I deeply appreciate my co-supervisors, Prof. Dr. Ken Furuya (Soka University) and Prof. Dr. Koji Hamasaki (The University of Tokyo), for the critical review of this dissertation.

I offer my gratitude to Prof. Dr. Tomohiko Kikuchi and Assoc. Prof. Dr. Shinji Shimode (Yokohama National University) for their cooperation in field investigation.

I am grateful to Prof. Dr. Toshihiko Takemura (Kyushu University) and the developers of SPRINTARS for the use of the data of aerosol deposition flux.

I cannot thank all students and staffs of Laboratory of Restoration Ecology enough, especially Dr. Kenji Tsuchiya (National Institute for Environmental Studies), for their supports and advice.

This dissertation cannot be accomplished without continuous support and encouragement by my family and friends.

Last but not least, I dedicate this dissertation to the founder of Soka University, Dr. Daisaku Ikeda, for his encouragement and expectation for the success of my life.

ABSTRACT

The sea surface microlayer (SML), defined as less than 1,000 μm uppermost layer of the ocean water column, is located at the interface between the atmosphere and the ocean and plays critical roles in global biogeochemical cycles and climate change through air-sea gas exchange. To clarify the enrichment of organic matter and microorganisms in the SML of temperate coastal waters and its roles in air-sea gas exchange, the seasonality in organic matter concentration and microbial abundance in the SML (Study 1) and the dynamics of carbon monoxide (CO) in the SML produced photochemically and consumed biologically (Study 2) were investigated in coastal waters of Sagami Bay, Japan. In Study 1, the concentration of organic matter (dissolved and particulate organic carbon, chromophoric dissolved organic matter [CDOM], and transparent exopolymer particles) and the abundance of microorganisms (phytoplankton, bacteria, and autotrophic and heterotrophic nanoflagellates) in the SML were significantly higher compared to the subsurface water (SSW, 0.5 m depth) throughout the year and particularly increased during spring (April 2014 and May 2015). The particular increase during spring was probably due to phytoplankton blooms in the SML induced by the external supply of inorganic nutrients (phosphate), which showed the seasonality of chemical and biological factors in the SML of temperate coastal waters. In Study 2, photochemical CO production rate in the SML normalized by the integrated solar irradiance during the incubation period was relatively high (3.85 ± 3.09 nM [kWh m^{-2}]$^{-1}$) from spring to autumn (from June to November 2017 and from March to June 2018) when significant enrichment of CDOM was observed. On the other hand, biological CO consumption rate constant in the SML was relatively high (0.060 ± 0.010 h^{-1}) from spring to autumn (from June to November 2017 and from May to June 2018) during the period of relatively high water temperature. Although sea-air CO flux (*F*) showed a similar variation with CO concentration in the SSW, CO concentration in the SML particularly increased (15.0 nM) during a spring phytoplankton bloom (June 2017), which indicates

the suppression of air-sea CO exchange by the enrichment of biogenic surfactants in the SML derived from phytoplankton. Comparison among the turnover time of the photochemical production, biological consumption, and sea-air emission of CO in the SML (τ_{prod}, τ_{cons}, and $\tau_{sea\text{-}air}$, respectively) showed that τ_{cons} (13.5–27.8 h) was much higher than $\tau_{sea\text{-}air}$ (0.003–0.079 h) throughout the year, suggesting that biological CO consumption in the SML can be ignored in air-sea CO exchange. However, τ_{prod} (0.36 h) was relatively comparable to $\tau_{sea\text{-}air}$ ($\tau_{sea\text{-}air}/\tau_{prod}$ = 21.9%) in August 2017, which suggests that photochemical CO production in the SML enhances *F* during summer under intense light, active biological production, and weak wind conditions.

Chapter 1

General Introduction

1.1. Global Warming and the Role of the Ocean

In the Fifth Assessment Report, the Intergovernmental Panel on Climate Change (IPCC) reported that global mean surface temperature has linearly increased by 0.85°C from 1880 to 2012 (Hartmann et al. 2013). Because the surface temperature increase observed during the last 30 years was unprecedented and the highest over the last thousands of years, the IPCC concluded that global warming is unequivocal.

The extent of greenhouse effect is expressed as radiative forcing defined as the change in energy flux at the tropopause (the boundary between the troposphere and the stratosphere) due to the change of the drivers of climate change. In 2011, anthropogenic radiative forcing relative to 1750 (2.29 W m^{-2}) was much higher than natural radiative forcing caused by the change in solar irradiance (0.05 W m^{-2}) (Myhre & Shindell 2013). Among all anthropogenic drivers, the largest contribution to radiative forcing was made by the increase in the atmospheric concentration of greenhouse gases (GHGs) such as carbon dioxide (CO_2) (1.68 W m^{-2}), methane (CH_4) (0.97 W m^{-2}), carbon monoxide (CO) (0.23 W m^{-2}), and nitrous oxide (N_2O) (0.17 W m^{-2}). CO_2, CH_4, and N_2O themselves act as the drivers of climate change whereas CO is known as an indirect GHG because CO concentration regulates the concentration of various GHGs in the atmosphere including CH_4, halocarbons, and ozone with high global warming potential.

Climate change is predicted under the Coupled Model Intercomparison Project Phase 5 (CMIP5) by simulating anthropogenic effect on climate in the future based on the scenarios of human activity, called the representative concentration pathways (RCPs) which show radiative forcing in 2100 relative to 1750. In the RCP 8.5 scenario which assumes more GHG emission by human activity in the future, the increase in global mean surface temperature and sea surface

temperature is estimated to be 3.7°C and more than 3°C at the end of the 21st century relative to 1986–2005, respectively (Collins & Knutti 2013; Kirtman & Power 2013). For more accurate prediction of climate change, the understanding of feedback on global warming by the change of climate processes affecting GHG concentration in the atmosphere is essential.

Although the largest cause of global warming is GHG emission by human activity, not all amount of GHGs emitted anthropogenically accumulates in the atmosphere because some amount of the GHGs is absorbed by the land and the ocean. Of the two, the ocean has much higher storage capacity of some GHGs compared to the land. For example, the ocean is calculated to have absorbed much more carbon (127 pgC) from 1850 to 2005 compared to the land (2 pgC) and is expected to continue carbon uptake during the 21st century in all RCP scenarios (Ciais & Sabine 2013). Thus, the ocean plays vital roles in global warming through air-sea gas exchange.

1.2. Air-sea Gas Exchange

The classical model of air-sea gas exchange, the two-layer (thin film) model, considers thin films, which are tens to hundreds of μm thick (Zhang et al. 1998; Zhang et al. 2003; Carpenter & Nightingale 2015; Engel et al. 2017), on either side of flat interface between the atmosphere and the ocean (Liss & Slater 1974; Upstill-Goddard 2006) (Fig. 1-1a). Turbulent mixing determines gas transfer outside thin films whereas turbulence dramatically attenuates near thin films due to the viscosity of the ocean surface. In thin films, gas transfer is dominated by molecular diffusion, and gas concentration gradient develops. Excluding wave breaking and bubble ebullition, the strongest resistance to gas transfer is molecular diffusion in thin films, which substantially regulates gas exchange across the air-sea interface. For relatively insoluble gases including most of the GHGs, the air-side thin film can be practically ignored, and air-sea gas exchange exclusively depends on gas transfer in the sea-side thin film.

Air-sea gas flux is calculated by the product of gas transfer velocity (k_w) and the difference

between gas concentration in the atmosphere and the ocean (ΔC). Because k_w cannot be measured directly, the measurement of air-sea gas flux and ΔC allows the estimation of apparent k_w. Practically, to calculate air-sea gas flux, ΔC is measured, and apparent k_w is parameterized using an empirical relationship between wind speed and apparent k_w based on the assumption that air-sea gas exchange depends on wind and wind-related processes such as waves and bubbles (Liss & Merlivat 1986; Wanninkhof 1992; Wanninkhof & McGillis 1999; Nightingale et al. 2000). Thus, better understanding of apparent k_w is essential for more accurate calculation of air-sea gas flux because apparent k_w largely varies at similar wind speeds (Brooks et al. 2009; Garbe et al. 2014), which suggests the need to consider parameters not scaling with wind speed.

1.3. Sea Surface Microlayer (SML)

Tens to hundreds of μm of the sea-side thin film is also known as the sea surface microlayer (SML). The SML is defined as less than 1,000 μm uppermost layer of the ocean water column (Liss & Duce 1997). The SML is located at the interface between the atmosphere and the ocean and plays critical roles in global biogeochemical cycles and climate change through the regulation of the air-sea exchange of relatively insoluble, climate-related gases (Cunliffe et al. 2013). Due to its proximity to the atmosphere, the SML is physically different from the subsurface water (SSW) usually at 0.5–1 m depth (Cunliffe et al. 2011). For example, the SML is exposed to the most intense ultraviolet (UV) and visible solar radiation and subject to the largest magnitude of salinity change due to precipitation and freshwater inflow. These facts make the SML one of the most extreme environments in the ocean.

Field investigation in tropical, temperate, and polar regions by Wurl et al. (2011a) confirmed that the formation of the SML persisted at global mean wind speed of 6.6 m s^{-1} (Archer & Jacobson 2005) and even at 10 m s^{-1}. Further, they showed that a significant extent of the ocean surface is covered with the SML based on the world distribution of biological productivity and wind

condition. However, the thickness of the SML in natural environments changes depending on environmental conditions including water temperature and wind speed and remains unrevealed (Cunliffe et al. 2011). Thus, SML samples are operationally defined as seawater collected using SML samplers such as mesh screens (Garrett 1965), glass plates (Harvey 1966; Harvey & Burzell 1972), and polycarbonate filters (Crow et al. 1975; Kjelleberg et al. 1979), which typically collect 150–400 μm, 20–150 μm, and 40 μm layer of the ocean surface, respectively.

To date, the chemical and biological studies of the SML have been conducted in various oceanic areas from tropical to polar regions and from coastal to open waters (Table 1-1). Previous studies have shown the difference between the concentration of organic matter and the abundance of microorganisms in the SML and SSW using enrichment factors (EFs) calculated as the ratio of values in the SML to those in the SSW (e.g. Sieburth et al. 1976; Harvey & Young 1980). Most of the EFs reported by previous studies ranged from 0.9 to 2.7, which means approximately 1–3 times higher organic matter concentration and microbial abundance in the SML than in the SSW (e.g. Carlson 1983; Obernosterer et al. 2005; Joux et al. 2006; Wurl & Holmes 2008). Occasionally, particularly high EFs (up to 42.8) were also reported by Wurl et al. (2011b) and Wurl et al. (2016) who investigated the SML of visible slick areas where the wave-damped ocean surface caused by the accumulation of surface-active organic matter (surfactants) is observed and Nakajima et al. (2013) who investigated the SML of tropical coral reef waters. These studies show that the SML also forms chemically and biologically distinct environments compared to the SSW.

1.4. Air-sea Gas Exchange through SML

Conrad & Seiler (1988) and Upstill-Goddard et al. (2003) used a free-floating box in the tropical Atlantic Ocean and a closed tank in a laboratory, respectively, under the controlled turbulent condition to estimate both the apparent air-sea and sea-air k_w of gases such as CH_4 and CO. They found significant differences between the apparent air-sea and sea-air k_w, which can be only

attributed to gas uptake by microorganisms in the SML. This result indicates that gases can be actively produced and/or consumed in the SML enough to change apparent k_w depending on gases and environmental conditions while they pass through the SML via molecular diffusion. After that, Cen-Lin & Tzung-May (2013) pointed out that the chemical and biological reactions of gases in the SML are not considered in the two-layer model and proposed the three-layer model, a system composed of the air-side thin film at the bottom of bulk atmosphere, the sea-side thin film at the top of bulk seawater, and the SML on the sea-side thin film where gas concentration is uniform (Fig. 1-1b). In the three-layer model, chemical and biological gas reactions in the SML can change apparent k_w by acting as an additional source and/or sink of gases. If gases are chemically and biologically produced and/or consumed significantly in the SML, the parameterization of apparent k_w according to the two-layer model based on the assumption that air-sea gas exchange is only under physical control and the subsequent calculation of air-sea gas flux will be erroneous.

Apparent k_w can also change due to the accumulation of organic matter in the SML. For example, Salter et al. (2011) added a surfactant (oleyl alcohol) to seawater in the northeast Atlantic Ocean and estimated apparent k_w using air-sea gas flux measured by a dual tracer ($^3He/SF_6$) technique and ΔC. They found the decrease in apparent k_w by < 55% at wind speed of < 7.2 m s^{-1} in artificially surfactant-covered areas relative to natural areas. This result indicates that air-sea gas exchange can be largely suppressed because organic film formed in the SML acts as a physical barrier and changes turbulent energy transfer in surface waters.

These researches suggest that the study of the enrichment of organic matter and microorganisms in the SML is required to understand gas production and consumption in the SML and their effect on air-sea gas exchange. Further, because the SML is the first in the ocean to be exposed to the increase in water temperature due to global warming and changes in the SML by water temperature increase in turn affect the atmosphere, the evaluation of feedback on global warming due to the changes of gas production and/or consumption in the SML by the increase in

water temperature is required to understand the processes of the ocean-climate feedback and to develop climate models.

CO_2, CH_4, CO, and N_2O are atmospheric trace gases which largely contribute to radiative forcing and global warming (Myhre & Shindell 2013). The ocean is globally a sink of the atmospheric CO_2 although the regional air-sea CO_2 flux can be both positive and negative depending on the difference between the partial pressure of CO_2 in the atmosphere and the ocean (Gruber et al. 2009; Takahashi et al. 2009). For CH_4, CO, and N_2O, the ocean generally acts as a source because they are supersaturated in surface waters with respect to the atmospheric concentration (Conrad et al. 1982; Bange et al. 1994; Bange 2006). In the ocean, CO_2 production and consumption mainly occur due to respiration and photosynthesis. Methanogenesis by methanogenic archaea in anoxic environments using CO_2 or acetic acid as substrates and aerobic oxidation by methanotrophic bacteria under the oxic condition are responsible for CH_4 production and consumption, respectively (e.g. Cicerone & Oremland 1988). CO is produced by the photochemical degradation of chromophoric dissolved organic matter (CDOM) and consumed aerobically by CO-oxidizing bacteria (Conrad et al. 1982; Zafiriou et al. 2003). Nitrifying and denitrifying bacteria produce N_2O as a by-product of hydroxylamine oxidation through nitrification and as an intermediate between nitric oxide and molecular nitrogen through denitrification under the oxic and anoxic conditions, respectively whereas denitrifying bacteria consume N_2O through denitrification in anoxic environments (e.g. Schropp & Schwarz 1983).

Interestingly, previous studies reported the enrichment of CDOM in the SML exposed to the most intense solar radiation in the ocean (Table 1-1) (Carlson 1983; Obernosterer et al. 2008; Wurl et al. 2009), which suggests active photochemical reactions in the SML by the photodegradation of CDOM. Significantly higher bacterial abundance in the SML than in the SSW was also reported (Table 1-1) (e.g. Kuznetsova et al. 2004; Stolle et al. 2010), suggesting active biochemical reactions in the SML by bacteria. Further, anoxic processes are considered not to occur

actively in the SML in contact with the atmosphere. Based on these facts, among GHGs above, CO, an indirect GHG, is expected to be most actively produced and consumed in the SML.

1.5. Objectives

Temperate coastal waters are one of the most productive areas in the ocean, and the seasonal patterns of vertical structure, chemical distribution, and biological productivity are clearly observed in the water column. Sugai et al. (2016) conducted field investigation from May 2012 to May 2013 at Station M (St. M, 120 m depth) in coastal waters of Sagami Bay, Japan (Fig. 1-2) and showed the seasonal and vertical variations in chemical and biological parameters such as the concentrations of dissolved organic carbon (DOC) and chlorophyll (chl.) *a* as well as seawater density (σ_t). Thermal stratification developed from spring (May) 2012 to autumn (October) and during spring (April–May) 2013, and the water column was vertically well-mixed from autumn (November) to spring (March) 2013 (Fig. 1-3a). DOC concentration increased in surface waters during spring (May) 2012 and summer (August) (Fig. 1-3b) when or after phytoplankton blooms occurred during spring (May) 2012 and summer (July) (Fig. 1-3c). These seasonal events observed in the water column are also expected in the SML, and the enrichment of organic matter and microorganisms in the SML may also show seasonality in temperate coastal waters. However, most of the previous studies of the SML have been conducted by opportunistic samplings (Table 1-1), and the annual variations in chemical and biological parameters in the SML have never been investigated. Time-series investigation at the same sampling station will provide information on dynamic and complex temporal interactions in the SML (Cunliffe et al. 2013). Further, since the sampling of the SML takes much time and the sample volume of the SML is limited, relationships between parameters in the SML have remained unrevealed.

Therefore, the objective of the present study was to clarify the enrichment of organic matter and microorganisms in the SML of temperate coastal waters and its roles in air-sea gas

exchange. First, the seasonal variations in organic matter concentration and microbial abundance and relationships between parameters in the SML were investigated by a two-year, monthly field survey (Chapter 2). Then, a one-year, monthly field survey and incubation experiments were conducted to investigate the seasonality of CO production and consumption in the SML and to evaluate their significance in air-sea CO exchange (Chapter 3). The changes in CO production and consumption rates in the SML by the increase in water temperature were also examined to assess feedback on global warming in Chapter 3. Finally, the biogeochemical roles of the SML in temperate coastal waters and air-sea gas exchange considering gas dynamics and organic matter accumulation in the SML are discussed (Chapter 4).

Table 1-1. Mean enrichment factors (EF) of organic matter and microorganisms reported by previous and the present studies. SML: surface microlayer, DOC: dissolved organic carbon, CDOM: chromophoric dissolved organic matter, POC: particulate organic carbon, TEP: transparent exopolymer particles, Chl *a*: chlorophyll *a*, ANF: autotrophic nanoflagellates, Bac: bacteria, HNF: heterotrophic nanoflagellates, Ref: references, NA: not available, MS: mesh screen, GP: glass plate, PF: polycarbonate filter. Modified from Sugai et al. (2018)

Study area (No. of sampling station)	Study period (No. of sampling time)	SML sampling	EF								Ref
			DOC	CDOM	POC	TEP	Chl *a*	ANF	Bac	HNF	
North Atlantic (Block Island–Azores Islands) (9)	Jul–Aug 1975 (9)	MS	1.6				1.4				a
Palo Alto Salt Marsh, USA (1)	May 1978 (10)	MS							1.7		b
Damariscotta River Estuary, USA (NA)	May 1978–Sep 1980 (NA)	GP	1.3	1.5	10.1						c
Sequim Bay, USA (1)	Feb–Jul 1983 (5)	PF					1.8				d
East Coast of Isla Cedros, Mexico (2)	Nov 1983 (2)	MS	1.2		3.5		1.0		1.4		e
NW Mediterranean Sea, France & Spain (2)	Mar 2001–Jul 2002 (8)	MS					1.8		1.1	5.4	f
NW Atlantic (Woods Hole–Sargasso Sea) (16)	Jun 2001 (16)	MS							1.4		g
NW Mediterranean Sea, France & Spain (2)	Mar–Sep 2001 (4)	MS	1.0		1.4		2.0				h
Bay of Banyuls-sur-Mer, France (1)	May–Jul 2003 (3)	MS	1.3		14.0				1.2	2.7	i
Bay of Banyuls-sur-Mer, France (1)	Mar 2001–Jul 2002 (4)	MS					1.3	3.7	1.1	3.7	j
South Pacific (West of Marquise Islands) (1)	Oct 2004 (1)	MS	0.9	1.9	1.9		1.2	1.2	1.0	1.8	k
Western Mediterranean Sea (Algerian basin) (11)	Sep–Oct 2003 (11)	GP	1.8						1.1		l
Singapore Strait, Singapore (8)	Jan–May 2007 (22)	GP	1.3			1.3					m
Santa Barbara Channel, USA (1)	Sep 2008 (26)	GP		1.6		1.7					n
SW Baltic Sea, Germany (1)	May 2008 (4)	GP	1.1		13.9				2.1		o
NE Pacific, Offshore Hawaii, and Canadian Arctic (non-slick) (14)	Jun–Oct 2009 (14)	GP				2.0					p
NE Pacific and Offshore Hawaii (slick) (3)	Jun–Aug 2009 (3)	GP				10.5					p
West Coast of Bidong Island, Malaysia (1)	Jun 2011 (3)	MS	1.2				7.1	18.8	6.0	22.6	q
Central Arctic (ice edge) (8)	Aug–Sep 2012 (8)	GP	1.2			1.1			1.0		r
NE Pacific, NW South China Sea, and SW Baltic Sea (non-slick) (44)	Jan–Sep 2013 (44)	GP	1.2		2.3	1.6			1.2		s
NE Pacific, NW South China Sea, and SW Baltic Sea (slick) (16)	Jan–Sep 2013 (16)	GP	2.0		42.8	12.5			2.8		s
Sagami Bay, Japan (1)	Sep 2013–Sep 2015 (23) *	MS	1.2	1.4	2.0	1.4	1.5	2.9	1.6	4.0	t
Sagami Bay, Japan (1)	Apr 2014 (1)	MS	4.8	4.2	7.0	6.1	7.4	40.8	7.8	37.0	t
Sagami Bay, Japan (1)	May 2015 (1)	MS	2.9	3.2	3.1	3.0	3.9	4.6	6.9	4.7	t

a: Sieburth et al. (1976), b: Harvey & Young (1980), c: Carlson (1983), d: Hardy & Apts (1984), e: Carlucci et al. (1986), f: Agogué et al. (2004), g: Kuznetsova et al. (2004), h: Momzikoff et al. (2004), i: Obernosterer et al. (2005), j: Joux et al. (2006), k: Obernosterer et al. (2008), l: Reinthaler et al. (2008), m: Wurl & Holmes (2008), n: Wurl et al. (2009), o: Stolle et al. (2010), p: Wurl et al. (2011b), q: Nakajima et al. (2013), r: Galgani et al. (2016), s: Wurl et al. (2016), t: Present study, *: during the study period except in April 2014 and May 2015

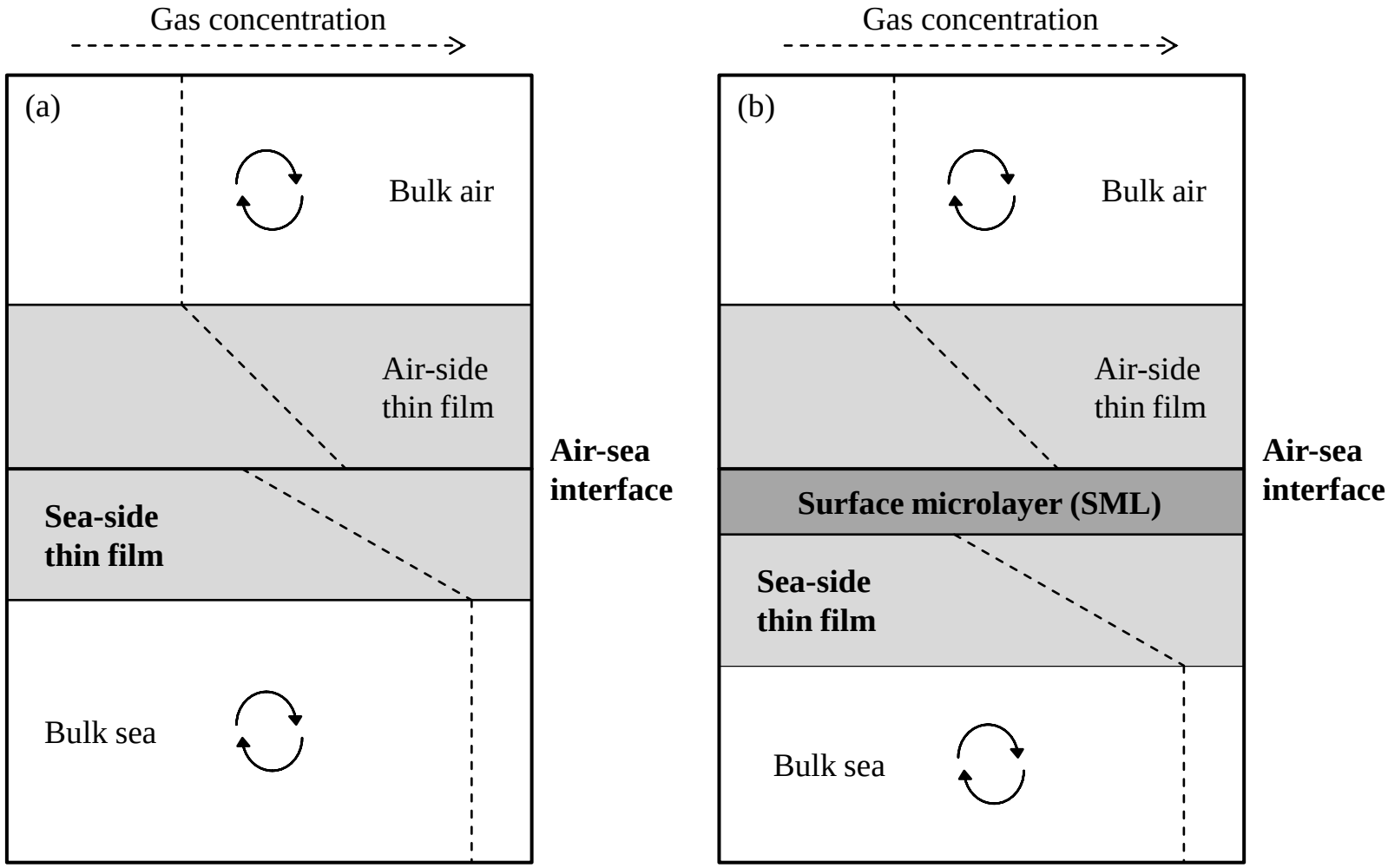

Fig. 1-1. (a) The two-layer (thin film) model (modified from Upstill-Goddard 2006) and (b) the three-layer model (modified from Cen-Lin & Tzung-May 2013) of air-sea gas exchange.

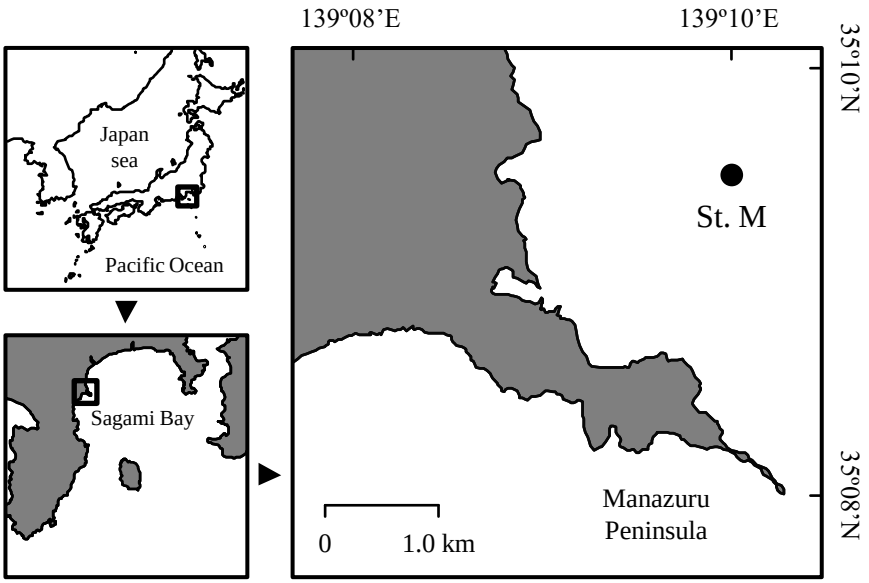

Fig. 1-2. Location of Station M (St. M, 120 m depth) in Sagami Bay, Japan

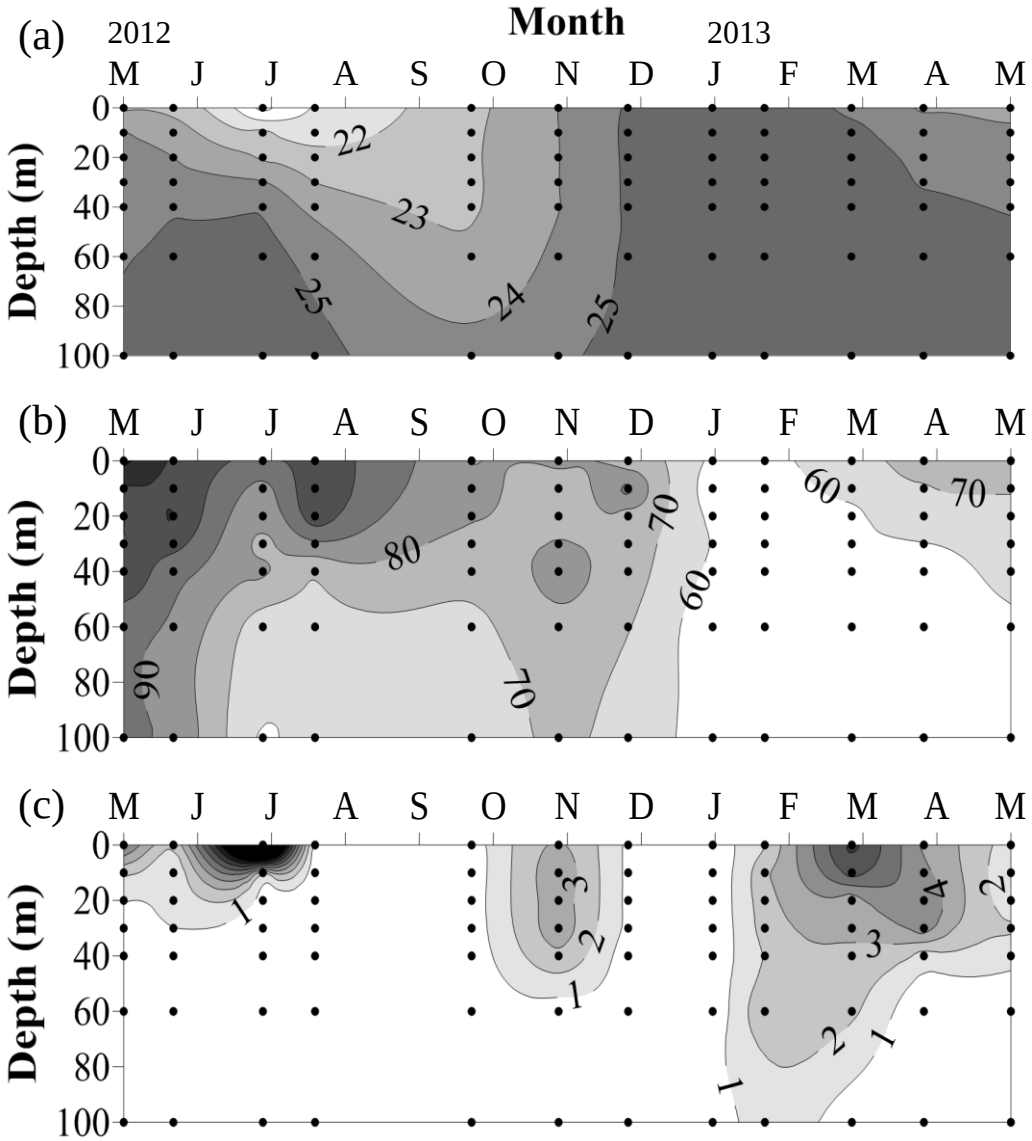

Fig. 1-3. Seasonal and vertical variations in (a) water density (σ_t, kg m^{-3}), (b) dissolved organic carbon (μmolC L^{-1}), and (c) chlorophyll *a* (μg L^{-1}) from May 2012 to May 2013 at St. M in Sagami Bay, Japan (Sugai et al. 2016)

Chapter 2

Seasonal Variation in the Enrichment of Organic Matter and Microorganisms in SML

2.1. Introduction

Most of the previous studies of the SML reported significantly higher organic matter concentration and microbial abundance in the SML than in the SSW of various ocean areas (e.g. Carlson 1983; Obernosterer et al. 2005; Joux et al. 2006; Wurl & Holmes 2008) (Table 1-1). The enrichment of organic matter and microorganisms in the SML results from higher production in the SML than in the SSW and/or upward transport in the water column through passive adsorption on rising bubbles and buoyant particles (Liss & Duce 1997).

Wurl & Holmes (2008) reported significant enrichment of transparent exopolymer particles (TEPs), known as buoyant particles, in the SML. Since then, the accumulation of TEPs in the SML has been considered as a process which enhances the enrichment of organic matter and microorganisms there and contributes to the formation of the SML (Cunliffe & Murrell 2009). TEPs are one of the most ubiquitous gelatinous particles in the ocean and operationally defined as the particles of acidic polysaccharides stainable with alcian blue solution (Alldredge et al. 1993). Previous studies showed that TEPs rapidly form aggregates with organic particles and microbial cells through passive adsorption on their sticky surface (Alldredge et al. 1993; Passow & Alldredge 1994; Mari & Kiørboe 1996; Verdugo et al. 2004). Interestingly, Azetsu-Scott & Passow (2004) experimentally demonstrated that TEP aggregates ascend in the water column due to low density of TEPs. These studies suggest that the enrichment of organic matter and microorganisms in the SML is enhanced by that of TEPs through the upward transport of TEP aggregates in the water column. Further, once gel-like particles, TEPs, accumulate in the SML, the viscosity of the SML may increase, probably resulting in the formation of the physically stable SML which is not easily

disrupted by wind-induced waves. Indeed, the biofilm-like properties of the SML with high EFs of both TEP concentration (12.5) and microbial abundance (2.8 for bacterial abundance) were observed in visible slick areas (Wurl et al. 2016). However, relationships between the enrichment of TEPs and other parameters in the SML have never been reported.

In the water column, TEPs are mainly formed abiotically by the spontaneous coagulation of dissolved precursors released by phytoplankton (Myklestad 1995; Chin et al. 1998; Zhou et al. 1998; Passow 2000), and the peaks of TEP concentration are generally associated with phytoplankton blooms (Passow & Alldredge 1994; Mari & Kiørboe 1996; Mari & Burd 1998; Passow et al. 2001). Thus, in temperate coastal waters where phytoplankton blooms are seasonally observed in the water column (Sugai et al. 2016), the amount of TEP aggregates transported upward and the subsequent enrichment of organic matter and microorganisms in the SML may also show seasonality, and high enrichment in the SML is expected during phytoplankton blooms. Therefore, Chapter 2 aimed to clarify the seasonal variation in the enrichment of organic matter and microorganisms and relationships between chemical and biological parameters in the SML of temperate coastal waters.

2.2. Materials and Methods

2.2.1. Study area

This study was conducted at St. M (35°09′45″N, 139°10′00″E) located 2 km northeast off the Manazuru Peninsula, in coastal waters of Sagami Bay, Japan (Fig. 1-2). Sagami Bay is on the southern coast of the central Japan and faces the northwest Pacific Ocean. About 20 rivers flow into Sagami Bay, and low-salinity water mass is often formed in nearshore areas. St. M is approximately 11 and 25 km far from the mouth of two large rivers, the Sakawa River and the Sagami River, respectively. Sagami Bay is considered as one of the representative temperate coastal waters where the hydrographic conditions of the water column change seasonally (Ara et al. 2011; Kuwahara et al.

2015), and physical, chemical, and biological environments have been intensively investigated in Sagami Bay (e.g. Kuwahara et al. 2000; Fujiki et al. 2004; Shimode et al. 2006; Sugai et al. 2016).

2.2.2. Samplings

Surveys were carried out monthly for two consecutive years from September 2013 to September 2015 on the R/V "Tachibana" of the Manazuru Marine Center for Environmental Research and Education (MMCER), Yokohama National University. Surface seawater for water temperature and salinity was collected using a bucket. Water temperature was measured with a mercury thermometer immediately after a bucket was recovered on the deck, and salinity was measured with an inductive salinometer (601 Mk IV, Yeo-Kal Electronics) within an hour in a laboratory.

SML samples were collected at the bow of the research vessel (12 m long) on the leeward side using a nylon mesh screen to collect organic matter and microorganisms with a wide range of size effectively and to collect a large amount of seawater over a relatively short period of time (Garrett 1965; Agogué et al. 2004; Momzikoff et al. 2004). Nylon mesh was used to avoid sample contamination due to the elution of metals and stretched over a 60 × 80 cm plastic frame. Nylon diameter (430 μm) and mesh size (1.25 mm) were determined based on Agogué et al. (2004) and Momzikoff et al. (2004). The mesh screen was lowered vertically through the ocean surface about 2 m away from the research vessel to collect the natural SML which is not disrupted, raised horizontally through the ocean surface, and tilted to drain SML samples into a 2-L polypropylene bottle. The first 100 mL of seawater draining from the mesh screen was discarded to remove seawater adhering to a plastic frame (Obernosterer et al. 2005; Nakajima et al. 2013). To collect 2-L SML samples, approximately 20–25 dips were performed within 1.5 hours. The thickness of the SML collected by the mesh screen was calculated to be 380 ± 9 μm according to Cunliffe & Wurl (2014). SSW samples were taken at 0.5 m depth using a horizontal Niskin bottle and collected in a

5-L polypropylene bottle. Seawater samples except for the analysis of TEPs were pre-filtered through 180-μm nylon mesh to remove large plankton and debris and brought back to a laboratory within an hour.

Wind speed data were obtained from the Japan Meteorological Agency at the Odawara Office (35°16’36”N, 139°09’18”E) (Japan Meteorological Agency 2015) located less than 15 km away from St. M.

2.2.3. Analytical methods

Triplicate subsamples for the analysis of inorganic nutrients were filtered through 0.45-μm pore size filters (Millex-HA, Merck), and the filtrate was stored at −20°C in 10-mL polyethylene tubes until analysis. Nitrate (NO_3), ammonium (NH_4), phosphate (PO_4), and silicate (SiO_2) concentrations were measured according to Parsons et al. (1984) using a two-channel nutrient autoanalyzer (SWAAT, BL TEC). The detection limit of NO_3, NH_4, PO_4, and SiO_2 concentrations were 0.03, 0.04, 0.02, and 0.08 μM, respectively.

Triplicate subsamples for the analysis of DOC were filtered through 0.22-μm pore size filters (Millex-GV, Merck) following Servais et al. (1989). The filtrate was transferred to 10-mL pre-combusted (450°C, 4 h) glass ampoules, which were immediately heat-sealed with a burner and frozen at −20°C until analysis. After the filtrate was acidified by hydrochloric acid (HCl) and sparged, DOC concentration was measured as non-purgeable organic carbon by a high temperature (680°C) Pt catalyst oxidation method using a total organic carbon analyzer (TOC-V_{CSH}, Shimadzu) equipped with a non-dispersive infrared detector as described by Ogawa et al. (2003). Potassium hydrogen phthalate (Wako) was used as a standard, and detection limit was 0.001 mgC L^{-1}. Triplicate subsamples for the analysis of CDOM were filtered through 0.22-μm pore size filters (Millex-GV, Merck) under the dark condition, and the filtrate was preserved at −20°C in 50-mL polyethylene bottles until analysis. Spectral absorbance was measured using a single-beam

UV-visible spectrophotometer (UV-2450, Shimadzu) with 10-cm pathlength quartz cells referenced against Milli-Q water. Spectral scan was performed from 250 to 850 nm, and baseline for each spectrum was corrected by absorbance at 700–800 nm (Green & Blough 1994). The absorption coefficient of CDOM at wavelength λ (a_{CDOM} [λ]) was determined by

$$a_{\mathrm{CDOM}}(\lambda) = 2.303\, D(\lambda)\, l^{-1}$$

where D (λ) is absorbance at wavelength λ and l is the pathlength of quartz cells.

Triplicate subsamples of 100–400 mL for the analysis of particulate organic carbon (POC) were filtered on pre-combusted (450°C, 4 h) Whatman GF/F filters (GE Healthcare Life Sciences), and the filters were treated with HCl for 2 h to remove inorganic carbon, dried in a dry oven at 60°C for 12 h, and stored in a desiccator until analysis. POC concentration was measured using an organic elemental analyzer (Flash 2000, Thermo Scientific). Acetanilide (Wako) was used as a standard, and detection limit was 0.006 mgC L^{-1}. TEP concentration was determined colorimetrically by a dye-binding assay according to Passow & Alldredge (1995) and Engel (2009). Triplicate subsamples of 20–80 mL were filtered on 0.4-μm pore size polycarbonate filters (Nuclepore Track-Etch Membrane Black, GE Healthcare Life Sciences) under low (< 20 kPa), constant vacuum. The filters were stained with 500 μL of 0.02% (w/v) alcian blue solution, rinsed twice with 1 mL of Milli-Q water, and frozen at –20°C until analysis. After the filters were soaked in 6 mL of 80% (v/v) sulfuric acid (H_2SO_4) for 3 h to dissolve dye, the absorbance of H_2SO_4 solution at 787 nm was measured using a single-beam UV-visible spectrophotometer (UV-2450, Shimadzu) with 1-cm pathlength quartz cells referenced against Milli-Q water. TEP concentration was expressed in the milligrams of Xanthan Gum (Sigma-Aldrich), a standard, equivalent per liter (mg X_{eq} L^{-1}). Detection limit was 0.04 mg X_{eq} L^{-1}.

Triplicate subsamples of 50–200 mL for the analysis of chl. *a* were filtered on Whatman GF/F filters (GE Healthcare Life Sciences), and the filters were preserved at −20°C in 20-mL glass vials pre-filled with 5 mL of *N*,*N*-dimethylformanide to extract chl. *a* pigment following Suzuki &

Ishimaru (1990). Chl. *a* concentration was measured fluorometrically using a fluorometer (10AU, Turner Design) as described by Welschmeyer (1994).

Subsamples for the analysis of bacteria were fixed with the buffered and pre-filtered (< 0.22 μm) formaldehyde (2% final concentration) and stored at −20°C in 10-mL polypropylene tubes until analysis. The subsamples were stained with a nucleic acid stain (SYBR Gold, Invitrogen) and filtered on 0.2-μm pore size polycarbonate filters (Nuclepore Track-Etch Membrane Black, GE Healthcare Life Sciences) according to Shibata et al. (2006). For each filter, at least 20 microscopic fields were examined, and more than 400 cells were counted at × 1000 magnification using an epifluorescence microscope (Axioskop 2 plus, Zeiss). Subsamples for the analyses of autotrophic and heterotrophic nanoflagellates (ANFs and HNFs, respectively) were fixed with glutaraldehyde (1 % final concentration) and preserved at 4°C in 100-mL polyethylene bottles until analysis. The subsamples were filtered on 0.8-μm pore size polycarbonate filters (Nuclepore Track-Etch Membrane Black, GE Healthcare Life Sciences) and stained with primulin (Sigma-Aldrich) as described by Sherr et al. (1993). More than 50 cells on each filter were enumerated at × 1000 magnification using the epifluorescence microscope. ANFs were distinguished from HNFs by the presence of autofluorescence signals, and mixotrophic nanoflagellates were counted as ANFs.

2.2.4. Data analysis

EFs were calculated as the ratio of values in the SML to those in the SSW (e.g. Sieburth et al. 1976; Harvey & Young 1980), and EFs more than and less than one mean enrichment and depletion in the SML, respectively. Values more than the third quartile + 1.5 × interquartile range (IQR) and less than the first quartile – 1.5 × IQR are regarded as outliers. Wilcoxon signed-rank test was conducted using the monthly medians of each parameter in the SML and SSW, and correlation analysis was performed using Pearson's correlation coefficient. Probability less than 0.05 ($p < 0.05$) was considered significant in all statistical analyses. Principal component analysis (PCA) was

conducted to show the seasonal variations in all chemical and biological parameters in the SML and SSW.

2.3. Results

2.3.1. Physical and meteorological parameters

Surface water temperature gradually decreased from 26.1°C in September 2013 to 13.0°C in March 2014 and increased to 24.8°C in August 2014 (Fig. 2-1a). From August 2014 to September 2015, water temperature showed a similar variation. Surface salinity was relatively high (> 33.0) during the study period except in October 2013 (30.6), June 2014 (32.6), July 2014 (32.3), October 2014 (32.4), July 2015 (30.4), and September 2015 (32.0) (Fig. 2-1b). Relatively low mean wind speed during samplings (< 3.3 m s^{-1}) was observed during the study period except in April 2014 (3.8 m s^{-1}), May 2014 (4.0 m s^{-1}), December 2014 (5.4 m s^{-1}), and March 2015 (7.3 m s^{-1}) (Fig. 2-1c).

2.3.2. Chemical and biological parameters in SML and SSW

NO_3 concentration ranged from under the detection limit to 14.4 μM in the SML and from under the detection limit to 13.2 μM in the SSW (Fig. 2-2a). During the study period, NO_3 concentration in the SML (median: 3.04 μM) was slightly but significantly higher compared to the SSW (2.27 μM) ($p < 0.001$). NH_4 concentration varied between 0.46 μM and 4.69 μM in the SML and between 0.46 μM and 2.72 μM in the SSW (Fig. 2-2b). No significant difference was observed between NH_4 concentration in the SML (1.10 μM) and in the SSW (0.88 μM) during the study period ($p = 0.07$). PO_4 concentration fluctuated from 0.02 μM to 0.74 μM in the SML and from 0.02 μM to 0.69 μM in the SSW (Fig. 2-2c). PO_4 concentration in the SML (0.19 μM) showed significantly higher values compared to the SSW (0.14 μM) during the study period ($p < 0.01$). SiO_2 concentration ranged between 2.56 μM and 39.6 μM in the SML and between 1.28 μM and 37.0

μM in the SSW (Fig. 2-2d). During the study period, significantly lower SiO_2 concentration was observed in the SML (10.9 μM) than in the SSW (11.2 μM) ($p < 0.05$).

DOC concentration was relatively high in April 2014 (6.60 mgC L^{-1}), May 2014 (3.36 mgC L^{-1}), and May 2015 (6.29 mgC L^{-1}) in the SML and in June 2014 (1.67 mgC L^{-1}) and May 2015 (2.18 mgC L^{-1}) in the SSW (Fig. 2-3a). Significantly higher DOC concentration was observed in the SML (1.20 mgC L^{-1}) than in the SSW (1.11 mgC L^{-1}) ($p < 0.001$). a_{CDOM} (320) showed relatively high values in April 2014 (1.72 m^{-1}) and May 2015 (3.08 m^{-1}) in the SML and in May 2015 (0.96 m^{-1}) and July 2015 (0.92 m^{-1}) in the SSW (Fig. 2-3b). a_{CDOM} (320) in the SML (0.45 m^{-1}) was significantly higher compared to the SSW (0.36 m^{-1}) ($p < 0.001$).

POC concentration was relatively high in April 2014 (5.17 mgC L^{-1}), May 2015 (1.98 mgC L^{-1}), June 2015 (1.60 mgC L^{-1}), and September 2015 (1.11 mgC L^{-1}) in the SML and in April 2014 (0.74 mgC L^{-1}), May 2015 (0.64 mgC L^{-1}), July 2015 (0.63 mgC L^{-1}), and September 2015 (0.67 mgC L^{-1}) in the SSW (Fig. 2-4a). Significantly higher POC concentration was observed in the SML (0.50 mgC L^{-1}) than in the SSW (0.27 mgC L^{-1}) ($p < 0.001$). TEP concentration showed relatively high values in April 2014 and May 2015 in the SML (5.44 mg X_{eq} L^{-1} and 2.11 mg X_{eq} L^{-1}, respectively) and SSW (0.89 mg X_{eq} L^{-1} and 0.71 mg X_{eq} L^{-1}, respectively) (Fig. 2-4b). TEP concentration in the SML (0.32 mg X_{eq} L^{-1}) was significantly higher compared to the SSW (0.26 mg X_{eq} L^{-1}) ($p < 0.001$).

Chl. *a* concentration was relatively high in April 2014 (129 μg L^{-1}), May 2015 (31.4 μg L^{-1}), and June 2015 (25.9 μg L^{-1}) in the SML and in September 2013 (8.82 μg L^{-1}), March 2014 (9.34 μg L^{-1}), April 2014 (17.5 μg L^{-1}), February 2015 (11.8 μg L^{-1}), May 2015 (7.99 μg L^{-1}), and September 2015 (10.5 μg L^{-1}) in the SSW (Fig. 2-5a). Significantly higher chl. *a* concentration was observed in the SML (3.67 μg L^{-1}) than in the SSW (3.25 μg L^{-1}) ($p < 0.05$). ANF abundance showed relatively high values in April 2014 (46.3×10^6 cells L^{-1}), May 2015 (25.5×10^6 cells L^{-1}), June 2015 (17.4×10^6 cells L^{-1}), and September 2015 (21.0×10^6 cells L^{-1}) in the SML and in July

2014 (5.48×10^6 cells L^{-1}), May 2015 (5.48×10^6 cells L^{-1}), and September 2015 (8.51×10^6 cells L^{-1}) in the SSW (Fig. 2-5b). ANF abundance in the SML (4.33×10^6 cells L^{-1}) was significantly higher compared to the SSW (1.35×10^6 cells L^{-1}) ($p < 0.001$).

Bacterial abundance was relatively high in April 2014 (16.1×10^9 cells L^{-1}), July 2014 (6.56×10^9 cells L^{-1}), May 2015 (10.4×10^9 cells L^{-1}), and September 2015 (4.97×10^9 cells L^{-1}) in the SML and in July 2014 (5.41×10^9 cells L^{-1}) in the SSW (Fig. 2-6a). Significantly higher bacterial abundance was observed in the SML (2.52×10^9 cells L^{-1}) than in the SSW (1.33×10^9 cells L^{-1}) ($p < 0.001$). HNF abundance showed relatively high values in April 2014 (69.9×10^6 cells L^{-1}), May 2015 (24.0×10^6 cells L^{-1}), and September 2015 (21.6×10^6 cells L^{-1}) in the SML and in July 2014 (4.73×10^6 cells L^{-1}), September 2014 (6.05×10^6 cells L^{-1}), May 2015 (5.10×10^6 cells L^{-1}), and September 2015 (6.62×10^6 cells L^{-1}) in the SSW (Fig. 2-6b). HNF abundance in the SML (6.50×10^6 cells L^{-1}) was significantly higher compared to the SSW (1.83×10^6 cells L^{-1}) ($p < 0.001$).

The median EF of POC concentration (1.77) was higher than those of TEP concentration (1.38), a_{CDOM} (320) (1.37), and DOC concentration (1.20), and the median EFs of HNF abundance (3.13) and ANF abundance (2.83) were higher than those of bacterial abundance (1.54) and chl. *a* concentration (1.25) (Fig. 2-7). In April 2014 and May 2015, the EFs of all parameters except POC concentration, ANF abundance, and HNF abundance in May 2015 were particularly high and regarded as outliers. EFs in April 2014 ranged from 4.18 (a_{CDOM} [320]) to 40.8 (ANF) and higher than those in May 2015 which varied between 2.89 (DOC) and 6.95 (bacterial abundance).

2.3.3. Principal component analysis

Principal component 1 (PC1) (60.4%) and 2 (PC2) (19.1%) explained 79.5% of the variances in chemical and biological parameters in the SML and SSW (Fig. 2-8a). In April 2014 and May 2015, SML samples showed particularly high positive values on PC1 (15.1 and 8.46,

respectively) and moderate positive values on PC2 (1.47 and 1.31, respectively). For SML samples except in April 2014 and May 2015 and SSW samples, relatively low values on PC1 (from −1.77 to 2.37) and a wide range of values on PC2 (from −1.85 to 3.58) were observed. SML samples in April 2014 and May 2015 were mainly characterized by particularly high concentration of organic matter and abundance of microorganisms and moderate concentrations of inorganic nutrients whereas SML samples except in April 2014 and May 2015 and SSW samples were characterized by relatively low organic matter concentration and microbial abundance and the variations in inorganic nutrient concentrations (Fig. 2-8b).

2.3.4. Relationships between parameters

Each chemical and biological parameter in the SML showed a significant positive correlation with that in the SSW during the study period except in April 2014 and May 2015 (Fig. 2-9, Fig. 2-10, Fig. 2-11). In April 2014, all parameters except NO_3 (Fig. 2-9a), NH_4 (Fig. 2-9b), and SiO_2 concentrations (Fig. 2-9d) in the SML were particularly higher compared to the SSW. In May 2015, particularly higher values in the SML were observed compared to the SSW for all parameters except SiO_2 concentration (Fig. 2-9d), POC concentration (Fig. 2-10c), ANF abundance (Fig. 2-11c), and HNF abundance (Fig. 2-11d).

No significant relationship was observed between mean wind speed during samplings and the EFs of organic matter concentration or microbial abundance during the study period except in April 2014 and May 2015. During the period, the EF of TEP concentration was significantly positively correlated with not DOC concentration ($p = 0.52$) (Fig. 2-12a), a_{CDOM} (320) ($p = 0.20$) (Fig. 2-12b), POC concentration ($p = 0.09$) (Fig. 2-12c), ANF abundance ($p = 0.19$) (Fig. 2-13b), bacterial abundance ($p = 0.14$) (Fig. 2-13c), and HNF abundance ($p = 0.41$) (Fig. 2-13d) but only chl. *a* concentration ($r = 0.469$, $n = 23$, $p < 0.05$) (Fig. 2-13a).

2.4. Discussion

2.4.1. Enrichment in SML except in April 2014 and May 2015

The mean EFs of organic matter concentration and microbial abundance during the study period except in April 2014 and May 2015 were within ranges reported by previous studies (Table 1-1). During the period, each chemical and biological parameter in the SML was significantly positively correlated with that in the SSW (Fig. 2-9, Fig. 2-10, Fig. 2-11), which shows that the seasonal variations in parameters in the SML were similar with those in the SSW. In the present study, during the study period except in April 2014 and May 2015, no significant relationship was observed between mean wind speed during samplings and the EFs of chemical and biological parameters. The insignificant relationships may be because wind speed at St. M and at the Odawara Office (the Japan Meteorological Agency) is different due to distance between the two sites (15 km).

In the water column, high TEP concentration is generally associated with phytoplankton blooms, and the relationship between chl. *a* (x) and TEP concentrations (y) can be fitted to $y = a\, x^{b}$ (Passow 2002). In the present study, the following regression formulae were obtained: $y = 231\, x^{0.292}$ ($r^2 = 0.531$, n = 23, $p < 0.001$) in the SML during the study period except in April 2014 and May 2015 and $y = 188\, x^{0.356}$ ($r^2 = 0.544$, n = 25, $p < 0.001$) in the SSW during the study period (Fig. 2-14). The exponent, b, of the regression formulae (0.292 and 0.356) is comparable to that in Bransfield Strait (0.317) (Corzo et al. 2005) and in Singapore Strait and Johor Strait (0.35) (Wurl & Holmes 2008) but considerably less than one. This result indicates the decrease in TEP production rate and/or the increase in TEP consumption rate as phytoplankton abundance increases, which is in agreement with the hypothesis that TEP production rate is a function of the growth rate rather than the abundance of phytoplankton (Waite et al. 1995; Engel et al. 2002).

To reveal whether or not the enrichment of TEPs in the SML enhances that of organic matter and microorganisms through the upward transport of TEPs in the water column forming

aggregates with organic particles and microbial cells, the relationships between the EFs of TEP concentration and those of organic matter concentration (Fig. 2-12) or microbial abundance (Fig. 2-13) were examined. However, no significant relationship was observed between them except the relationship between the EFs of the concentrations of TEPs and chl. *a* (Fig. 2-13a) during the study period except in April 2014 and May 2015. A significant positive correlation between the EFs of TEP and chl. *a* concentrations can result from the formation of TEPs through the extracellular release of TEP precursors by phytoplankton (Myklestad 1995; Chin et al. 1998; Zhou et al. 1998; Passow 2000) as well as the accumulation of phytoplankton in the SML due to that of TEP aggregates, which is supported by significant positive relationships between chl. *a* and TEP concentrations both in the SML and SSW (Fig. 2-14). These results suggest that the enrichment of organic matter and microorganisms in the SML is not enhanced by that of TEPs in temperate coastal waters. Organic matter and microorganisms were enriched in the SML probably due to a combination of higher production in the SML and passive adsorption on rising bubbles and buoyant particles (Liss & Duce 1997).

2.4.2. Enrichment in SML in April 2014 and May 2015

The EFs of organic matter concentration and microbial abundance except POC concentration, ANF abundance, and HNF abundance in May 2015 were particularly high during spring (in April 2014 and May 2015), which are comparable to those reported by Wurl et al. (2011b), Nakajima et al. (2013), and Wurl et al. (2016) (Table 1-1). This result clearly showed the seasonality of the enrichment of organic matter and microorganisms in the SML of temperate coastal waters.

Whether TEP aggregates ascend or sink in the water column depends on the density and the relative proportions of TEPs (positively buoyant) and solid particles (negatively buoyant) in the aggregates (Azetsu-Scott & Passow 2004). Wurl et al. (2011b) examined the ratio of TEP to POC

concentrations (TEP/POC ratio) using POC as an indicator of the amount of solid particles. They found high TEP/POC ratio in the water column, which possibly means relatively high proportion of TEPs compared to solid particles in TEP aggregates, and showed the possibility of the upward transport of the TEP aggregates in the water column. However, in the present study, TEP/POC ratio in the SSW was not high in April 2014 (1.20 mg X_{eq} mgC^{-1}) and May 2015 (1.10 mg X_{eq} mgC^{-1}) compared to the other months (1.09 ± 0.59 mg X_{eq} mgC^{-1}) (Fig. 2-15). This result indicates that particularly high enrichment of organic matter and microorganisms in the SML in April 2014 and May 2015 was due to particularly high production in the SML rather than the upward transport of TEP aggregates in the water column. Interestingly, in April 2014 and May 2015, relatively high PO_4 concentration, which is enough to relieve the P limitation of phytoplankton, was observed in the SML (0.61 µM and 0.52 µM, respectively) despite relatively low values in the SSW (0.02 µM and 0.05 µM, respectively) (Fig. 2-9c). In coastal waters of Sagami Bay, Fujiki et al. (2004) measured the *in situ* concentration of inorganic nutrients in every two days and conducted bioassay experiments by adding inorganic nutrients to surface seawater in every eight days from spring to summer. Their study indicated that phytoplankton growth is limited by the lack of PO_4 in surface waters of coastal Sagami Bay during the period as reported in estuaries and coastal areas where a larger amount of N than P is supplied by freshwater inflow (Harrison et al. 1990; Turner et al. 1990; Thingstad et al. 1998; Labry et al. 2002). In the present study, although bioassay experiments were not conducted, the possible limitation of phytoplankton growth by the lack of inorganic nutrients can be assessed by a combination of inorganic nutrient concentrations and ratios (PO_4 limitation if PO_4 concentration < 0.2 µM, dissolved inorganic nitrogen [DIN]/PO_4 ratio > 20, SiO_2/PO_4 ratio > 20) determined based on the concentrations less than half-saturation constant for uptake) (Dortch & Whitledge 1992; Justić et al. 1995). In the SSW, PO_4 concentration, DIN/PO_4 ratio, and SiO_2/PO_4 ratio were 0.02 µM, 39.2, and 374 in April 2014 and 0.05 µM, 41.1, and 26.6 in May 2015, respectively (Fig. 2-2), which indicates that phytoplankton growth was limited by PO_4

unavailability in surface waters in April 2014 and May 2015. Because chl. *a* concentration in the SML particularly increased in April 2014 (129 μg L^{-1}) and May 2015 (31.4 μg L^{-1}) (Fig. 2-5a), these results suggest that the production of organic matter and microorganisms in the SML was particularly high in April 2014 and May 2015 due to phytoplankton blooms there induced by the supply of PO_4. Possibly, PO_4 was externally supplied by freshwater inflow because heavy precipitation was observed eight days and 11 days before the sampling day in April 2014 (51.5 mm) and May 2015 (38.5 mm), respectively (Japan Meteorological Agency 2015), although salinity in the SML was not measured in the present study. PO_4 may have been also supplied by the atmospheric deposition of anthropogenic materials on the ocean surface, which can be a source of PO_4 in surface waters of the coastal areas of the northwest Pacific Ocean (Zhang & Liu 1994), because relatively high deposition flux of sulfate was observed six days and 11 days before the sampling day in April 2014 (0.5–1 μg m^{-2} s^{-1}) and May 2015 (0.2–0.5 μg m^{-2} s^{-1}), respectively (Kyushu University 2019). The present study suggests that chemical and biological parameters show seasonality in the SML of temperate coastal waters depending on by the seasonal events of the external supply of inorganic nutrients.

Particularly high enrichment of organic matter and microorganisms in the SML was observed in April 2014 and May 2015 probably also because the viscous, stable SML was formed due to the accumulation of TEPs (5.44 mg X_{eq} L^{-1} and 2.11 mg X_{eq} L^{-1}, respectively) (Fig. 2-4b) without the disruption of the SML by wind-induced waves at wind speed of 3.8 m s^{-1} and 2.8 m s^{-1}, respectively (Fig. 2-1c). The formation of the stable SML was indicated by Wurl & Holmes (2008) who showed significant enrichment of the sulphate half-ester group ($-OSO_3^-$) of TEPs in the SML. Further, TEPs protect microorganisms from intense solar radiation (Ortega-Retuerta et al. 2009) and provide microhabitats favorable for the growth of microorganisms (Wurl et al. 2016).

Interestingly, although all EFs of organic matter concentration and microbial abundance particularly increased in April 2014, the enrichment of POC, ANF, and HNF was not particularly

high in May 2015 (3.09, 4.65, and 4.70, respectively) (Fig. 2-7). This result probably shows the difference between time periods from phytoplankton blooms to samplings and thus between the extent of the development of microbial communities in the SML in April 2014 and May 2015. First, because the dominance of *Leptocylindrus* spp. was observed in the SML both in April 2014 (75.1%) and May 2015 (89.3%), the blooms of phytoplankton dominated by diatoms may have occurred in the SML. Then, phytoplankton probably released organic matter extracellularly, which rapidly stimulated bacterial growth, followed by the growth of flagellates and the increase in POC.

2.4.3. Difference in the enrichment of organic matter and microorganisms in SML

The median EFs of organic matter concentration and microbial abundance were largely different (Fig. 2-7). The enrichment of POC in the SML (median EF: 1.77) was higher compared to TEPs (1.38), CDOM (1.37), and DOC (1.20) as reported by previous studies (e.g. Carlucci et al. 1986; Stolle et al. 2010). This result was probably due to the formation of particles in the SML promoted by the compression and dilation of the ocean surface (Wheeler 1975; Carlson 1993) and the atmospheric deposition of aerosol particles on the ocean surface. Interestingly, higher EF of a_{CDOM} (320) than that of DOC concentration was observed despite more rapid removal of CDOM in the SML under more intense solar radiation. Carlson (1983) and Obernosterer et al. (2008) also reported the selective enrichment of CDOM in the SML, which may have resulted from more effective adsorption of CDOM on rising bubbles and buoyant particles compared to low-molecular weight (LMW) dissolved organic matter. Higher enrichment of CDOM in the SML even under more intense light condition suggests the continuous supply of CDOM and active photochemical reactions by the photodegradation of CDOM there.

The median EFs of HNF (3.13) and ANF abundance (2.83) were higher than those of bacterial abundance (1.54) and chl. *a* concentration (1.25) as reported by previous studies (e.g. Agogué et al. 2004; Obernosterer et al. 2005; Joux et al. 2006; Nakajima et al. 2013). Although UV

radiation causes DNA damage and the production of reactive oxygen species, previous studies reported that flagellates had higher resistance to UV radiation compared to bacteria and diatoms (Buma et al. 2001; Wängberg et al. 2008), which indicates adaptation by flagellates to the light condition of the SML. The depletion of ciliates (EF: 0.63) was reported in the SML of temperate coastal waters (Agogué et al. 2004), and lower abundance of the predators of flagellates in the SML than in the SSW is possibly another reason although ciliate abundance was not measured in the present study. Joux et al. (2006) and Nakajima et al. (2013) showed that the ratio of bacterial abundance to HNF abundance (BA/HNFA ratio), an indicator of grazing pressure on bacteria by HNFs (e.g. Gasol 1994; Lekunberri et al. 2012), was lower in the SML than in the SSW, which indicates higher grazing pressure on bacteria in the SML. In the present study, significantly lower BA/HNFA ratio in the SML (median: 281) was observed compared to the SSW (735) ($p < 0.001$). This results indicates that lower EF of bacterial abundance than that of HNF abundance was due to stronger top-down control on bacteria by HNFs in the SML. The lowest EF of chl. *a* concentration among biological parameters probably resulted from a smaller amount of chl. *a* pigment per cell in the SML than in the SSW under more intense light condition (Richardson et al. 1983; Geider 1987). Further, Agogué et al. (2004) and Joux et al. (2006) showed higher EF of the concentration of phaeophytin (9.97 and 9.2, respectively), a chlorophyll-degraded product, compared to chl. *a* concentration (1.76 and 1.3, respectively), indicating more rapid photooxidation of chl. *a* in the SML than in the SSW. These results suggest different chemical composition and microbial community structure in the SML and SSW.

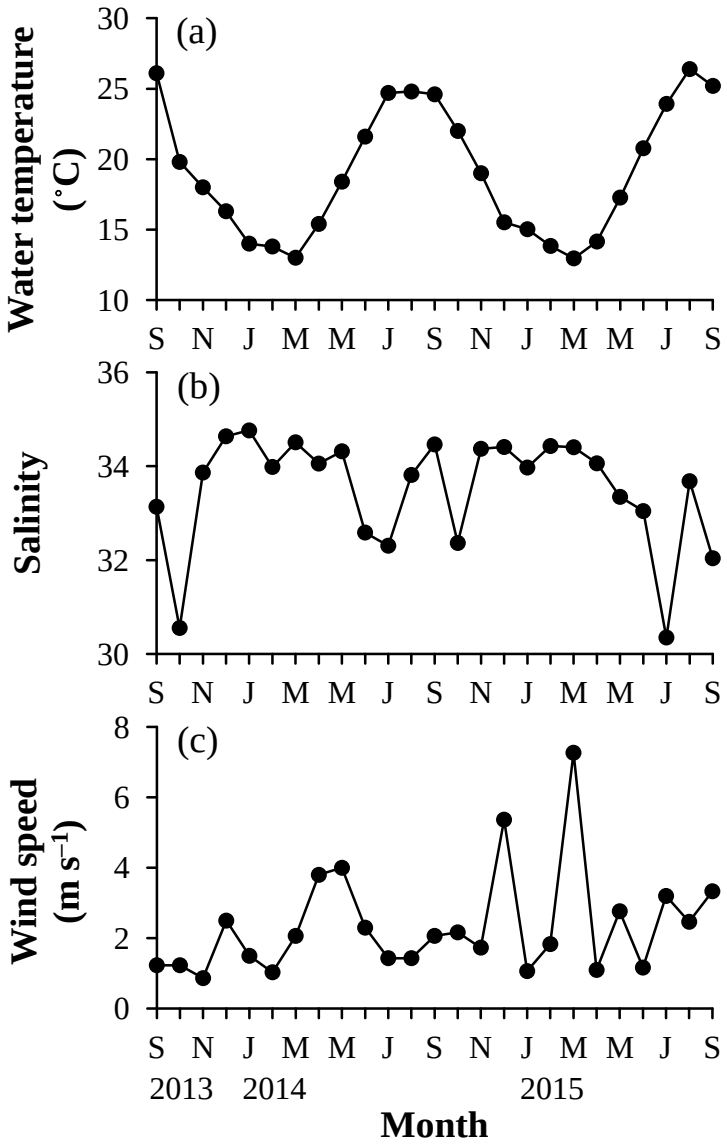

Fig. 2-1. Monthly variations in (a) surface water temperature, (b) surface salinity, and (c) mean wind speed during samplings (Sugai et al. 2018)

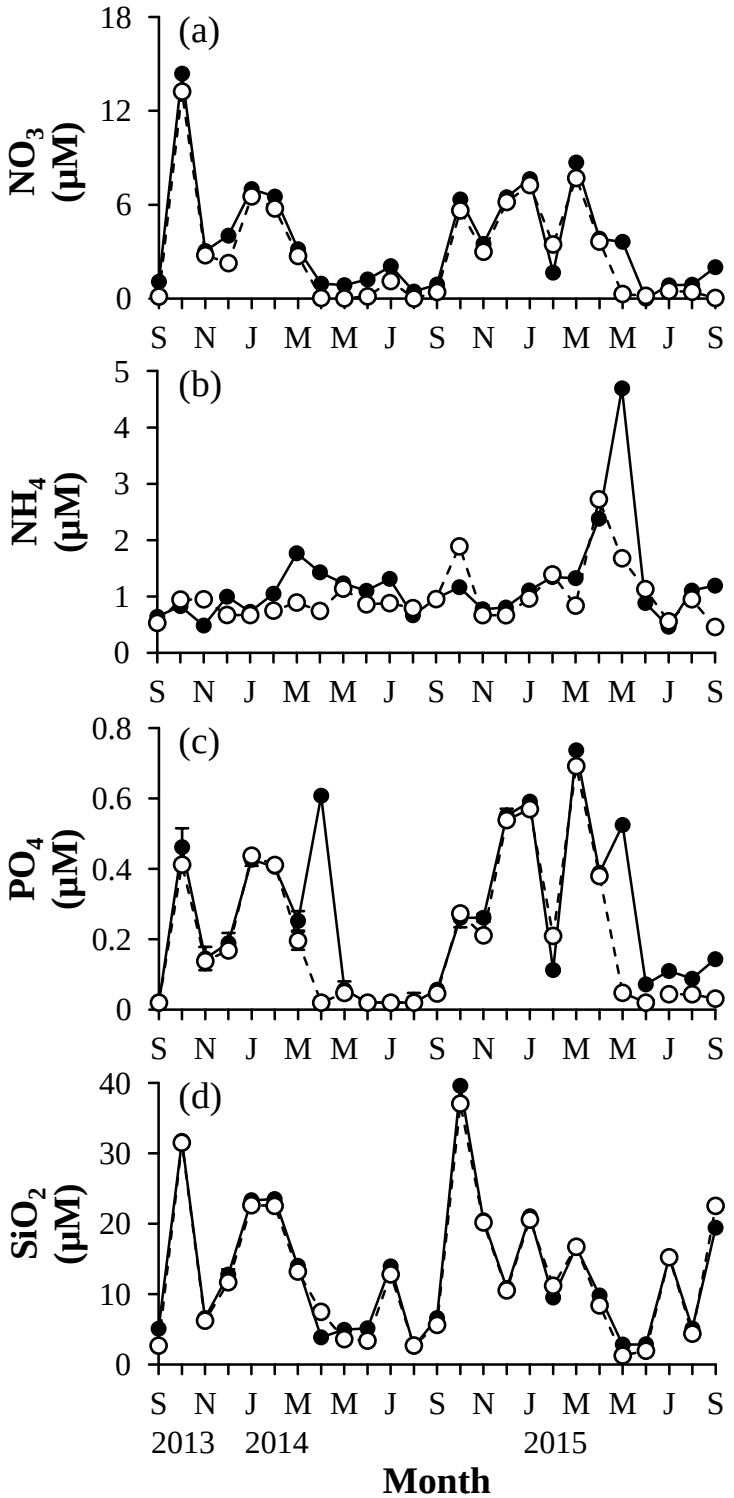

Fig. 2-2. Monthly variations in (a) nitrate (NO_3), (b) ammonium (NH_4), (c) phosphate (PO_4), and (d) silicate (SiO_2) in the surface microlayer (closed circles) and subsurface water (open circles) (Sugai et al. 2018)

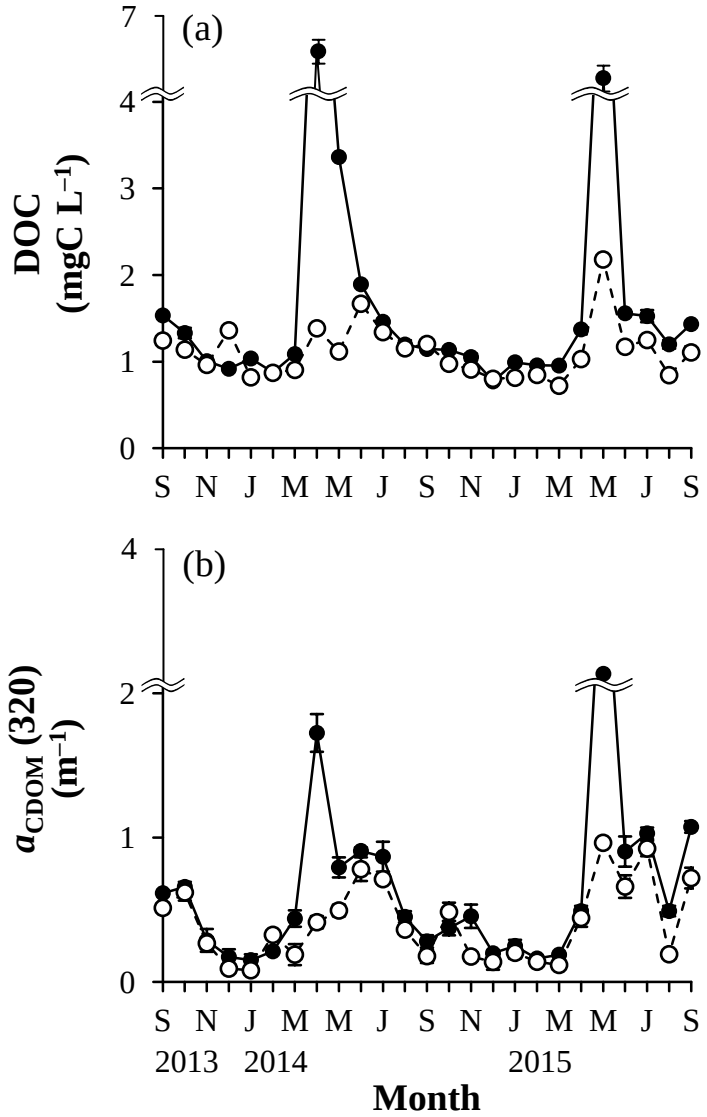

Fig. 2-3. Monthly variations in (a) dissolved organic carbon (DOC) and (b) the absorption coefficient of chromophoric dissolved organic matter at 320 nm (a_{CDOM} [320]) in the surface microlayer (closed circles) and subsurface water (open circles) (Sugai et al. 2018)

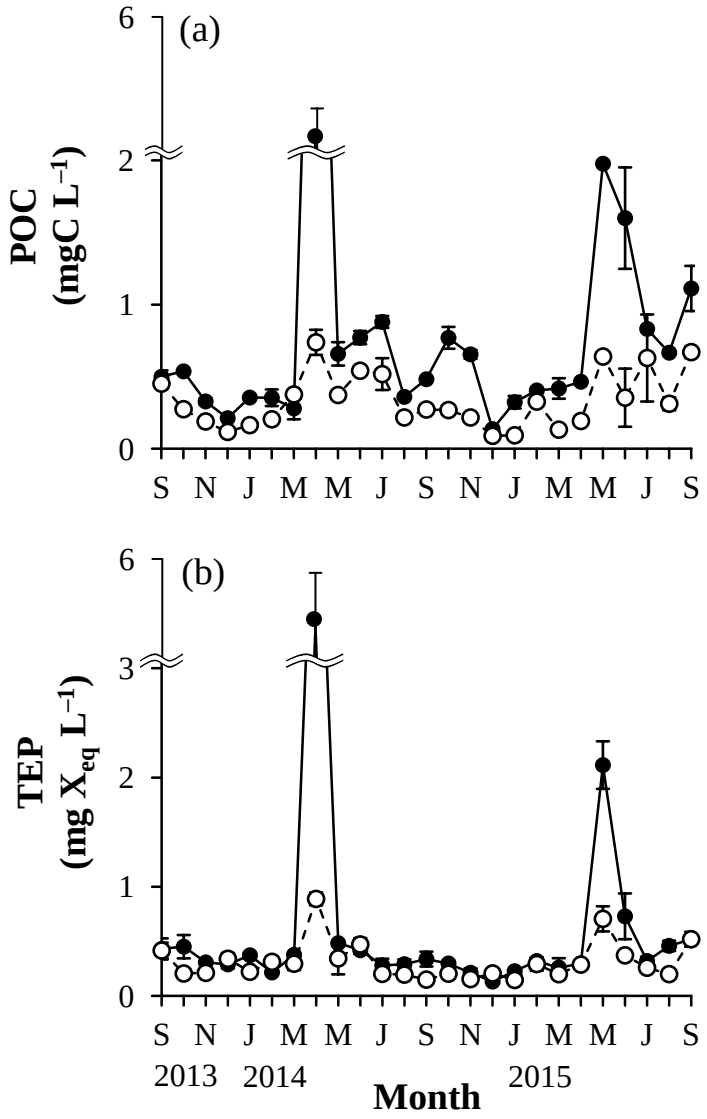

Fig. 2-4. Monthly variations in (a) particulate organic carbon (POC) and (b) transparent exopolymer particles (TEP) in the surface microlayer (closed circles) and subsurface water (open circles) (Sugai et al. 2018)

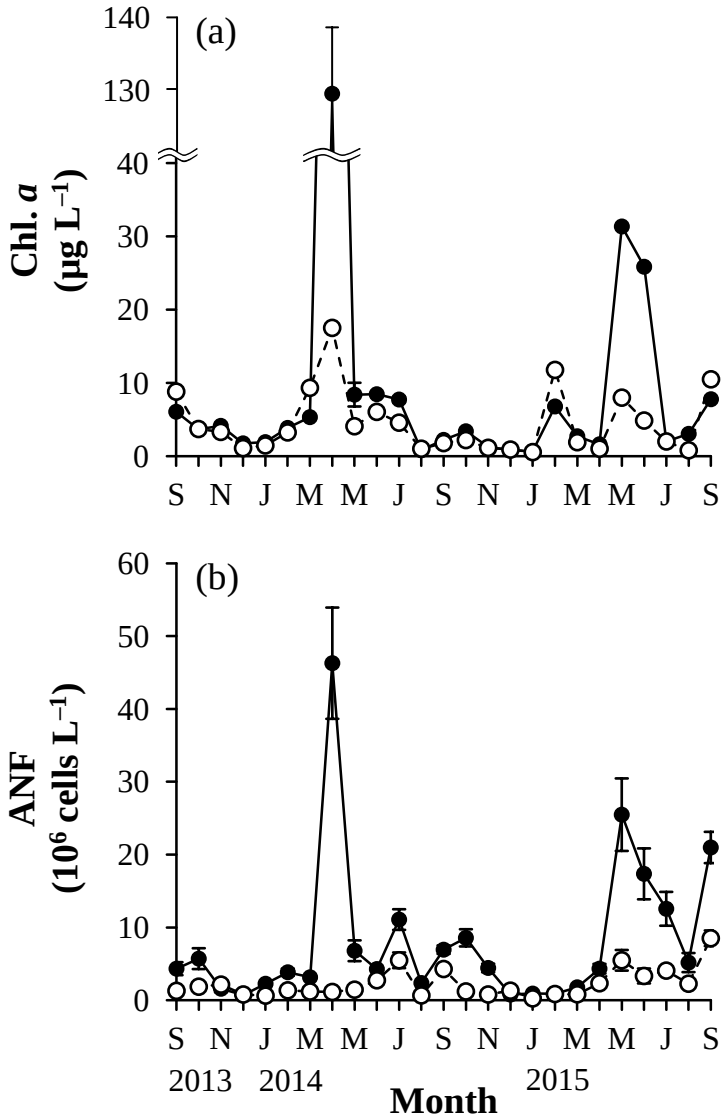

Fig. 2-5. Monthly variations in (a) chlorophyll (chl.) *a* and (b) autotrophic nanoflagellates (ANF) in the surface microlayer (closed circles) and subsurface water (open circles) (Sugai et al. 2018)

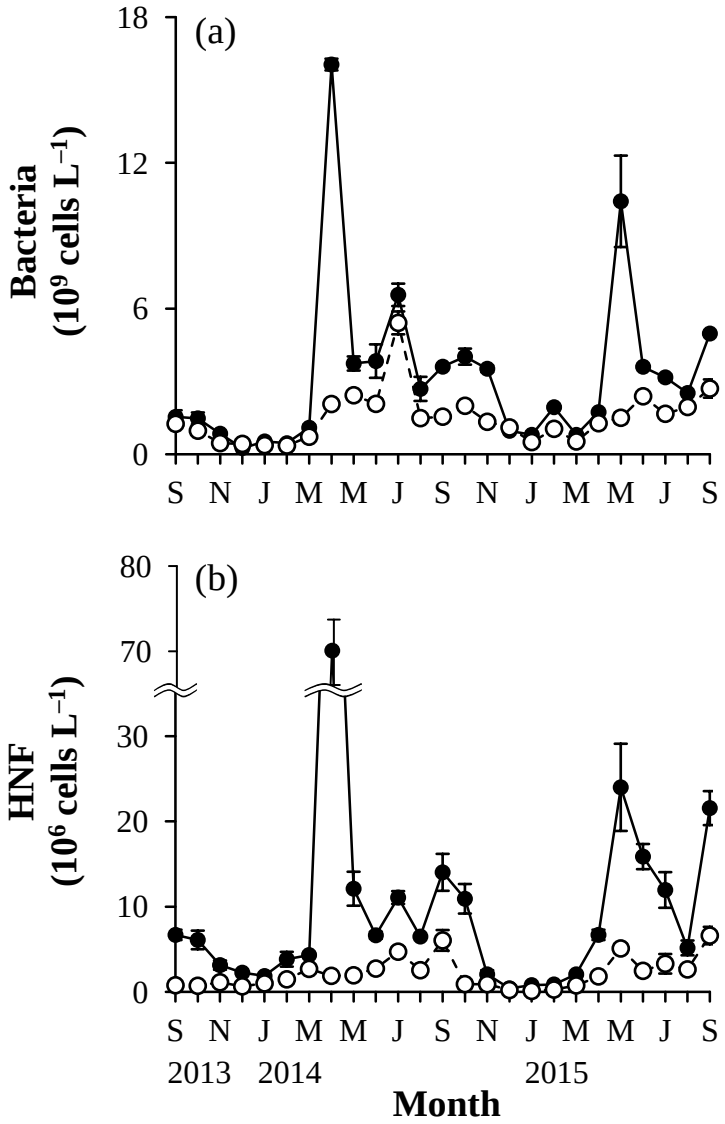

Fig. 2-6. Monthly variations in (a) bacteria and (b) heterotrophic nanoflagellates (HNF) in the surface microlayer (closed circles) and subsurface water (open circles) (Sugai et al. 2018)

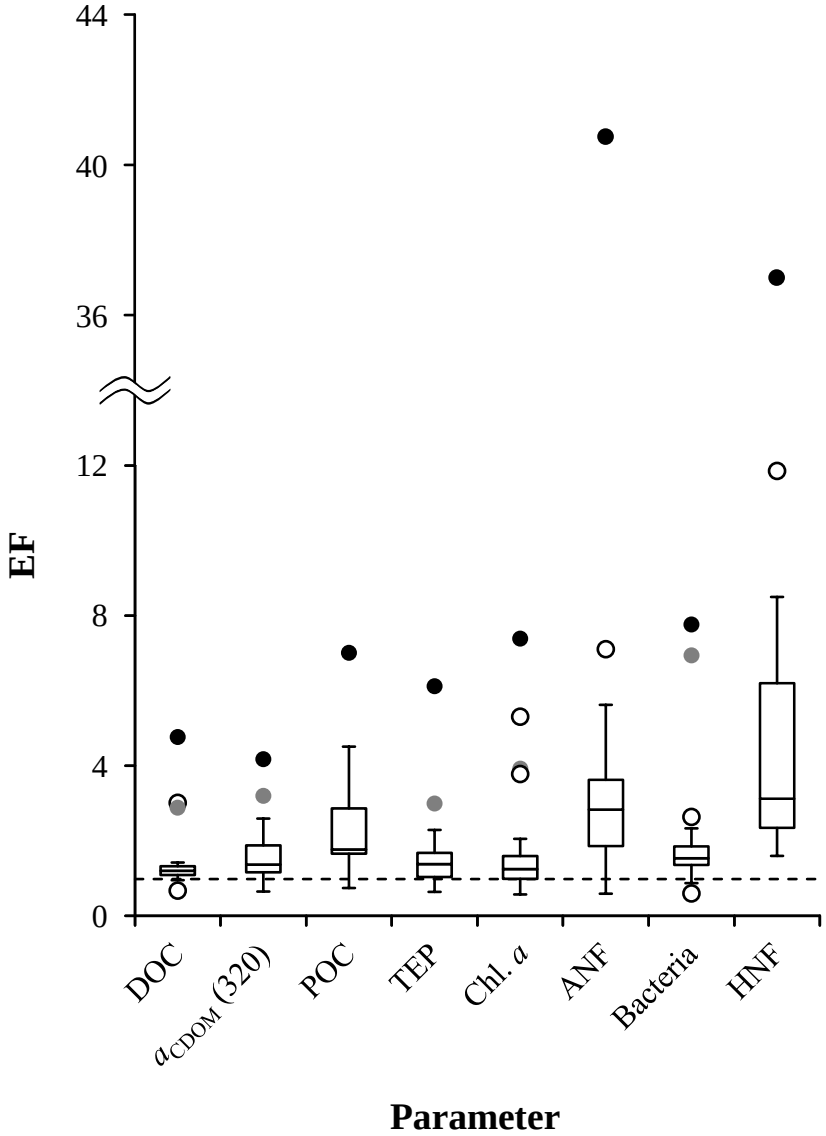

Fig. 2-7. Enrichment factors (EF) of organic matter and microorganisms. Closed black circles, closed gray circles, and open circles represent outliers in April 2014, May 2015, and the other months, respectively. Dashed line indicates EF = 1. DOC: dissolved organic carbon, a_{CDOM} (320): the absorption coefficient of chromophoric dissolved organic matter at 320 nm, POC: particulate organic carbon, TEP: transparent exopolymer particles, chl. *a*: chlorophyll *a*, ANF: autotrophic nanoflagellates, HNF: heterotrophic nanoflagellates

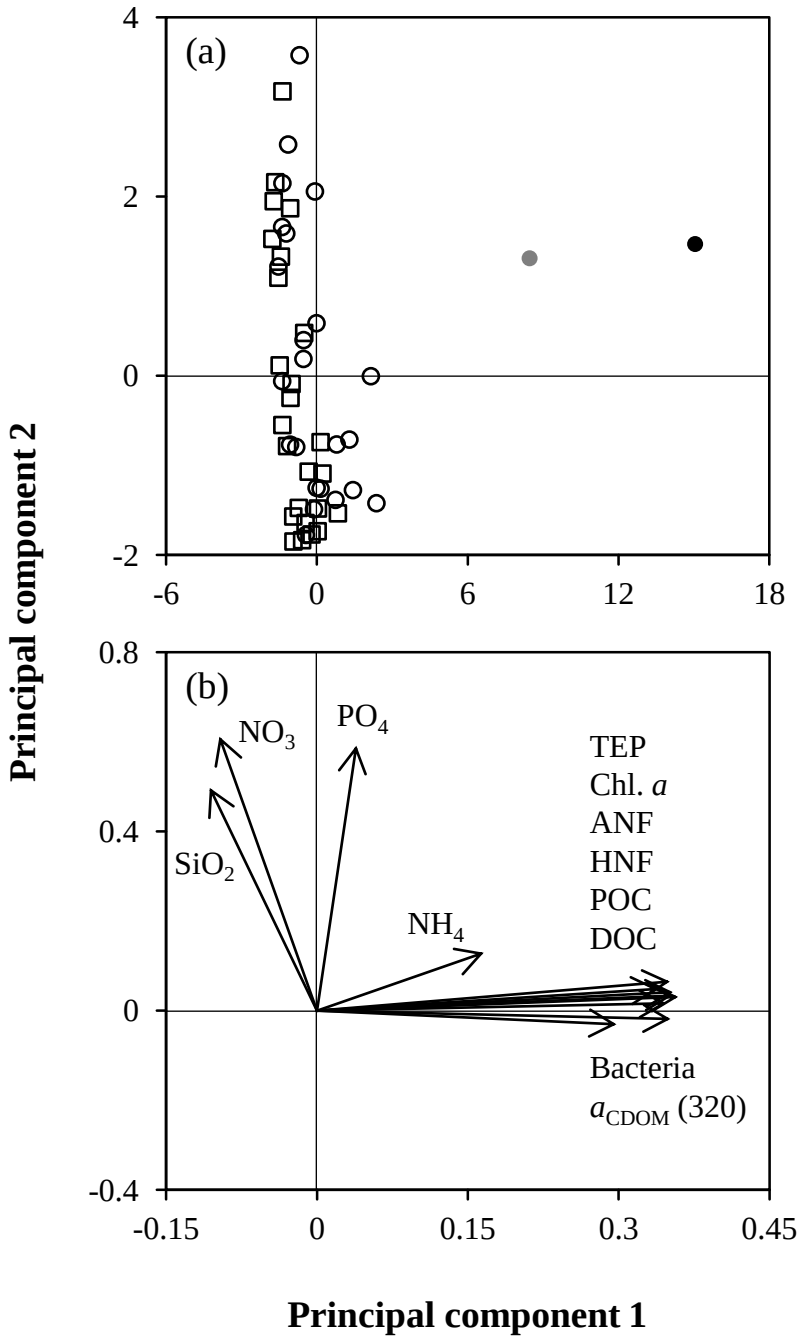

Fig. 2-8. Distribution of (a) monthly samples and (b) the eigenvectors of parameters. Closed black circle, closed gray circle, open circles, and open squares represent the surface microlayer (SML) in April 2014, in May 2015, and in the other months, and the subsurface water, respectively. NO_3: nitrate, NH_4: ammonium, PO_4: phosphate, SiO_2: silicate, DOC: dissolved organic carbon, a_{CDOM} (320): the absorption coefficient of chromophoric dissolved organic matter at 320 nm, POC: particulate organic carbon, TEP: transparent exopolymer particles, chl. *a*: chlorophyll *a*, ANF: autotrophic nanoflagellates, HNF: heterotrophic nanoflagellates

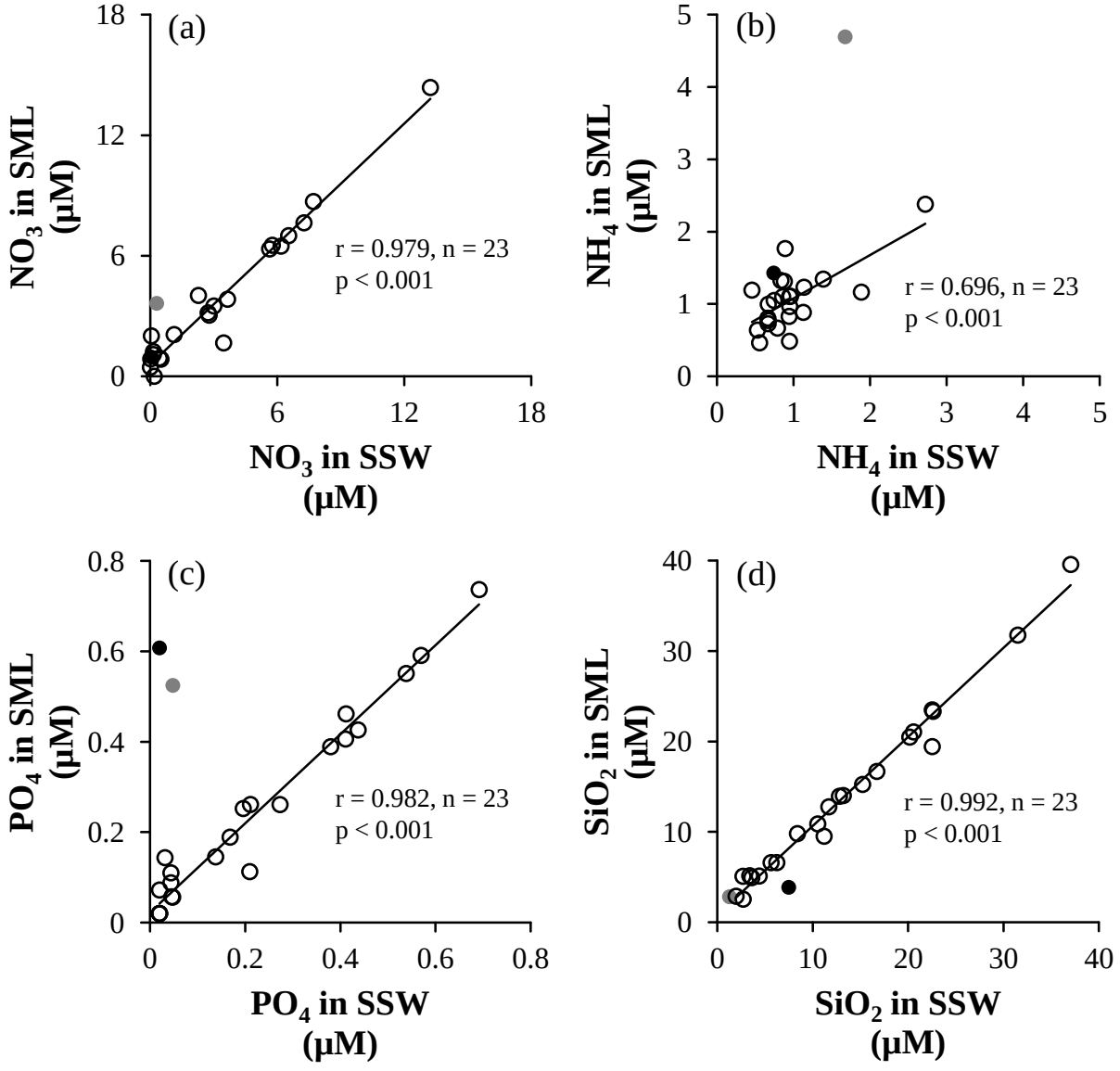

Fig. 2-9. Relationships between (a) nitrate (NO_3), (b) ammonium (NH_4), (c) phosphate (PO_4), and (d) silicate (SiO_2) in the surface microlayer (SML) and subsurface water (SSW). Closed black circles, closed gray circles, and open circles represent April 2014, May 2015, and the other months, respectively. Relationships were examined excluding data in April 2014 and May 2015

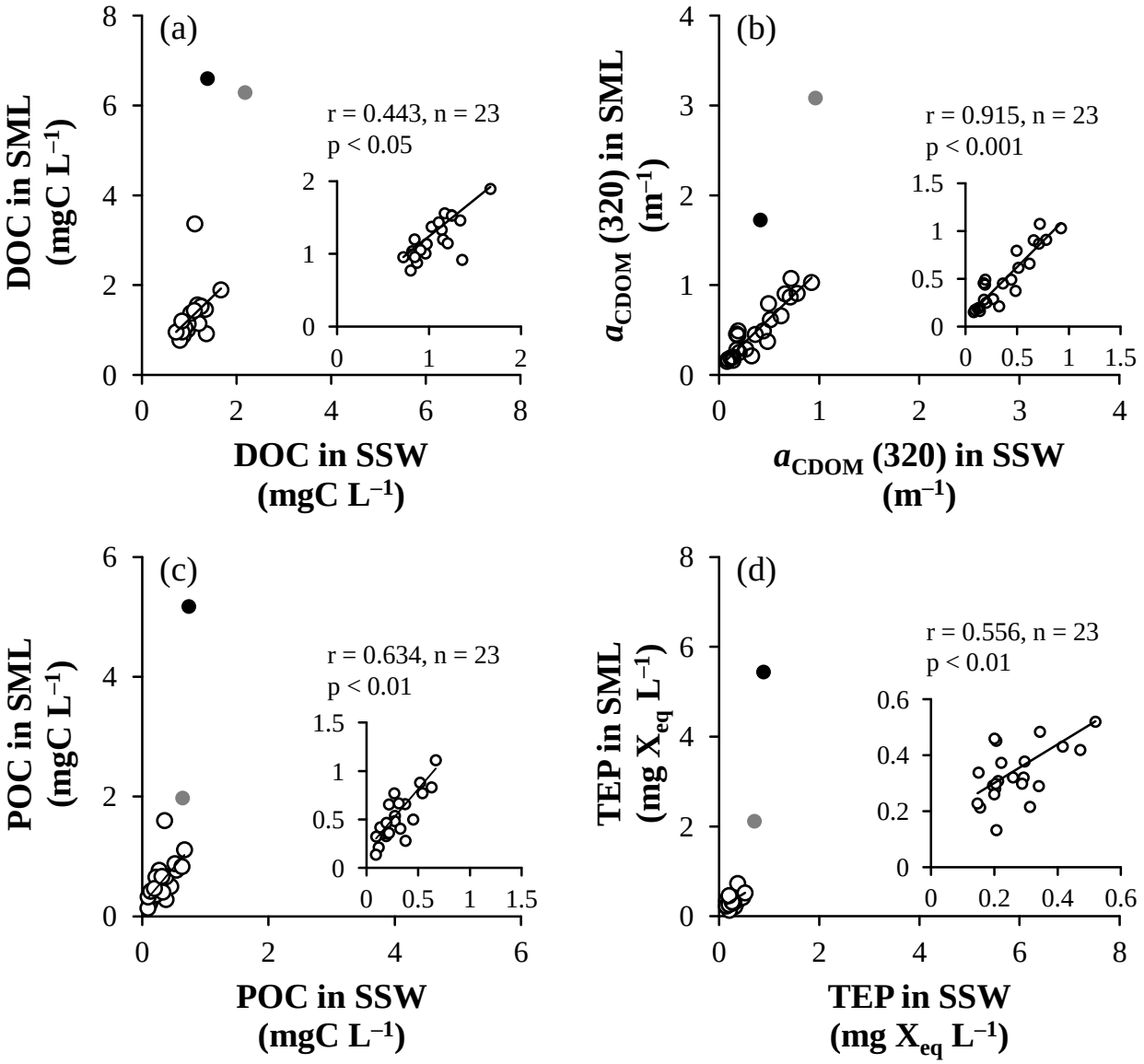

Fig. 2-10. Relationships between (a) dissolved organic carbon (DOC), (b) the absorption coefficient of chromophoric dissolved organic matter at 320 nm (a_{CDOM} [320]), (c) particulate organic carbon (POC), and (d) transparent exopolymer particles (TEP) in the surface microlayer (SML) and subsurface water (SSW). Closed black circles, closed gray circles, and open circles represent April 2014, May 2015, and the other months, respectively. Relationships were examined excluding data in April 2014 and May 2015. Insets show the magnified views of each figure

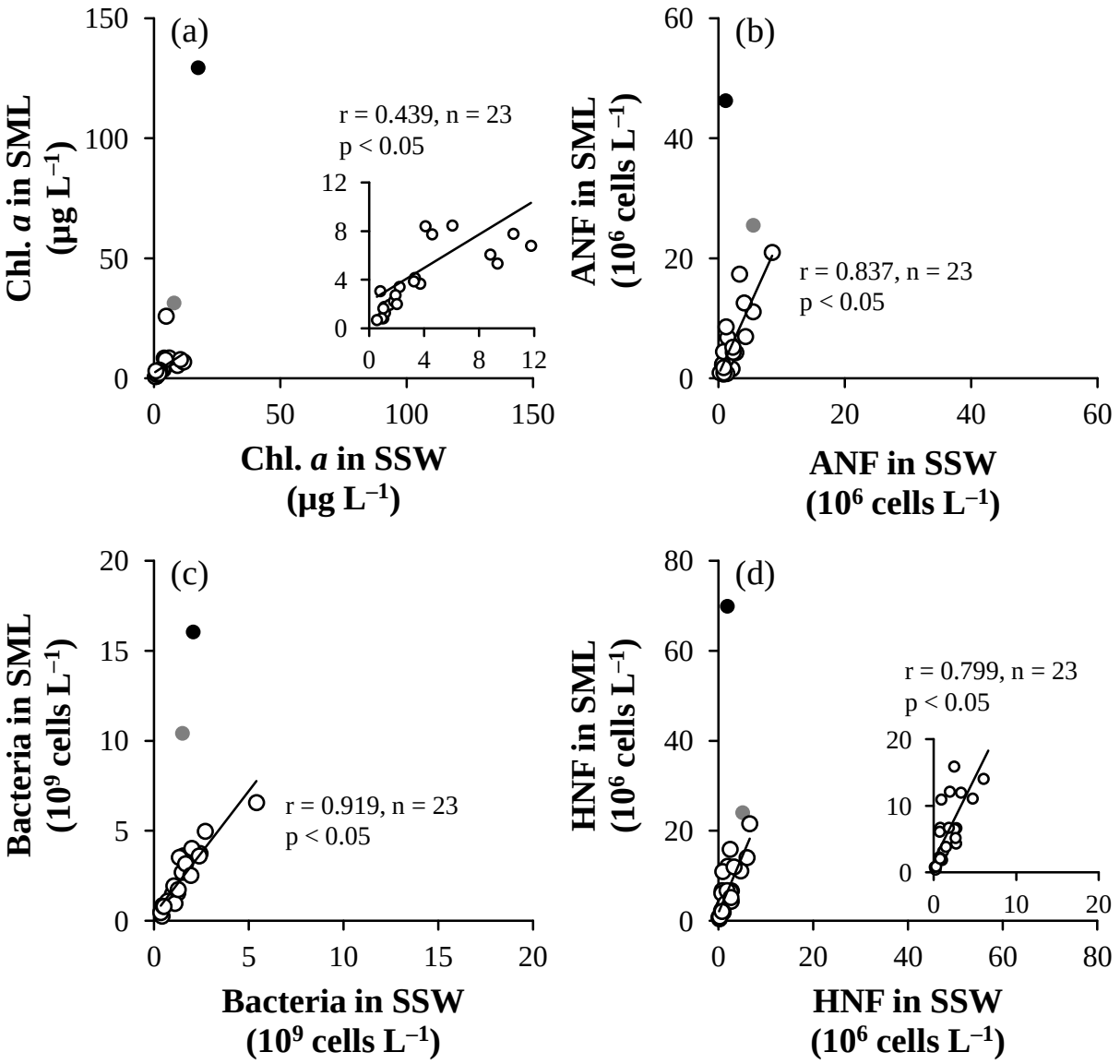

Fig. 2-11. Relationships between (a) chlorophyll (chl.) *a*, (b) autotrophic nanoflagellates (ANF), (c) bacteria, and (d) heterotrophic nanoflagellates (HNF) in the surface microlayer (SML) and subsurface water (SSW). Closed black circles, closed gray circles, and open circles represent April 2014, May 2015, and the other months, respectively. Relationships were examined excluding data in April 2014 and May 2015. Insets show the magnified views of each figure

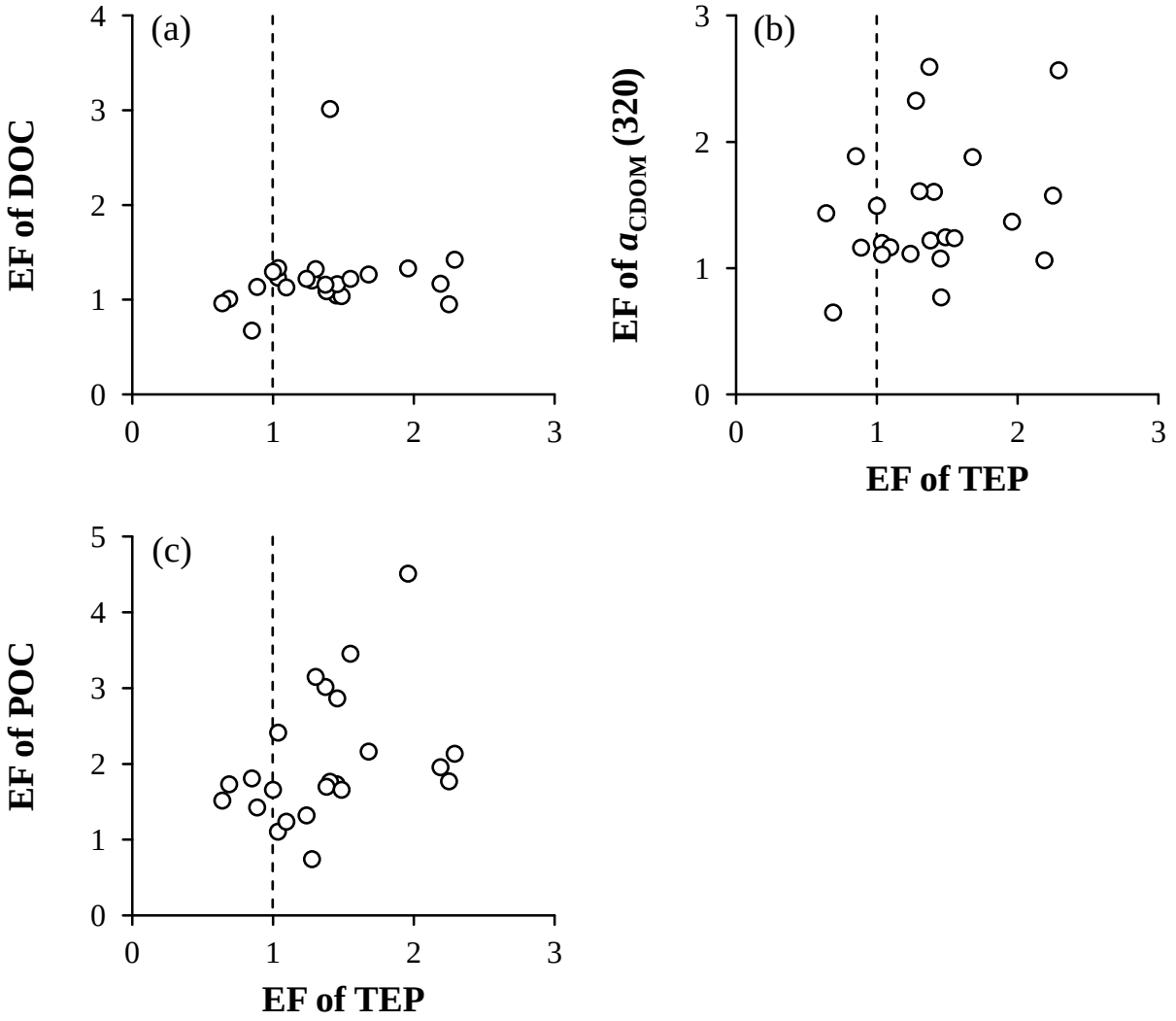

Fig. 2-12. Relationships between the enrichment factors (EF) of transparent exopolymer particles (TEP) and (a) dissolved organic carbon (DOC), (b) the absorption coefficient of chromophoric dissolved organic matter at 320 nm (a_{CDOM} [320]), and (c) particulate organic carbon (POC) during the study period except in April 2014 and May 2015. Dashed lines indicate EF of TEP = 1

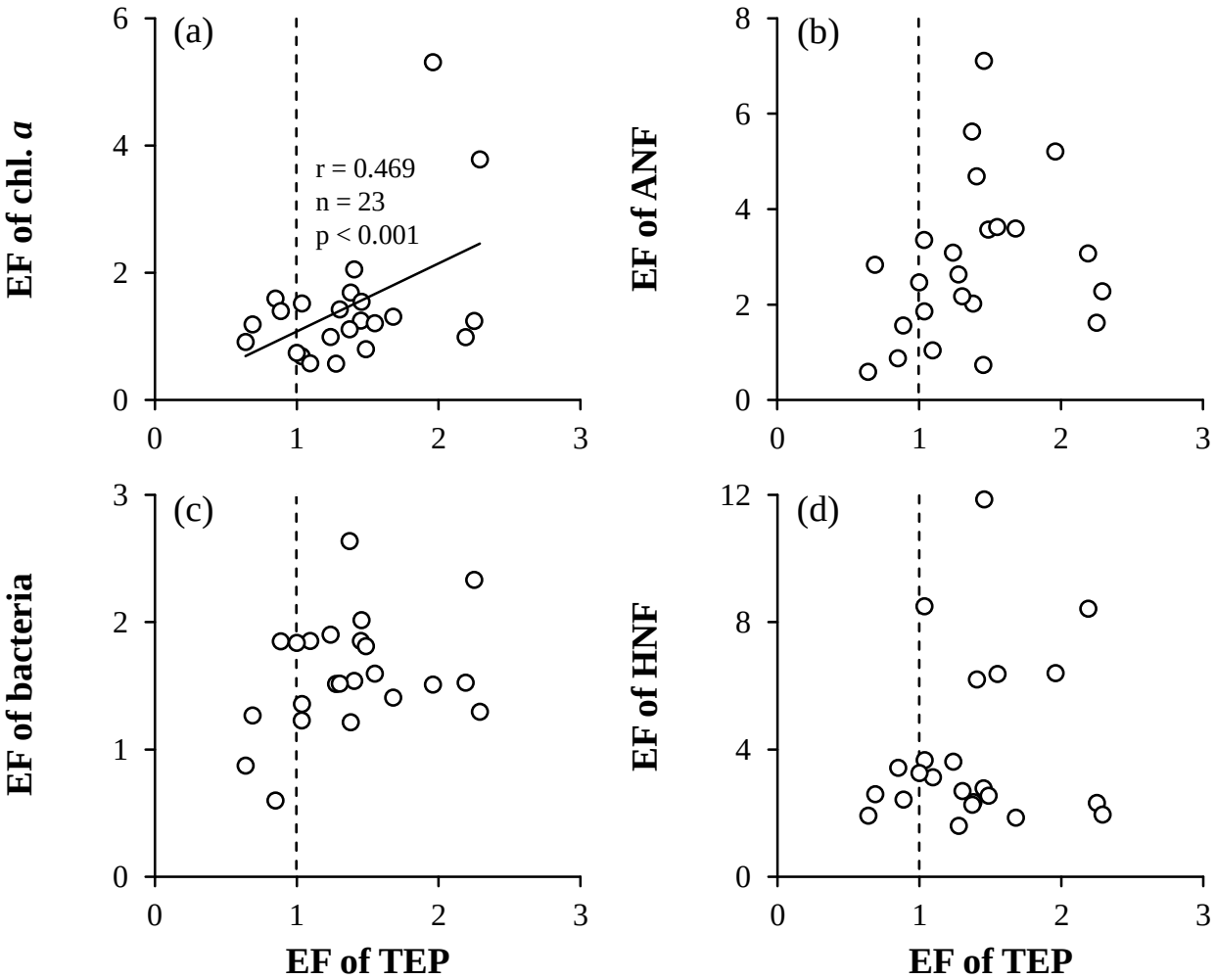

Fig. 2-13. Relationships between the enrichment factors (EF) of transparent exopolymer particles (TEP) and (a) chlorophyll (chl.) *a*, (b) autotrophic nanoflagellates (ANF), (c) bacteria, and (d) heterotrophic nanoflagellates (HNF) during the study period except in April 2014 and May 2015. Dashed lines indicate EF of TEP = 1 (Sugai et al. 2018)

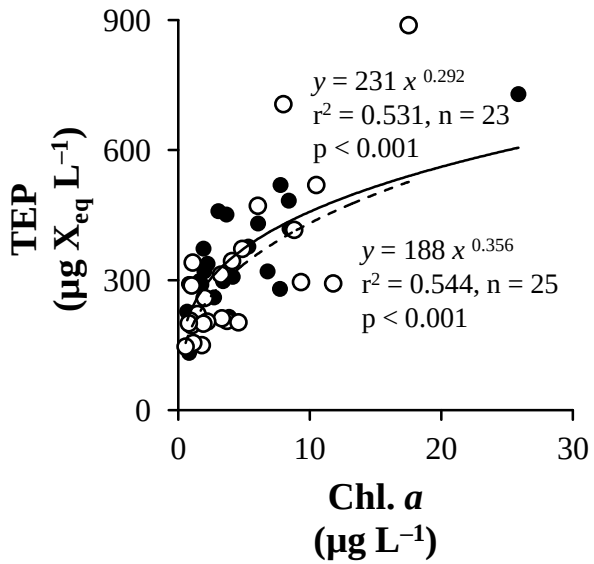

Fig. 2-14. Relationships between chlorophyll (chl.) *a* and transparent exopolymer particles (TEP) in the surface microlayer during the study period except in April 2014 and May 2015 (closed circles, solid line) and subsurface water during the study period (open circles, dashed line) (Sugai et al. 2018)

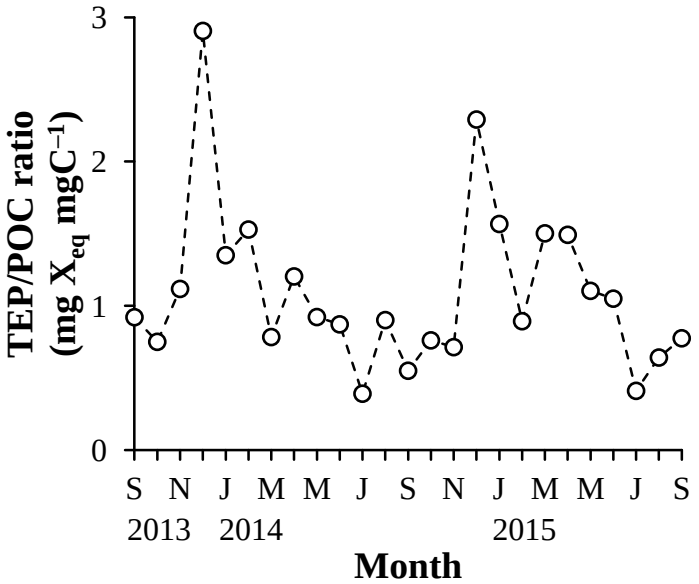

Fig. 2-15. Monthly variations in the ratio of transparent exopolymer particles to particulate organic carbon (TEP/POC ratio) in the subsurface water

Chapter 3

Carbon Monoxide (CO) Production and Consumption in SML and Emission to the Atmosphere

3.1. Introduction

Interestingly, in temperate coastal waters, CDOM was significantly enriched in the SML exposed to the most intense solar radiation (Fig. 2-3b), which suggests active photochemical reactions in the SML by the photodegradation of CDOM. Significant enrichment of bacteria in the SML was also observed (Fig. 2-6a), suggesting active biochemical reactions in the SML by bacteria. Based on these results, CO was expected to be most actively produced and consumed in the SML among GHGs.

In the troposphere, CO is one of the dominant sinks of hydroxyl radical, a reactive oxygen species with high oxidative capacity, and largely contributes to radiative forcing as an indirect GHG through the change of the concentrations of GHGs including CH_4, halocarbons, and ozone (Logan et al. 1981; Thompson & Cicerone 1986; Crutzen & Zimmermann 1991; Thompson 1992). Sea-air CO flux (F) ranges over two orders of magnitude due to large temporal and spatial variations in wind speed and CO concentration ([CO]) in the ocean and is estimated to be 3.7–600 Tg CO $year^{-1}$, which is equivalent to 0.30–77.9% of the total CO emission (770–1230 Tg CO $year^{-1}$) (Bates et al. 1995; Ehhalt & Prather 2001; Stubbins et al. 2006a; Yang et al. 2011). In addition to photochemical production and biological consumption, CO is also lost by emission to the atmosphere in surface waters (Conrad et al. 1982; Zafiriou et al. 2003). Although more intense solar radiation and the enrichment of CDOM and bacteria suggest more active CO production and consumption in the SML than in the SSW, which potentially changes apparent k_w and subsequently F, CO production and consumption rates in the SML have not been investigated. Therefore, Chapter 3 aimed to investigate the seasonal variations in the photochemical production and biological consumption

rates of CO in the SML and evaluate the significance of CO production and consumption in the SML in air-sea CO exchange by comparing them with emission to the atmosphere. Further, the changes in CO production and consumption rates in the SML by the increase in water temperature were assessed to clarify feedback on global warming.

3. 2. Materials and Methods

3.2.1. Study area and samplings

This study was conducted monthly from June 2017 to June 2018 at St. M in coastal waters of Sagami Bay, Japan (Fig. 1-2). The details of the study area and samplings are described in Chapter 2. Briefly, surveys were carried out on the R/V “Tachibana” of the MMCER, Yokohama National University. Surface seawater was collected using a bucket, and water temperature and salinity were measured with a mercury thermometer and an inductive salinometer (601 Mk IV, Yeo-Kal Electronics), respectively. The data of wind speed at 10 m height in Odawara (35°16’36” N, 139°09’18” E) located less than 15 km away from St. M were obtained from Japan Meteorological Agency (2018). Solar irradiance was recorded every hour during the study period with a pyranometer sensor (LI-200SA, LI-COR) placed on the roof of the MMCER located less than 2 km away from St. M.

SML samples were collected from 9 a.m. to 11 a.m. (LT) in a 2-L polypropylene bottle using a nylon mesh screen (nylon diameter: 430 μm, mesh size: 1.25 mm) at the bow of the research vessel on the leeward side (Garrett 1965; Agogué et al. 2004; Momzikoff et al. 2004). Compared to a glass plate, SML samples collected by a mesh screen have a smaller unavoidable CO loss during samplings and a smaller variation in the thickness of the SML (Yang et al. 2001). The nylon mesh screen collected 380 ± 9 μm of the SML. Immediately after the 2-L bottle was filled, seawater was gently transferred to 50-mL glass tubes with glass stopcocks at both ends and 200-mL quartz bottles using a Teflon tube. SSW samples were taken at 0.5 m depth using a horizontal

Niskin bottle, and seawater was collected in a 5-L polypropylene bottle and gently drawn to the glass tubes and quartz bottles. Caution was taken to expose all materials such as the glass tubes and quartz bottles to a minimum amount of light in all procedures, and the glass tubes and quartz bottles were confirmed not to contain air bubbles after threefold volume of overflow. Seawater samples were brought back to a laboratory within 1 h.

After $HgCl_2$ solution (0.5 mM final concentration) was added, the glass tubes were stored at 4°C under the dark condition for a few days until analysis (Ohta et al. 2000; Nakagawa et al. 2004). The quartz bottles were used for incubation experiments to estimate the photochemical production and biological consumption rates of CO. For photochemical CO production rate, after $HgCl_2$ solution (0.5 mM final concentration) was added to stop bacterial activity, the quartz bottles were incubated for 2–8 h under the *in situ* water temperature and light conditions. Seawater in the quartz bottles was gently drawn to the glass tubes using a Teflon tube and preserved as described above. For biological CO consumption rate, the quartz bottles were incubated for 4–12 h under the *in situ* water temperature and dark light conditions without the addition of $HgCl_2$ solution (e.g. Xie et al. 2005). Seawater in the quartz bottles was gently drawn to the glass tubes and stored as described above after the addition of $HgCl_2$ solution (0.5 mM final concentration).

3.2.2. Seawater warming experiments

During autumn (November 2017), winter (February 2018), spring (May 2018), and summer (August 2018), SML samples were collected in coastal waters of Sagami Bay, Japan. To evaluate the effect of water temperature increase on CO production and consumption at the ocean surface, CO production and consumption rates in the SML were estimated as described above except for the conditions of water temperature. The quarts bottles were incubated at 3°C higher (21.3°C, 18.5°C, 23.5°C, and 31.4°C, respectively) (the + 3°C condition) and the *in situ* water temperature (18.3°C, 15.5°C, 20.5°C, and 28.4°C, respectively) (the control condition) during

autumn, winter, spring, and summer since the increase in global mean sea surface temperature by more than 3°C is estimated at the end of the 21st century relative to 1986–2005 in the RCP 8.5 scenario (Kirtman & Power 2013).

3.2.3. Analytical methods

The details of the analyses of CDOM, chl. *a*, and bacteria are described in Chapter 2. Briefly, for the analysis of CDOM, seawater was filtered through 0.22-μm pore size filters (Millex-GV, Merck) under the dark condition. Spectral absorbance from 250 to 850 nm was measured using a single-beam UV-visible spectrophotometer (UV-2450, Shimadzu) with 10-cm pathlength quartz cells referenced against Milli-Q water. $a_{\mathrm{CDOM}}(\lambda)$ was determined by

$$a_{\mathrm{CDOM}}(\lambda) = 2.303\, D(\lambda)\, l^{-1}$$

where $D(\lambda)$ and l are absorbance at wavelength λ and the pathlength of quartz cells, respectively. For the analysis of chl. *a*, seawater was filtered using Whatman GF/F filters (GE Healthcare Life Sciences), and chl. *a* pigment on the filters was extracted with *N*,*N*-dimethylformamide (Suzuki & Ishimaru 1990). Chl. *a* concentration was measured using a fluorometer (10AU, Turner Designs) (Welschmeyer 1994). For the analysis of bacteria, seawater was fixed with the buffered and pre-filtered (< 0.22 μm) formalin (2% final concentration) and stained with a nucleic acid stain (SYBR Gold, Invitrogen) (Shibata et al. 2006). At least 400 cells filtered on each 0.2-μm pore size polycarbonate filter (Nuclepore Track-Etch Membrane Black, GE Healthcare Life Sciences) were counted using an epifluorescence microscope (Axioskop 2 plus, Zeiss).

[CO] was measured by headspace analysis (Xie et al. 2002) and GC-FID analysis (Ohta 1997; Ohta et al. 2000). Seawater of about 6 mL in 50-mL glass tubes with glass stopcocks at both ends was replaced by air, and the glass tubes were vigorously shaken for 3 min using a vortex mixer and kept standing for 5 min to complete the equilibrium between [CO] in headspace air and seawater in the glass tubes. The equilibrated headspace air of 2 mL was injected into a gas

chromatograph (G-3000, Hitachi) fitted with a chromato-integrator (D-2500, Hitachi) using a gastight glass syringe. CO was separated by Molecular Sieve 13X-S (60/80 mesh) (GL Sciences) heated at 40°C in a stainless column (inside diameter: 2.2 mm, length: 1 m), reduced to CH_4 by a methanizer (MT221, GL Sciences) heated at 320°C, and detected by a flame ionization detector at career gas (G1-grade He, Taiyo Nippon Sanso) flow rate of 35 mL min^{-1}. A standard CO gas was obtained from Taiyo Nippon Sanso.

3.2.4. Calculations

According to Xie et al. (2002), [CO] in natural seawater was calculated based on CO mass balance in the glass tubes before and after equilibrium using [CO] in the equilibrated headspace air, the Bunsen solubility coefficient of CO, which is a function of water temperature and salinity (Wiesenburg & Guinasso 1979), and the volume of headspace air and seawater in the glass tubes.

Photochemical CO production rate was determined by dividing the difference between [CO] in seawater in quartz bottles before and after incubation experiments by incubation period. Because [CO] in natural seawater does not usually exceed half-saturation concentration, biological CO consumption was evaluated by first-order kinetics using the following equation unless it is assessed by the ^{14}C-CO method (Johnson & Bates 1996; Zafiriou et al. 2003; Xie et al. 2005), which often causes too high [CO] in seawater (zero-order kinetics) (Jones 1991; Jones & Amador 1993):

$$[CO]_t = [CO]_0 \, e^{-k_{CO} t}$$

where $[CO]_t$ and $[CO]_0$ are [CO] at time t and 0, respectively, and k_{CO} is biological CO consumption rate constant.

Instantaneous F was calculated by

$$F = k_w (C_{sw} - C_{eq})$$

where C_{sw} and C_{eq} are [CO] in the SSW and seawater equilibrated with the atmospheric [CO],

respectively. In this study, the atmospheric [CO] of 117 ppbv, the common atmospheric [CO] in the Japanese coastal areas under the influence of urban air (Ohta et al. 2000), was used. Apparent k_w was estimated the quadratic polynomial, wind-driven turbulent diffusion model (Nightingale et al. 2000):

$$k_w = (0.333\ u + 0.222\ u^2)\ (Sc_{CO} / 660)^{-0.5}$$

where u is wind speed 10 m above the ocean surface and Sc_{CO} is the Schmidt number of CO determined by

$$Sc_{CO} = -0.0553\ T^3 + 4.38\ T^2 - 140\ T + 2134$$

where T is water temperature (Zafiriou et al. 2008).

The turnover time of the photochemical production (τ_{prod}), biological consumption (τ_{cons}), and emission to the atmosphere ($\tau_{sea\text{-}air}$) of CO in the SML was calculated by the following equations (Zhou & Mopper 1997; Yang et al. 2001; Yang & Tsunogai 2005; Yang et al. 2005):

$$\tau_{prod} = \text{[CO] in the SML / photochemical CO production rate in the SML}$$

$$\tau_{cons} = 1 / k_{CO} \text{ in the SML}$$

$$\tau_{sea\text{-}air} = \text{[CO] in the SML} \times \text{SML thickness (380 μm)} / F$$

3.2.5. Data analysis

Paired *t*-test was conducted using the monthly means of each parameter in the SML and SSW, and correlation analysis was performed using a Pearson's correlation coefficient. Probability less than 0.05 ($p < 0.05$) was considered significant in all statistical analyses.

3.3. Results

3.3.1. Environmental factors and CO concentration

Surface water temperature increased from 21.7°C in June 2017 to 26.1°C in August and gradually decreased until February (13.6°C) (Fig. 3-1a). After that, water temperature increased

again to 22.0°C in June 2018. Surface salinity was relatively high (> 33.6) during the study period expect in August (32.4) and October (30.1) (Fig. 3-1b). Mean wind speed during samplings was relatively low in August (1.1 m s^{-1}), October (1.9 m s^{-1}), November (1.4 m s^{-1}), and January (1.7 m s^{-1}) and relatively high in April (4.1 m s^{-1}) (Fig. 3-1c). The integrated solar irradiance during the incubation period ranged from 0.11 kW m^{-2} in September to 2.58 kW m^{-2} in March (Fig. 3-1d).

a_{CDOM} (320) was relatively high in June 2017 (1.48 m^{-1}), August (1.22 m^{-1}), and September (0.84 m^{-1}) in the SML and in June 2017 (0.63 m^{-1}), and August (0.61 m^{-1}) in the SSW (Fig. 3-2a). a_{CDOM} (320) in the SML (0.69 ± 0.38 m^{-1}) showed significantly higher values compared to the SSW (0.39 ± 0.15 m^{-1}) from spring to autumn (June 2017–November and March–June 2018) ($p < 0.01$). During winter (from December to February), no significant difference was observed between a_{CDOM} (320) in the SML (0.16 ± 0.09 m^{-1}) and SSW (0.19 ± 0.05 m^{-1}) ($p = 0.63$). Chl. *a* concentration was particularly high in June 2017 (43.4 µg L^{-1}) and relatively high in August (6.41 µg L^{-1}) in the SML and relatively high in August (2.78 µg L^{-1}) in the SSW (Fig. 3-2b). During the study period except in June 2017, chl. *a* concentration in the SML (1.59 ± 1.70 µg L^{-1}) was not significantly different compared to the SSW (1.20 ± 0.83 µg L^{-1}) ($p = 0.25$). Bacterial abundance was relatively high both in the SML and SSW in August (6.39×10^9 cells L^{-1} and 5.71×10^9 cells L^{-1}, respectively) and June 2018 (6.22×10^9 cells L^{-1} and 7.61×10^9 cells L^{-1}, respectively) (Fig. 3-2c). Bacterial abundance in the SML ($2.78 \pm 1.98 \times 10^9$ cells L^{-1}) and SSW ($2.27 \pm 2.11 \times 10^9$ cells L^{-1}) showed no significant difference during the study period ($p = 0.07$).

[CO] was particularly high in June 2017 (15.0 nM) in the SML and in June 2017 (7.70 nM) and April (9.98 nM) in the SSW (Fig. 3-2d). No significant difference was observed between [CO] in the SML (3.53 ± 3.61 nM) and SSW (3.59 ± 2.63 nM) during the study period ($p = 0.95$).

3.3.2. CO production, consumption, and emission to atmosphere

Photochemical CO production rate normalized by the integrated solar irradiance during the

incubation period was relatively high both in the SML and SSW in June 2017 (10.5 nM [kWh $m^{-2}]^{-1}$ and 2.22 nM [kWh $m^{-2}]^{-1}$, respectively), August (7.58 nM [kWh $m^{-2}]^{-1}$ and 2.14 nM [kWh $m^{-2}]^{-1}$, respectively), and October (5.51 nM [kWh $m^{-2}]^{-1}$ and 1.98 nM [kWh $m^{-2}]^{-1}$, respectively) (Fig. 3-3a). From spring to autumn (June 2017–November and March–June 2018), the light-normalized CO production rate in the SML (3.85 ± 3.09 nM [kWh $m^{-2}]^{-1}$) was significantly higher compared to the SSW (1.22 ± 0.65 nM [kWh $m^{-2}]^{-1}$) ($p < 0.01$). On the other hand, no significant difference was observed between the light-normalized CO production rate in the SML (0.84 ± 0.31 nM [kWh $m^{-2}]^{-1}$) and SSW (0.65 ± 0.60 nM [kWh $m^{-2}]^{-1}$) during winter (from December to February) ($p = 0.41$). k_{CO} was relatively high both in the SML and SSW from spring to autumn (June 2017–November and May–June 2018) (Fig. 3-3b). During the period, k_{CO} in the SML (0.060 ± 0.010 h^{-1}) was significantly lower compared to the SSW (0.074 ± 0.016 h^{-1}) ($p < 0.05$). In contrast, k_{CO} was significantly higher in the SML (0.049 ± 0.015 h^{-1}) than in the SSW (0.025 ± 0.013 h^{-1}) from winter to spring (from December to April) ($p < 0.05$).

Apparent k_w ranged from 0.53 cm h^{-1} in August to 5.81 cm h^{-1} in April (2.72 ± 1.46 cm h^{-1}). *F* varied over two orders of magnitude from 8.55 nmol m^{-2} h^{-1} to 574 nmol m^{-2} h^{-1} (116 ± 152 nmol m^{-2} h^{-1}) with relatively high values in June 2017 (256 nmol m^{-2} h^{-1}) and April (574 nmol m^{-2} h^{-1}) (Fig. 3-4).

3.3.3. Relationships between parameters

During the study period except in June 2017, the EF of [CO] (*y*) showed a significant negative relationship with [CO] in the SSW (*x*) ($y = 1.74\ e^{-0.213\,x}$, $r^2 = 0.373$, $n = 12$, $p < 0.05$) (Fig. 3-5) although no significant relationship was observed with surface water temperature ($p = 0.76$), surface salinity ($p = 0.68$), and mean wind speed during samplings ($p = 0.16$). *F* was significantly positively correlated with [CO] in the SSW ($r = 0.925$, $n = 13$, $p < 0.001$) rather than apparent k_w ($r = 0.767$, $n = 13$, $p < 0.01$).

The light-normalized CO production rate (y) showed significant positive correlations with a_{CDOM} (320) (x) both in the SML (y = 6.60 x – 0.58, r^2 = 0.801, n = 13, $p < 0.001$) and SSW (y = 2.99 x + 0.06, r^2 = 0.514, n = 13, $p < 0.01$) (Fig. 3-6a). Significant positive correlations were observed between surface water temperature (x) and k_{CO} (y) both in the SML (y = 0.0018 x + 0.0209, r^2 = 0.298, n = 13, $p < 0.05$) and SSW (y = 0.0061 x – 0.0662, r^2 = 0.726, n = 13, $p < 0.001$) (Fig. 3-6b).

3.3.4. Turnover in SML

τ_{prod} was relatively low in July (0.65 h), August (0.36 h), and May (0.52 h) (Table 3-1). τ_{cons} ranged from 13.5 h in August to 27.8 h in April and was higher compared to τ_{prod} during the study period. Relatively high $\tau_{sea\text{-}air}$ was observed in August (0.079 h) and January (0.068 h). The ratio of $\tau_{sea\text{-}air}$ to τ_{prod} ($\tau_{sea\text{-}air}/\tau_{prod}$ ratio) was low (< 3.03%) during the study period except in August (21.9%). During the study period, τ_{cons} was much higher compared to $\tau_{sea\text{-}air}$, and the ratio of $\tau_{sea\text{-}air}$ to τ_{cons} ($\tau_{sea\text{-}air}/\tau_{cons}$ ratio) was low (< 0.58%).

3.3.5. Seawater warming experiments

The light-normalized CO production rate of the + 3°C and control conditions did not show difference throughout the year (Fig. 3-7a). On the other hand, k_{CO} was higher under the + 3°C condition compared to the control condition during autumn, winter, and spring although no difference was observed during summer (Fig. 3-7b). However, even under the + 3°C condition, τ_{cons} (27.8–55.6 h) was much higher compared to $\tau_{sea\text{-}air}$ (0.002–0.017 h), and $\tau_{sea\text{-}air}/\tau_{cons}$ ratio was low (< 0.047%) (Table 3-2).

3.4. Discussion

3.4.1. Photochemical CO production

Photochemical CO production rate normalized by the integrated solar irradiance during the incubation period was significantly positively correlated with a_{CDOM} (320) both in the SML and SSW (Fig. 3-6a). This result indicates that photochemical CO production was mainly regulated by light intensity and CDOM absorbance. Previous studies showed a significant relationship between a_{CDOM} and the apparent quantum yield of photochemical CO production (the ratio of the number of CO produced to that of photons absorbed at a given wavelength), which suggests that a_{CDOM} can be used as an indicator of CDOM photoreactivity (Stubbins 2001; Stubbins et al. 2006b; Zhang et al. 2006; Xie et al. 2009).

Because a_{CDOM} (320) in the SML was significantly higher compared to the SSW from spring to autumn (Fig. 3-2a), one reason for significantly higher light-normalized CO production rate in the SML than in the SSW during the period (Fig. 3-3a) was probably significantly higher concentration of CDOM in the SML. Kieber et al. (1990) reported that the photoproduction of carbonyl compounds was proportional to the concentration of dissolved organic matter. Further, the slopes of significant positive relationships between a_{CDOM} (320) and the light-normalized CO production rate in the SML and SSW were different, and higher slope was observed in the SML (6.60) than in the SSW (2.99) (Fig. 3-6a). This result indicates that another reason was higher photochemical degradability of CDOM in the SML under more intense light condition. Previous studies showed the dependence of photochemical CO production by the photodegradation of CDOM on light wavelength and the exponential decrease in the efficiency of CO production with increasing wavelength (Zafiriou et al. 2003; Ziolkowski & Miller 2007; Kitidis et al. 2011; Stubbins et al. 2011). For example, photochemical CO production occurs efficiently at 280–320 nm in lakes and rivers (Valentine & Zepp 1993), at 300–365 nm in the Pacific and Southern Ocean (Zafiriou et al. 2003), and at 310–340 nm in the Pacific Ocean (Kettle 1994). In the water column, the different

wavelength of solar radiation penetrates differently, and UV radiation attenuates much more rapidly with depth compared to visible radiation. For example, Plane et al. (1997) estimated that only 40% of UV radiation at 310 nm reaches 1 m depth although 99% of visible radiation at 500 nm penetrates through 1 m depth in productive waters. These results suggest that photochemical CO production is the most active in the SML among marine environments as reported for the photoproduction of LMW carbonyl compounds (aldehydes and ketones) (Zhou & Mopper 1997). They showed up to 24.5 times higher production rate of glyoxylic acids in the SML than in the SSW of coastal Hatchet Bay, Bahamas and Biscayne Bay, USA.

a_{CDOM} (320) (y) showed significant positive relationships with not salinity ($p = 0.28$ and $p = 0.24$, respectively) but chl. *a* concentration (x) in the SML ($y = 0.271 \ln [x] + 0.477$, $r^2 = 0.848$, $n = 13$, $p < 0.001$) and SSW ($y = 0.143 x + 0.165$, $r^2 = 0.545$, $n = 13$, $p < 0.01$) (Fig. 3-8) as reported by previous studies (Nelson et al. 1998; Nelson et al. 2004; Sasaki et al. 2005). This result indicates that CDOM was mainly supplied from autochthonous phytoplankton, not allochthonous terrestrial source in the study area. The difference between the relationships in the SML and SSW was probably due to more rapid removal of CDOM in the SML under more intense light condition.

3.4.2. Biological CO consumption

k_{CO} in the SML was significantly higher from winter to spring but significantly lower from spring to autumn compared to the SSW (Fig. 3-3b). Tolli & Taylor (2005) estimated k_{CO} in Sargasso Sea during spring–summer by incubating seawater both under the light and dark conditions using the ^{14}C-CO method. They showed significantly lower k_{CO} when seawater was incubated under the light condition, which indicates the inhibitory effect of solar radiation on the activity of CO-oxidizing bacteria. Thus, significantly lower k_{CO} in the SML from spring to autumn in the present study was probably due to the photoinhibition of the activity of CO-oxidizing bacteria under relatively strong light condition during the period. From winter to spring, the photoinhibitory effect

in the SML may have been alleviated under relatively weak light condition.

k_{CO} showed significant positive correlations with surface water temperature both in the SML and SSW (Fig. 3-6b). This result indicates that the activity of CO-oxidizing bacteria was mainly regulated by water temperature. Less active CO consumption by bacteria at lower water temperature was also reported by previous studies (Zafiriou et al. 2003; Xie et al. 2005). However, the slopes of the relationships in the SML (0.0018) and SSW (0.0061) were different. Cunliffe et al. (2008), who analyzed the community structure of CO-oxidizing bacteria in the coastal North Sea using a functional gene which encodes CO dehydrogenase (*coxL*), found totally different community structure in the SML and SSW. Thus, the difference between the slopes in the SML and SSW was possibly due to different community structure of CO-oxidizing bacteria.

3.4.3. CO concentration and emission to atmosphere

In surface waters, [CO] generally shows a clear diurnal variation, which is caused by the imbalance between the photochemical production (source) and biological consumption (sink) of CO (Conrad et al. 1982; Johnson & Bates 1996; Ohta 1997; Yang et al. 2011). Previous studies reported that the lowest [CO] is observed before dawn due to biological consumption during the night whereas [CO] is the highest in the early afternoon because photochemical production exceeds biological consumption in the morning in surface seawater. The two processes are in balance in the early afternoon, and then biological consumption overtakes photochemical production. Thus, sampling time must be taken into account to discuss [CO] in surface waters. In the present study, samplings were conducted from 9 a.m. to 11 a.m. (LT), which may result in relatively high [CO]. Further, the diurnal variation in [CO] was probably larger in the SML than in the SSW as reported for the concentrations of LMW carbonyl compounds (Zhou & Mopper 1997).

Gases dissolved in the SML are inevitably lost during samplings. For example, for dimethylsulfide (DMS), a volatile gas with large concentration difference between the atmosphere

and the ocean, laboratory experiments and the *in situ* field investigation showed about 50–70% of loss from SML samples collected using a mesh screen (Yang et al. 2001; Yang & Tsunogai 2005). Brooks et al. (2009) showed that 89% of sulfur hexafluoride, an inert tracer, in the SML was lost by samplings using a mesh screen. However, in June 2017, [CO] in the SML was much higher (15.0 nM), which was equivalent to 16,650% supersaturation, compared to the other months (2.58 ± 1.14 nM during the study period except in June 2017) despite possible CO loss during samplings (Fig. 3-2d). Previous studies reported that organic film in the SML formed by the accumulation of surfactants largely suppressed air-sea gas exchange by acting as a physical barrier and changing turbulent energy transfer in surface waters. For example, air-sea oxygen exchange experiments in a laboratory which added natural surfactants derived from phytoplankton (Goldman et al. 1988; Frew et al. 1990) and synthetic surfactants (Frew 1997; Bock et al. 1999) to surface seawater showed the decrease in apparent k_w by 5–50% and < 90%, respectively. In the northeast Atlantic Ocean, Salter et al. (2011) released artificial surfactants (oleyl alcohol), and the $^3He/SF_6$-derived apparent k_w decreased in artificially surfactant-covered waters by < 55% and < 5% compared to natural areas at wind speed of < 7.2 m s^{-1} and < 10.7 m s^{-1}, respectively. Interestingly, in June 2017, particularly high concentrations of not only chl. *a* (43.4 μg L^{-1}) (Fig. 3-2b) but also TEPs (2.25 mg X_{eq} L^{-1}) were observed in the SML. These results indicate that the accumulation of organic matter derived from phytoplankton prevented the emission of CO in the SML to the atmosphere and the estimation of apparent k_w and the subsequent calculation of *F* are probably erroneous in June 2017. The suppression of air-sea gas exchange by high concentration of gelatinous particles in the SML was also suggested by Engel & Galgani (2016) and Wurl et al. (2016). The present study suggests that the accumulation of biogenic surfactants in the SML changes apparent k_w and subsequently *F*.

During the study period except in June 2017 when the suppression of air-sea CO exchange is indicated, the EF of [CO] showed a significant negative relationship with [CO] in the SSW (Fig. 3-5). This result indicates that large gradient in air-sea [CO] increases CO loss from SML samples

as reported for DMS by Yang et al. (2001). No significant relationship between surface water temperature, surface salinity, or mean wind speed during samplings and the EF of [CO] may have been because the effect of CO solubility and wind-induced turbulence on CO loss during samplings was masked by that of CO supersaturation in seawater. The insignificant relationship may be because wind speed at the Odawara Office (the Japan Meteorological Agency) and the *in situ* wind speed could be different due to distance between the Odawara Office and sampling station (15 km).

3.4.4. Effect of CO dynamics in SML on air-sea CO exchange

During the study period, τ_{cons} was about three orders of magnitude higher compared to $\tau_{sea\text{-}air}$ with the highest $\tau_{sea\text{-}air}/\tau_{cons}$ ratio of only 0.58% (Table 3-1). This result suggests that biological CO consumption in the SML by CO-oxidizing bacteria is not significant and can be ignored in air-sea CO exchange. Previous studies which investigated the production and consumption rates in the SML and the sea-air flux of DMS in the northwest Pacific Ocean reported much shorter turnover time of sea-air DMS emission (on the order of minutes) than that of DMS consumption (on the order of days) (Yang et al. 2001; Yang & Tsunogai 2005; Yang et al. 2005). Zhou & Mopper (1997) also showed that the turnover time of LMW carbonyl compounds by air-sea exchange (0.20–1.2 min) was much shorter compared to photochemical production (< 1 h). On the other hand, although τ_{prod} and $\tau_{sea\text{-}air}$ were two orders of magnitude different during most of the study period, τ_{prod} (0.36 h) can be relatively comparable to $\tau_{sea\text{-}air}$ (0.079 h) in August with $\tau_{sea\text{-}air}/\tau_{prod}$ ratio of 21.9% (Table 3-1). In August, moderate solar irradiance (205 W m^{-2} h^{-1}) and relatively high a_{CDOM} (320) (1.22 m^{-1}), which was probably due to relatively high chl. *a* concentration (6.41 μg L^{-1}) as supported by a significant positive relationship between chl. *a* concentration and a_{CDOM} (320) in the SML (Fig. 3-8), were observed in addition to relatively low wind speed (1.1 m s^{-1}). These results suggest that photochemical CO production in the SML by the degradation of CDOM is significant in air-sea CO exchange and enhance *F* during summer under intense light, active biological

production, and weak wind conditions. The comparison among τ_{prod}, τ_{cons}, and $\tau_{sea\text{-}air}$ indicates that CO loss by emission to the atmosphere largely dominates over that by biological consumption and that photochemical production only cannot counteract the CO loss to maintain the balance of [CO] in the SML, which suggests the overestimation of *F* and the importance of another source of CO in the SML such as gas transfer from the underlying water.

The present study suggests that photochemical CO production in the SML is active enough to change apparent k_w and subsequently *F*. In this case, the two-layer model cannot be applied to consider CO dynamics in the SML, which requires the reconstruction of air-sea gas exchange model. Cen-Lin & Tzung-May (2013) proposed the three-layer model to explain the difference in the measured and calculated gas fluxes determined according to the two-layer model. They demonstrated that the calculation of the change of acetone concentration in the SML due to chemical and biological reactions there successfully explained the observed acetone flux in the Pacific Ocean. The present study suggests that the three-layer model must be applied during summer to accurately calculate *F*.

Although photochemical CO production in the SML did not show difference throughout the year (Fig. 3-7a), seawater warming experiments indicated the stimulation of biological CO consumption in the SML by the increase in water temperature from spring to autumn (Fig. 3-7b). During summer, the effect of water temperature increase on the activity of CO-oxidizing bacteria in the SML was not observed probably due to high *in situ* water temperature (28.4°C). Because the increase in k_{CO} in the SML decreases *F*, the present study suggests that the warming of seawater leads to negative feedback on global warming in temperate coastal waters from spring to autumn. However, the comparison between τ_{cons} and $\tau_{sea\text{-}air}$ under the + 3°C condition indicates that the negative feedback is not significant (Table 3-2).

Table 3-1. Turnover time of the photochemical production (τ_{prod}), biological consumption (τ_{cons}), and emission to the atmosphere ($\tau_{sea\text{-}air}$) of carbon monoxide and the ratios ($\tau_{sea\text{-}air}/\tau_{prod}$ and $\tau_{sea\text{-}air}/\tau_{cons}$) in the surface microlayer

Month	τ_{prod} **(h)**	τ_{cons} **(h)**	$\tau_{sea\text{-}air}$ **(h)**	$\tau_{sea\text{-}air}/\tau_{prod}$ **(%)**	$\tau_{sea\text{-}air}/\tau_{cons}$ **(%)**
Jun 2017	1.68	15.6	0.022	1.33	0.14
Jul	0.65	15.6	0.007	1.15	0.05
Aug	0.36	13.5	0.079	21.9	0.58
Sep	11.5	15.9	0.013	0.12	0.09
Oct	2.88	14.9	0.037	1.29	0.25
Nov	5.11	23.8	0.022	0.43	0.09
Dec	5.84	27.0	0.010	0.18	0.04
Jan 2018	2.23	14.7	0.068	3.03	0.46
Feb	1.30	23.3	0.009	0.71	0.04
Mar	1.09	16.1	0.014	1.29	0.09
Apr	1.56	27.8	0.003	0.16	0.01
May	0.52	17.5	0.007	1.43	0.04
Jun	1.21	20.8	0.022	1.79	0.10

Table 3-2. Turnover time of the photochemical production (τ_{prod}), biological consumption (τ_{cons}), and emission to the atmosphere ($\tau_{sea\text{-}air}$) of carbon monoxide and the ratios ($\tau_{sea\text{-}air}/\tau_{prod}$ and $\tau_{sea\text{-}air}/\tau_{cons}$) during seawater warming experiments. Surface microlayer samples were incubated at 3°C higher (+ 3°C) and the *in situ* water temperature (control)

Season	Condition	τ_{prod} (h)	τ_{cons} (h)	$\tau_{sea\text{-}air}$ (h)	$\tau_{sea\text{-}air}/\tau_{prod}$ (%)	$\tau_{sea\text{-}air}/\tau_{cons}$ (%)
AUT	+ 3°C	6.24	35.7	0.017	0.27	0.047
	Control	7.94	47.6		0.21	0.035
WTR	+ 3°C	4.51	55.6	0.011	0.25	0.020
	Control	4.52	71.4		0.25	0.016
SPR	+ 3°C	0.81	27.8	0.002	0.28	0.008
	Control	0.86	47.6		0.27	0.005
SMR	+ 3°C	0.28	21.3	0.006	2.26	0.030
	Control	0.27	19.2		2.37	0.033

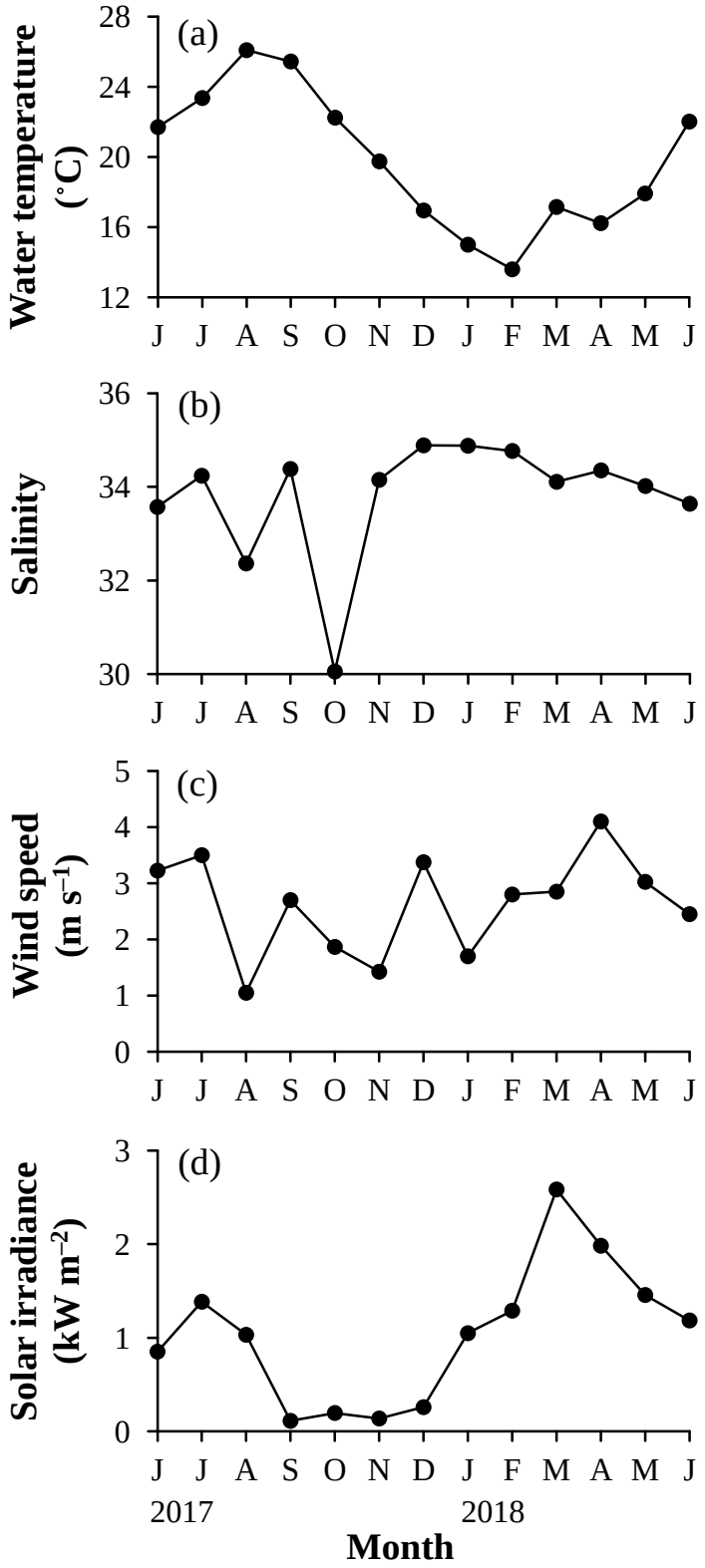

Fig. 3-1. Monthly variations in (a) surface water temperature, (b) surface salinity, (c) mean wind speed during samplings, and (d) the integrated solar irradiance during the incubation period

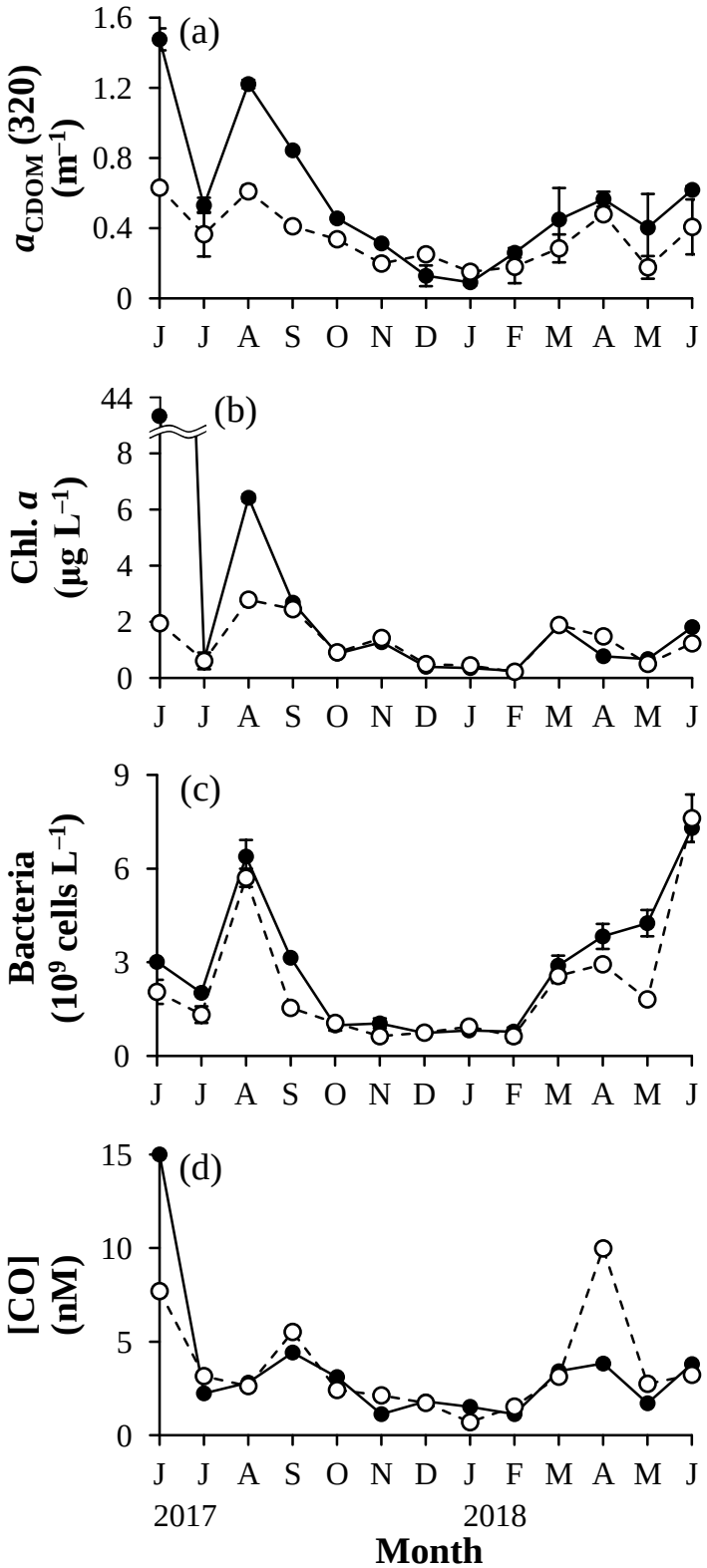

Fig. 3-2. Monthly variations in (a) the absorption coefficient of chromophoric dissolved organic matter at 320 nm (a_{CDOM} [320]), (b) chlorophyll (chl.) *a*, (c) bacteria, and (d) carbon monoxide concentration ([CO]) in the surface microlayer (closed circles) and subsurface water (open circles)

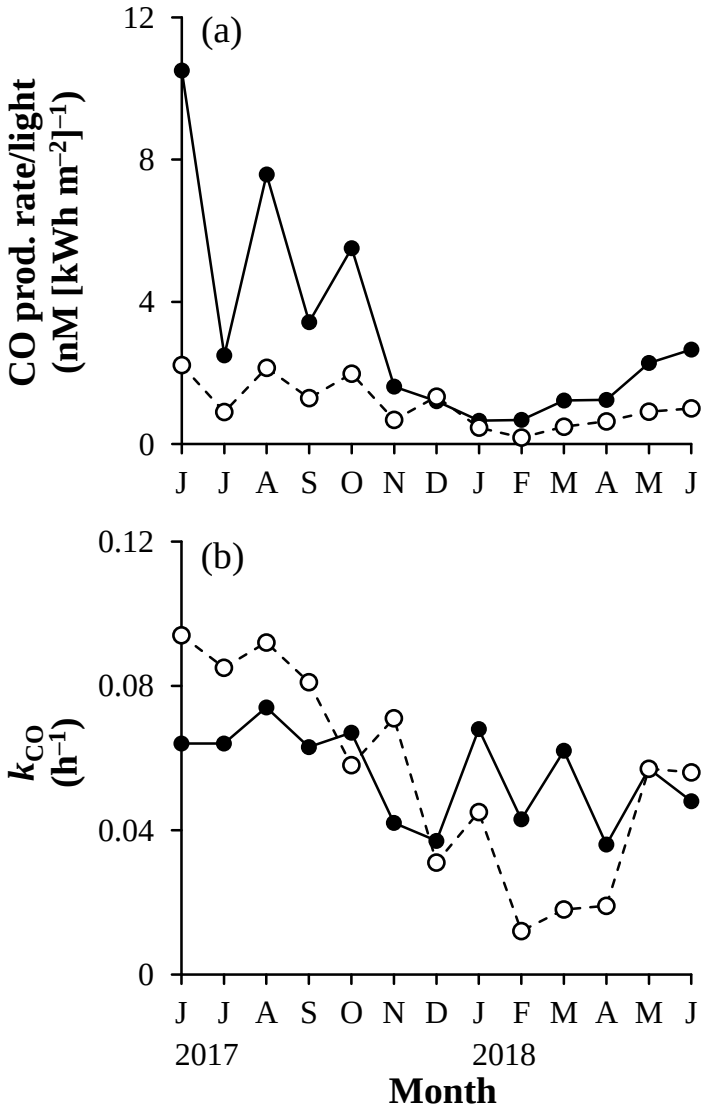

Fig. 3-3. Monthly variations in (a) the photochemical production rate of carbon monoxide (CO) normalized by the integrated solar irradiance during the incubation period (CO prod. rate/light) and (b) biological CO consumption rate constant (k_{CO}) in the surface microlayer (closed circles) and subsurface water (open circles)

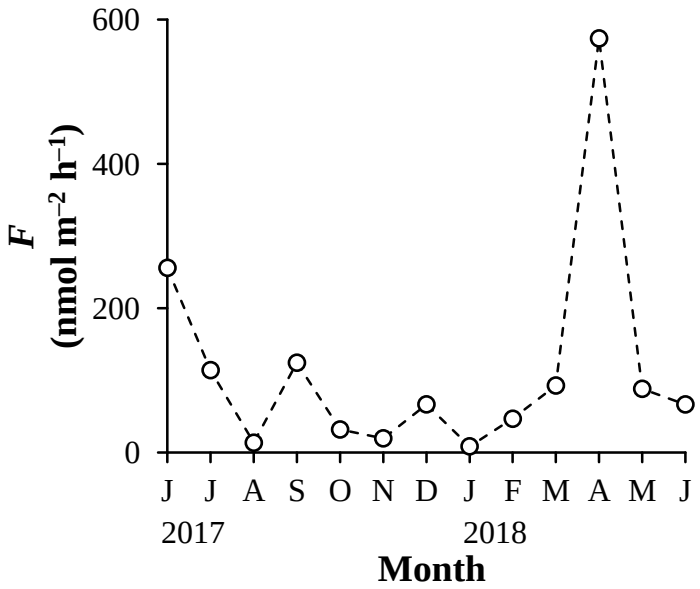

Fig. 3-4. Monthly variation in sea-air carbon monoxide flux (*F*)

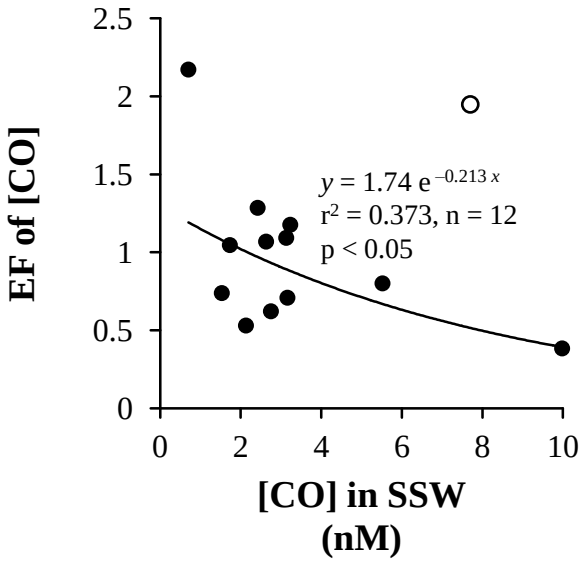

Fig. 3-5. Relationship between carbon monoxide concentration ([CO]) in the subsurface water (SSW) and the enrichment factor (EF) of [CO]. Relationship was examined excluding data in June 2017 (open circle).

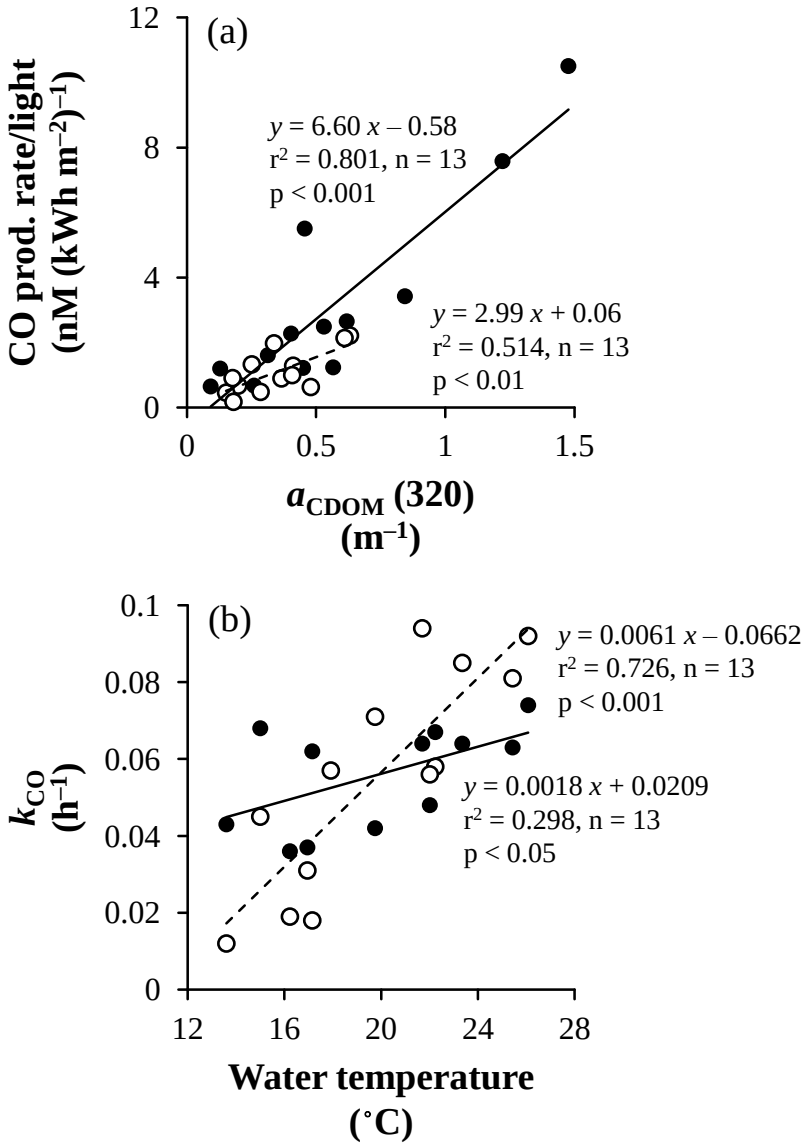

Fig. 3-6. Relationships between (a) the absorption coefficient of chromophoric dissolved organic matter at 320 nm (a_{CDOM} [320]) and the photochemical production rate of carbon monoxide (CO) normalized by the integrated solar irradiance during the incubation period (CO prod. rate/light) and (b) surface water temperature and biological CO consumption rate constant (k_{CO}) in the surface microlayer (closed circles, solid lines) and subsurface water (open circles, dashed lines)

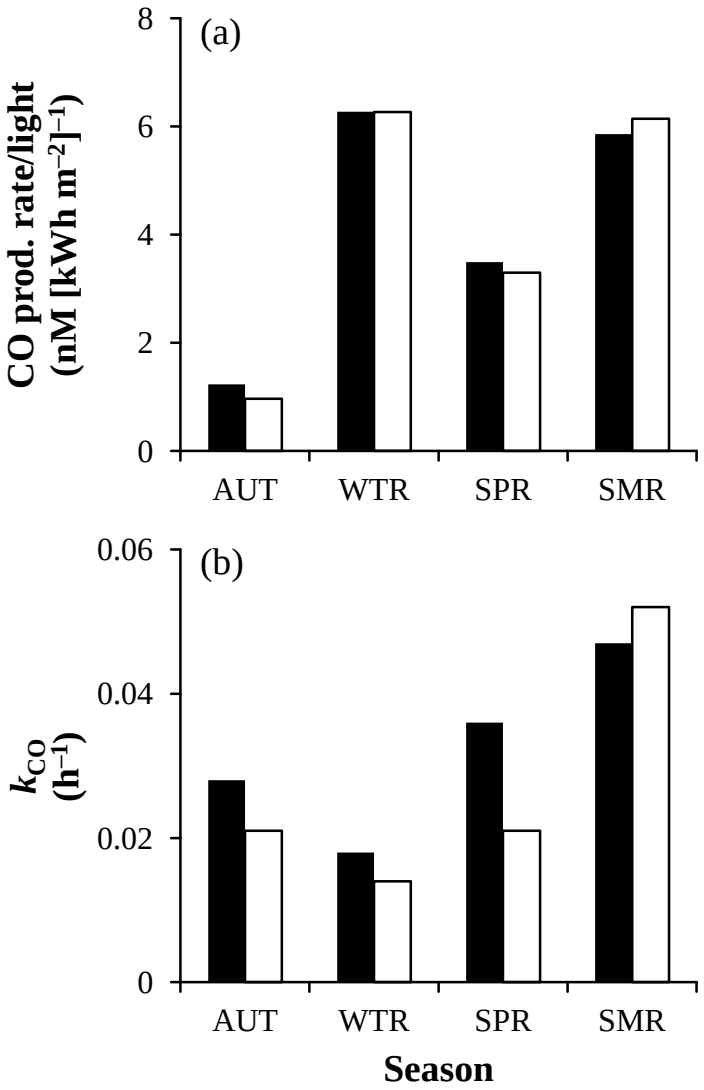

Fig. 3-7. (a) The photochemical production rate of carbon monoxide (CO) normalized by the integrated solar irradiance during the incubation period (CO prod. rate/light) and (b) biological CO consumption rate constant (k_{CO}) during seawater warming experiments at 3˚C higher (closed bars) and the *in situ* water temperature (open bars)

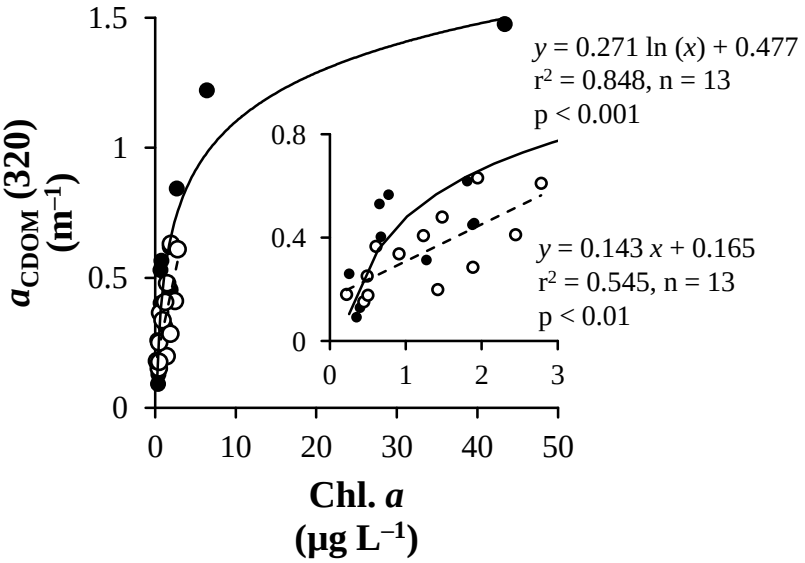

Fig. 3-8. Relationships between chlorophyll (chl.) *a* and the absorption coefficient of chromophoric dissolved organic matter at 320 nm (a_{CDOM} [320]) in the surface microlayer (closed circles, solid lines) and subsurface water (open circles, dashed lines). Inset shows the magnified view.

Chapter 4

General Discussion

4.1. Methodological Concerns in the Study of SML

The SML is considered to be tens to hundreds of μm thick in natural environments (Zhang et al. 1998; Zhang et al. 2003; Carpenter & Nightingale 2015; Engel et al. 2017). The thickness of the SML changes depending on the water temperature and wind conditions and is just operationally defined by SML samplers (Cunliffe et al. 2011). Cunliffe & Wurl (2014) proposed the standard sampling methods of the SML, and mesh screens (Garrett 1965), glass plates (Harvey 1966; Harvey & Burzell 1972), and polycarbonate membrane filters (Crow et al. 1975; Kjelleberg et al. 1979) are currently most used to typically collect 150–400 μm, 20–150 μm, and 40 μm thick ocean surface layers, respectively (Cunliffe et al. 2011) (Table 1-1). SML samplers are selected depending on the aim of a study and the desired volume of seawater because they each have specific advantages and disadvantages. The results of the study of the SML critically depend on sampling methods applied, and the characteristics of SML samples collected by each SML sampler has to be recognized.

In the present study, a mesh screen was used to collect SML samples. First, a mesh screen allows the effective sampling of dissolved and particulate materials with a wide range of sizes to compare different chemical and biological parameters (Agogué et al. 2004; Momzikoff et al. 2004). For example, Agogué et al. (2004) investigated the enrichment of various sizes of microorganisms in the SML ranging from bacteria to ciliates using both a mesh screen and glass plate. They found that the EF of bacterial abundance was similar for SML samples taken by a mesh screen (1.09) and glass plate (1.18) but that of ciliate abundance was significantly lower for SML samples collected by a glass plate (0.29) compared to a mesh screen (0.63). This result indicates that larger microorganisms, especially larger than flagellates, have lower values in the SML and thus EFs but that a mesh screen has much lower size selectivity due to smaller contact area with seawater

compared to a glass plate. The chemical compositions and microbial community structure in SML samples were affected by SML samplers. Further, a mesh screen collects a large volume of SML samples during a short period and considered to be appropriate for studies which examines relationships between multiple parameters and which requires a large amount of samples for analysis. Specifically, a mesh screen reduces CO loss during samplings and the variability in thickness (Yang et al. 2001). DMS loss during the samplings of the SML was smaller for SML samples collected by a mesh screen than by a glass plate. However, a mesh screen collects much thicker SML samples compared to other samplers. In the present study, the calculated thickness of the SML was 380 ± 9 μm and possibly thicker than the thickness of the sea-side thin film in natural environments. Thus, caution must be taken that SML samples may have been diluted by the underlying water during samplings and values in the SML and EFs may have been underestimated.

EFs, which numerically express the extent of enrichment in the SML, have been used in the study of the SML to distinguish the variations in parameters in the SML due to those in the SSW from due to the enrichment or depletion of materials in the SML and to compare the enrichment of different chemical and biological parameters in the SML. In addition to the sampling methods of the SML, the depth of the SSW, usually 0.5–1 m, can also be a concern to interpret values in the SSW and EFs. Traditionally, the measurement of water temperature by buoys has shown that the vertical variation near the ocean surface (0.5–2 m depth) is not significant and typically less than 0.5°C (Emery et al. 2001). Agogué et al. (2004) examined the SSW depth of less than 5 m (0.5 and 5 m depth) and found significant effect on results, and Brooks et al. (2009) showed that the vertical profile of DMS concentration in the upper 2 m of the water column was vertically similar. However, Momzikoff et al. (2004) showed that the surface ocean (0.05–1 m depth) is not necessarily homogeneous. The vertical homogeneity of parameters in the ocean surface depends on the water column structure, and the thermal stratification seasonally plays important roles to interpret values in the SSW and EFs.

Traditionally, the difference between water temperature in the SML and SSW has been reported (Saunders 1967; Soloviev & Schlüssel 1994; Fairall et al. 1996; Wick et al. 1996). The SML temperature, often referred to as the skin sea surface temperature (SST), is defined as water temperature measured by an infrared radiometer. On the other hand, water temperature in the SSW, the bulk SST, is defined as water temperature below the ocean surface measured by ships and buoys. The difference between the skin and bulk SST (ΔT) varies rapidly and depends on wind speed and air-sea heat flux, which mean the renewal and the heating or cooling of the skin, respectively (Emery et al. 2001). In the present study, we measured only the bulk SST using seawater taken from the SSW with a bucket, which does not represent water temperature just at the ocean surface (in the SML). However, because instantaneous ΔT is usually up to 2°C even under intense light and weak wind conditions (Garçon et al. 2014), the bulk SST can be used instead of the skin SST to calculate the Bunsen solubility coefficient of CO and Sc_{CO} in the SML and to incubate SML samples, which does not significantly affect the conclusions of the present study.

4.2. SML in Temperate Coastal Waters

The present study clarified the seasonality of organic matter and microorganisms in the SML of coastal waters of Sagami Bay where the seasonal patterns of physical, chemical, and biological factors are clearly observed in the water column (Sugai et al. 2016). The EFs of organic matter concentration and microbial abundance particularly increased during spring when phytoplankton blooms occurred in the SML (Fig 2-7), which is comparable to EFs reported by Wurl et al. (2011b) and Wurl et al. (2016), which collected SML samples in visible slick areas, and Nakajima et al. (2013), conducted in tropical coral reef waters (Table 1-1). In coastal areas of Sagami Bay, PO_4 is depleted in surface waters throughout the year except during winter when PO_4 is supplied from deeper waters (Sugai et al. 2016), and phytoplankton growth is indicated to be limited by PO_4 unavailability in the surface ocean from spring to summer (Fujiki et al. 2004).

Coastal Sagami Bay occasionally receives the allochthonous input of inorganic nutrients through processes such as freshwater inflow and the atmospheric deposition of aerosols on the ocean surface. The episodic, external supply of PO4 in such areas may result in phytoplankton blooms in the SML and the formation of viscous, stable SML.

Based on results obtained in Chapter 2 and Chapter 3, the possible formation of the stable SML in temperate coastal waters and its implication in air-sea gas exchange can be proposed. In Chapter 2, when phytoplankton blooms in the SML were observed during spring, the increase in the EFs of organic matter concentration and microbial abundance was largely different between April 2014 and May 2015 probably due to the difference in time period from phytoplankton blooms to samplings (Fig. 2-7). In April 2014, the EFs of all chemical and biological parameters particularly increased and were the highest during the study period. On the other hand, although the EFs of DOC concentration (2.89), a_{CDOM} (320) (3.20), TEP concentration (2.99), chl. *a* concentration (3.92), and bacterial abundance (6.95) showed particularly high values enough to be determined as outliers, those of POC concentration (3.09), ANF abundance (4.65), and HNF abundance (4.70) remained moderate in May 2015. If the time lag between the occurrence of phytoplankton blooms in the SML and samplings was longer compared to May 2015, the extent of the development of microbial communities in the SML may have been possibly different between April 2014 and May 2015. Possibly, the blooms of phytoplankton dominated by diatoms caused the extracellular release of dissolved organic matter and TEPs, which results in the formation of the viscous, stable SML. Then, phytoplankton-derived materials stimulated bacterial growth. However, relatively a large amount of time is required for the growth of flagellates and subsequently the increase in POC concentration. This hypothesis is also supported by the results obtained in Chapter 3. In June 2017 when a phytoplankton bloom was observed (Fig. 3-2b), high EF was observed for only a_{CDOM} (320) (2.34) (Fig. 3-2a) and TEP concentration (10.8) and not for bacterial abundance (1.47) (Fig. 3-2c), which indicates that phytoplankton extracellularly release CDOM and TEPs rapidly.

Once viscous, stable SML is formed, active chemical and biological reactions are expected to occur in the SML. In Chapter 3, during a phytoplankton bloom in June 2017, the EF of photochemical CO production rate normalized by the integrated solar irradiance during seawater incubation was the highest (4.74) during the study period (Fig. 3-3a), which potentially increases *F*. However, particularly high [CO] in the SML (15.0) was also observed despite possible CO loss from SML samples during samplings (Fig. 3-2d), which indicates the suppression of air-sea gas exchange and thus the decrease in *F* by the formation of the organic film in the SML due to the accumulation of surfactants. Thus, the formation of the viscous, stable SML causes active chemical and biological reactions which potentially promote air-sea gas exchange but simultaneously forms the organic film which prevents air-sea interactions. Under such a condition, the estimation of apparent k_w and subsequently the calculation *F* can be erroneous.

During the study period except in spring (April 2014 and May 2015), the EF of each chemical and biological parameter was within values reported by previous studies (Table 1-1). This result indicates that the enrichment of organic matter and microorganisms in the SML of temperate coastal waters is similar to that of various oceanic areas from tropical to polar regions and coastal to oceanic waters. Nevertheless, although the enrichment of bacteria in the SML did not cause significant biological CO consumption in air-sea gas exchange (Table 3-1), the enrichment of CDOM in the SML led to high photochemical CO production enough to potentially enhance *F* under intense light and weak wind conditions.

In temperate coastal waters, the enhancement of *F* by photochemical CO production in the SML was probably lower compared to areas where higher solar radiation and CDOM concentration are observed. For example, tropical coastal areas are expected to show active photochemical CO production. Mizubayashi et al. (2013) reported high concentration of CDOM mainly derived from terrestrial water in tropical coral reef waters, especially during monsoon seasons. Further, Nakajima et al. (2013) found particularly high enrichment of organic matter in the SML of high coral

coverage areas although they did not take CDOM samples (Table 1-1), which indicates the contribution of organic matter derived from benthic communities to the formation of the SML. Indeed, photochemical CO production rate was as high as 15.0 nM h^{-1} in the SML of the west coast of Bidong Island, Malaysia in October 2017, which is much higher than that observed in the present study (0.22–8.95 nM h^{-1}). Photochemical CO production in the SML may enhance not only regional but also global *F*, which suggests the reassessment of the relative importance of the ocean as a source of [CO] in the atmosphere.

4.3. Future Studies

Traditionally, gas concentration at some depth in the surface ocean has been usually used as C_{sw}. To re-evaluate air-sea gas flux, the *in situ* gas concentration in the SML should be used as C_{sw} due to the expected significant difference in the SML and SSW. However, the *in situ* gas concentration cannot be measured at present, and the sampling method of the SML which does not allow gas volatilization during samplings has to be developed. Current sampling techniques do not allow the collection of SML samples for the measurement of the *in situ* dissolved gas concentration. The determination of dissolved gas concentration in the SML and subsequently air-sea gas flux requires new sampling techniques which prevent gas volatilization from the SML during samplings. One approach, a cryogenic technique, which samples the SML as an ice layer, was suggested by Turner & Liss (1989), but no significant difference was observed between the DMS concentration of SML samples collected by a mesh screen and a cryogenic technique and the effect of freezing by liquid nitrogen on the chemical compositions and biological activity of SML samples remains an issue. The development of a new SML sampling method without exposure to the atmosphere provides better understanding of gas concentration difference in the atmosphere and ocean.

The SML probably have important roles in the air-sea exchange of other GHGs such as CH_4 and N_2O. The measurement of oxygen using microelectrodes showed that anaerobic

microenvironments exist in particles, especially in biogenic gels, due to low oxygen permeability by gelatinous films and high oxygen consumption rate by bacteria (e.g. Ploug 2008). Indeed, active CH_4 production in the ocean water column was confirmed near the pycnocline where high particle concentration was observed (e.g. Yoshida et al. 2011). In the present study, the most ubiquitous gelatinous particles, TEPs, accumulated in the SML, and the production and consumption processes of CH_4 and N_2O may be active in the anaerobic microenvironments of the SML although it is in contact with the atmosphere. Future studies should investigate the production and consumption rates of CH_4 and N_2O in the SML when the accumulation of gelatinous particles is observed and their effect on the air-sea flux of CH_4 and N_2O.

4.4. Conclusions

This study investigated various organic matter and microorganisms in the SML throughout the year for the first time and the role of their enrichment in the SML in air-sea CO exchange in temperate coastal waters. Organic matter concentration and microbial abundance in the SML showed clear seasonality, and their EFs was particularly high during spring probably due to phytoplankton blooms in the SML induced by the external supply of inorganic nutrients. When a phytoplankton bloom occurred in the SML, particularly high [CO] was observed there, which indicates the suppression of air-sea CO exchange by the accumulation of biogenic surfactants in the SML. Throughout the year, although bacteria were significantly enriched in the SML, biological CO consumption by bacterial activity in the SML can be ignored in air-sea CO exchange. However, significant enrichment of CDOM in the SML can result in active photochemical CO production by the photodegradation of CDOM there enough to promote air-sea CO exchange during summer under intense light and weak wind conditions. These results suggests that, in temperate coastal waters, the accumulation of organic matter in the SML decreases apparent k_w during spring whereas photochemical CO production in the SML increases apparent k_w during summer and that the

three-layer model including the SML must be applied to accurately calculate the sea-air flux of CO.

References

Agogué H, Casamayor EO, Joux F, Obernosterer I, Dupuy C, Lantoine F, Catala P, Weinbauer MG, Reinthaler T, Herndl GJ, Lebaron P (2004) Comparison of samplers for the biological characterization of the sea surface microlayer. *Limnology and Oceanography: Methods*, 2:213−225

Alldredge AL, Passow U, Logan BE (1993) The abundance and significance of a class of large, transparent organic particles in the ocean. *Deep-Sea Research Part I: Oceanographic Research Papers*, 40:1131−1140

Ara K, Yamaki K, Wada K, Fukuyama S, Okutsu T, Nagasaka S, Shiomoto A, Hiromi J (2011) Temporal variability in physicochemical properties, phytoplankton standing crop and primary production for 7 years (2002–2008) in the neritic area of Sagami Bay, Japan. *Journal of Oceanography*, 67:87–111

Archer CL, Jacobson MZ (2005) Evaluation of global wind power. *Journal of Geophysical Research*, 110:D12110

Azetsu-Scott K, Passow U (2004) Ascending marine particles: significance of transparent exopolymer particles (TEP) in the upper ocean. *Limnology and Oceanography*, 49:741−748

Bange HW (2006) New directions: the importance of oceanic nitrous oxide emissions. *Atmospheric Environment*, 40:198–199

Bange HW, Bartell UH, Rapsomanikis S, Andreae MO (1994) Methane in the Baltic and North Seas and a reassessment of the marine emissions of methane. *Global Biogeochemical Cycles*, 8:465–480

Bates TS, Kelly KC, Johnson JE, Gammon RH (1995) Regional and seasonal variations in the flux of oceanic carbon monoxide to the atmosphere. *Journal of Geophysical Research*,

100:23093−23101

Bock EJ, Hara T, Frew NM, McGillis WR (1999) Relationship between air-sea gas transfer and short wind waves. *Journal of Geophysical Research*, 104:25821–25831

Brooks IM, Yelland MJ, Upstill-Goddard RC, Nightingale PD, Archer S, d'Asaro E, Beale R, Beatty C, Blomquist B, Bloom AA, Brooks BJ, Cluderay J, Coles D, Dacey J, DeGrandpre M, Dixon J, Drennan WM, Gabriele J, Goldson L, Hardman-Mountford N, Hill MK, Horn M, Hsueh P, Huebert B, de Leeuw G, Leighton TG, Liddicoat M, Lingard JJN, McNeil C, McQuaid JB, Moat BI, Moore G, Neill C, Norris SJ, O'Doherty S, Pascal RW, Prytherch J, Rebozo M, Sahlee E, Salter M, Schuster U, Skjelvan I, Slagter H, Smith MH, Smith PD, Srokosz M, Stephens JA, Taylor PK, Telszewski M, Walsh R, Ward B, Woolf DK, Young D, Zemmelink H (2009) Physical exchanges at the air–sea interface: UK–SOLAS field measurements. *Bulletin of the American Meteorological Society*, 90:629−644

Buma AGJ, Helbing EW, de Boer MK, Villafañe VE (2001) Patterns of DNA damage and photoinhibition in temperate South-Atlantic picophytoplankton exposed to solar ultraviolet radiation. *Journal of Photochemistry and Photobiology B*, 62:9−18

Carlson DJ (1983) Dissolved organic materials in surface microlayers: temporal and spatial variability and relation to sea state. *Limnology and Oceanography*, 28:415−431

Carlson DJ (1993) The early diagenesis of organic matter: reaction at the air–sea interface. In: Engel MH, Macko SA (eds) *Organic Geochemistry*, Plenum Press, New York, p 255–267

Carlucci AF, Craven DB, Robertson KJ, Williams PM (1986) Surface-film microbial populations: diel amino acid metabolism, carbon utilization, and growth rates. *Marine Biology*, 92:289−297

Carpenter LJ, Nightingale PD (2015) Chemistry and release of gases from the surface ocean. *Chemical Reviews*, 115:4015−4034

Cen-Lin HE, Tzung-May FU (2013) Air-sea exchange of volatile organic compounds: a new model

with microlayer effects. *Atmospheric and Oceanic Science Letters*, 6:97–102

Chin WC, Orellana MV, Verdugo P (1998) Spontaneous assembly of marine dissolved organic matter into polymer gels. *Nature*, 391:568−572

Ciais O, Sabine C (2013) Carbon and other biogeochemical cycles. In: Stocker TF, Qin D, Plattner GK, Tignor M, Allen SK, Boschung J, Nauels A, Xia Y, Bex V, Midgley PM (eds) *Climate Change 2013 the Physical Science Basis: Contribution of Working Group I to the Fifth Assessment Report of the Intergovernmental Panel on Climate Change*, Cambridge University Press, Cambridge, p 465−570

Cicerone RJ, Oremland RS (1988) Biogeochemical aspects of atmospheric methane. *Global Biogeochemical Cycles*, 2:299−327

Collins M, Knutti R (2013) Long-term climate change: projections, commitments and irreversibility. In: Stocker TF, Qin D, Plattner GK, Tignor M, Allen SK, Boschung J, Nauels A, Xia Y, Bex V, Midgley PM (eds) *Climate Change 2013 the Physical Science Basis: Contribution of Working Group I to the Fifth Assessment Report of the Intergovernmental Panel on Climate Change*, Cambridge University Press, Cambridge, p 1029−1136

Conrad R, Seiler W (1988) Influence of the surface microlayer on the flux of nonconservative trace gases (CO, H_2, CH_4, N_2O) across the ocean-atmosphere interface. *Journal of Atmospheric Chemistry*, 6:83−94

Conrad R, Seiler W, Bunse G, Giehl H (1982) Carbon monoxide in seawater (Atlantic Ocean). *Journal of Geophysical Research: Oceans*, 87:8839−8852

Corzo A, Rodríguez-Gálvez S, Lubian L, Sangrá P, Martínez A, Morillo JA (2005) Spatial distribution of transparent exopolymer particles in the Bransfield Strait, Antarctica. *Journal of Plankton Research*, 27:635–646

Crow SA, Ahern DG, Cook WL, Bourquin AW (1975) Densities of bacteria and fungi in coastal surface films as determined by a membrane-adsorption procedure. *Limnology and*

Oceanography, 20:644–646

Crutzen PJ, Zimmermann PH (1991) The changing photochemistry of the troposphere. *Tellus B: Chemical and Physical Meteorology*, 43:136−151

Cunliffe M, Engel A, Frka S, Gašparovi B, Guitart C, Murrell JC, Salter M, Stolle C, Upstill-Goddard RC, Wurl O (2013) Sea surface microlayers: a unified physicochemical and biological perspective of the air-ocean interface. *Progress in Oceanography*, 109:104−116

Cunliffe M, Murrell JC (2009) The sea-surface microlayer is a gelatinous biofilm. *The ISME Journal*, 3:1001−1003

Cunliffe M, Schafer H, Harrison E, Cleave S, Upstill-Goddard RC, Murrell JC (2008) Phylogenetic and functional gene analysis of the bacterial and archaeal communities associated with the surface microlayer of an estuary. *The ISME Journal*, 2:776−789

Cunliffe M, Upstill-Goddard RC, Murrell JC (2011) Microbiology of aquatic surface microlayers. *FEMS Microbiology Reviews*, 35:233−246

Cunliffe M, Wurl O (2014) *Guide to Best Practices to Study the Ocean's Surface*. Occasional Publication of the Marine Biological Association of the United Kingdom, Plymouth

Dortch Q, Whitledge TE (1992) Does nitrogen or silicon limit phytoplankton production in the Mississippi River plume and nearby regions? *Continental Shelf Research*, 12:1293–1309

Ehhalt D, Prather M (2001) Atmospheric chemistry and greenhouse gases. In: Houghton JT, Ding Y, Griggs DJ, Noguer M, van der Linden PJ, Dai X, Maskell K, Johnson CA (eds) *Climate Change 2001 the Scientific Basis: Contribution of Working Group I to the Third Assessment Report of the Intergovernmental Panel on Climate Change*, Cambridge University Press, Cambridge, p 239−288

Emery WJ, Castro S, Wick GA, Schluessel P, Donlon C (2001) Estimating sea surface temperature from infrared satellite and in situ temperature data. *Bulletin of the American*

Meteorological Society, 82:2773−2786

Engel A (2009) Determination of marine gel particles. In: Wurl O (ed) *Practical Guidelines for the Analysis of Seawater*, CRC Press, Boca Raton, p 125−142

Engel A, Bange HW, Cunliffe M, Burrows SM, Friedrichs G, Galgani L, Herrmann H, Hertkorn N, Johnson M, Liss PS, Quinn PK, Schartau M, Soloviev A, Stolle C, Upstill-Goddard RC, van Pinxteren M, Zäncker B (2017) The ocean's vital skin: toward an integrated understanding of the sea surface microlayer. *Frontiers in Marine Science*, 4:165

Engel A, Galgani L (2016) The organic sea-surface microlayer in the upwelling region off the coast of Peru and potential implications for air–sea exchange processes. *Biogeosciences*, 13:989−1007

Engel A, Goldthwait S, Passow U, Alldredge AL (2002) Temporal decoupling of carbon and nitrogen dynamics during the course of a mesocosm diatom bloom. *Limnology Oceanography*, 47:753–761

Fairall CW, Bradley EF, Godfrey JS, Wick GA, Edson JB, Young GS (1996) Cool skin and warm layer effects on sea surface temperature. *Journal of Geophysical Research*, 101:1295−1308

Frew NM (1997) The role of organic films in air-sea gas exchange. In: Liss PS, Duce RA (eds) *The Sea Surface and Global Change*, Cambridge University Press, Cambridge, p 121–172

Frew NM, Goldman JC, Dennett MR, Johnson AS (1990) Impact of phytoplankton-generated surfactants on air-sea gas exchange. *Journal of Geophysical Research*, 95:3337–3351

Fujiki T, Toda T, Kikuchi T, Aono H, Taguchi S (2004) Phosphorus limitation of primary productivity during the spring-summer blooms in Sagami Bay, Japan. *Marine Ecology Progress Series*, 283:29–38

Galgani L, Piontek J, Engel A (2016) Biopolymers form a gelatinous microlayer at the air-sea interface when Arctic sea ice melts. *Scientific Reports*, 6:29465

Garbe CS, Rutgersson A, Boutin J, de Leeuw G, Delille B, Fairall CW, Gruber N, Hare J, Ho DT,

Johnson MT, Nightingale PD, Pettersson H, Piskozub J, Sahlée E, Tsai W, Ward B, Woolf DK, Zappa CJ (2014) Transfer across the air-sea interface. In: Liss PS, Johnson MT (eds) *Ocean-Atmosphere Interactions of Gases and Particles*, Springer, Berlin, p 55−112

Garçon VC, Bell TG, Wallace D, Arnold SR, Baker A, Bakker DCE, Bange HW, Bates NR, Bopp L, Boutin J, Boyd PW, Bracher A, Burrows JP, Carpenter LJ, de Leeuw G, Fennel K, Font J, Friedrich T, Garbe CS, Gruber N, Jaeglé L, Lana A, Lee JD, Liss PS, Miller LA, Olgun N, Olsen A, Pfeil B, Quack B, Read KA, Reul N, Rödenbeck C, Rohekar SS, Saiz-Lopez A, Saltzman ES, Schneising O, Schuster U, Seferian R, Steinhoff T, Le Traon P, Ziska F (2014) Perspectives and Integration in SOLAS Science. In: Liss PS, Johnson MT (eds) *Ocean-Atmosphere Interactions of Gases and Particles*, Springer, Berlin, p 247−306

Garrett WD (1965) Collection of slick-forming materials from the sea surface. *Limnology and Oceanography*, 10:602−605

Gasol JM (1994) A framework for the assessment of top-down vs bottom-up control of heterotrophic nanoflagellate abundance. *Marine Ecology Progress Series*, 113:291–300

Geider RJ (1987) Light and temperature dependence of the carbon to chlorophyll *a* ratio in microalgae and cyanobacteria: implications for physiology and growth of phytoplankton. *New Phytologist*, 106:1−34

Goldman JC, Dennet MR, Frew NM (1988) Surfactant effects on air-sea gas exchange under turbulent conditions. *Deep-Sea Research*, 35:1953–1970

Green SA, Blough NV (1994) Optical absorption and fluorescence properties of chromophoric dissolved organic matter in natural waters. *Limnology and Oceanography*, 39:1903–1916

Gruber N, Gloor M, Fletcher SEM, Doney SC, Dutkiewicz S, Follows MJ, Gerber M, Jacobson AR, Joos F, Lindsay K, Menemenlis D, Mouchet A, Müller SA, Sarmiento JL, Takahashi T (2009) Oceanic sources, sinks, and transport of atmospheric CO_2. *Global Biogeochemical Cycles*, 23:GB1005

Hardy JT, Apts CW (1984) The sea-surface microlayer: phytoneuston productivity and effects of atmospheric particulate matter. *Marine Biology*, 82:293−300

Harrison PJ, Hu MH, Yang YP, Lu X (1990) Phosphate limitation in estuarine and coastal waters of China. *Journal of Experimental Marine Biology and Ecology*, 140:79–87

Hartmann DL, Klein Tank AMG, Rusticucci M (2013) Observations: atmosphere and surface. In: Stocker TF, Qin D, Plattner GK, Tignor M, Allen SK, Boschung J, Nauels A, Xia Y, Bex V, Midgley PM (eds) *Climate Change 2013 the Physical Science Basis: Contribution of Working Group I to the Fifth Assessment Report of the Intergovernmental Panel on Climate Change*, Cambridge University Press, Cambridge, p 159−254

Harvey GW (1966) Microlayer collection from the sea surface: a new method and initial results. *Limnology and Oceanography*, 11:608–613

Harvey GW, Burzell LA (1972) A simple microlayer method for small samples. *Limnology and Oceanography*, 11:156–157

Harvey RW, Young LY (1980) Enrichment and association of bacteria and particulates in salt marsh surface water. *Applied Environmental Microbiology*, 39:894−899

Japan Meteorological Agency (2015) Meteorological data acquisition system (AMeDAS). https://www.jma.go.jp/jma/ (accessed on 1 October 2015)

Japan Meteorological Agency (2018) Meteorological data acquisition system (AMeDAS). https://www.jma.go.jp/jma/ (accessed on 1 July 2018)

Johnson JE, Bates TS (1996) Sources and sinks of carbon monoxide in the mixed layer of the tropical South Pacific Ocean. *Global Biogeochemical Cycles*, 10:347−359

Jones RD (1991) Carbon monoxide and methane distribution and consumption in the photic zone of the Sargasso Sea. *Deep-Sea Research*, 38:625−635

Jones RD, Amador JA (1993) Methane and carbon monoxide production, oxidation, and turnover times in the Caribbean Sea as influenced by the Orinoco River. *Journal of Geophysical*

Research: Oceans, 98:2353−2359

Joux F, Agogué H, Obernosterer I, Dupuy C, Reinthaler T, Herndl GJ, Lebaron P (2006) Microbial community structure in the sea surface microlayer at two contrasting coastal sites in the northwestern Mediterranean Sea. *Aquatic Microbial Ecology,* 42:91−104

Justić D, Rabalais NN, Turner RE, Dortch Q (1995) Changes in nutrient structure of river-dominated coastal waters: stoichiometric nutrient balance and its consequences. *Estuarine, Coastal and Shelf Science,* 40:339–356

Kettle AJ (1994) A model of the temporal and spatial distribution of carbon monoxide in the mixed layer. *Ph. D. Dissertation*, Massachusetts Institute of Technology, Cambridge

Kieber RJ, Zhou X, Mopper K (1990) Formation of carbonyl compounds from UV-induced photodegradation of humic substances in natural waters: fate of riverine carbon in the sea. *Limnology and Oceanography*, 35:1503–1515

Kirtman B, Power SB (2013) Near-term climate change: projections and predictability. In: Stocker TF, Qin D, Plattner GK, Tignor M, Allen SK, Boschung J, Nauels A, Xia Y, Bex V, Midgley PM (eds) *Climate Change 2013 the Physical Science Basis: Contribution of Working Group I to the Fifth Assessment Report of the Intergovernmental Panel on Climate Change*, Cambridge University Press, Cambridge, p 953−1028

Kitidis V, Tilstone GH, Smyth TJ, Torres R, Law CS (2011) Carbon monoxide emission from a Mauritanian upwelling filament. *Marine Chemistry*, 127:123–133

Kjelleberg S, Stenstrom TA, Odham G (1979) Comparative study of different hydrophobic devices for sampling liquid surface films and adherent microorganisms. *Marine Biology*, 53:21–25

Kuwahara VS, Nozaki S, Nakano J, Toda T, Kikuchi T, Taguchi S (2015) 18-year variability of ultraviolet radiation penetration in the mid-latitude coastal waters of the western boundary Pacific. *Estuarine, Coastal and Shelf Science,* 160:1–9

Kuwahara VS, Ogawa H, Toda T, Kikuchi T, Taguchi S (2000) Variability of bio-optical factors

influencing the seasonal attenuation of ultraviolet radiation in temperate coastal waters of Japan. *Photochemistry and Photobiology*, 72:193–199

Kuznetsova M, Lee C, Aller J, Frew N (2004) Enrichment of amino acids in the sea surface microlayer at coastal and open ocean sites in the North Atlantic Ocean. *Limnology and Oceanography*, 49:1605−1619

Kyushu University (2019) Spectral Radiation-Transport Model for Aerosol Species (SPRINTARS) https://sprintars.riam.kyushu-u.ac.jp/ (accessed on 1 February 2019)

Labry C, Herbland A, Delmas D (2002) The role of phosphorus on planktonic production of the Gironde plume waters in the Bay of Biscay. *Journal of Plankton Research*, 24:97–117

Lekunberri I, Lefort T, Romera-Castillo C, Cardelús C, Coll-Lladó M, Ruiz-González C, Marrasé C, Gasol JM (2012) Relationship between induced phytoplankton blooms and the structure and dynamics of the free-living heterotrophic bacterial community. *Marine Ecology Progress Series*, 448:23–37

Liss PS, Duce RA (1997) *The Sea Surface and Global Change*, Cambridge University Press, Cambridge

Liss PS, Merlivat L (1986) Air-sea gas exchange rates: introduction and synthesis. In: Buat-Ménard P (ed) *The Role of Air-sea Exchange in Geochemical Cycling*, Springer, Dordrecht, p 113−127

Liss PS, Slater PG (1974) Flux of gases across the air-sea interface. *Nature*, 247:181–184

Logan JA, Prather MJ, Wofsy SC, McElroy MB (1981) Tropospheric chemistry: a global perspective. *Journal of Geophysical Research: Oceans*, 86:7210−7254

Mari X, Burd A (1998) Seasonal size spectra of transparent exopolymeric particles (TEP) in a coastal sea and comparison with those predicted using coagulation theory. *Marine Ecology Progress Series*, 163:63−76

Mari X, Kiørboe T (1996) Abundance, size distribution and bacterial colonization of transparent

exopolymer particles (TEP) in the Kattegat. *Journal of Plankton Research*, 18:969−986

Mizubayashi K, Kuwahara VS, Segaran TC, Zaleha K, Effendy AWM, Kushairi MRM, Toda T (2013) Monsoon variability of ultraviolet radiation (UVR) attenuation and bio-optical factors in the Asian tropical coral-reef waters. *Estuarine, Coastal and Shelf Science*, 126:34−43

Momzikoff A, Brinis A, Dallot S, Gondry G, Saliot A, Lebaron P (2004) Field study of the chemical characterization of the upper ocean surface using various samplers. *Limnology and Oceanography: Methods*, 2:374−386

Myhre G, Shindell D (2013) Anthropogenic and natural radiative forcing. In: Stocker TF, Qin D, Plattner GK, Tignor M, Allen SK, Boschung J, Nauels A, Xia Y, Bex V, Midgley PM (eds) *Climate Change 2013 the Physical Science Basis: Contribution of Working Group I to the Fifth Assessment Report of the Intergovernmental Panel on Climate Change*, Cambridge University Press, Cambridge, p 659−740

Myklestad SM (1995) Release of extracellular products by phytoplankton with special emphasis on polysaccharides. *Science of the Total Environment*, 165:155−164

Nakagawa F, Tsunogai U, Gamo T, Yoshida N (2004) Stable isotopic compositions and fractionations of carbon monoxide at coastal and open ocean stations in the Pacific. *Journal of Geophysical Research: Oceans*, 109:C06016

Nakajima R, Tsuchiya K, Nakatomi N, Yoshida T, Tada Y, Konno F, Toda T, Kuwahara VS, Hamasaki K, Othman BHR, Segaran TC, Effendy AWM (2013) Enrichment of microbial abundance in the sea-surface microlayer over a coral reef: implications for biogeochemical cycles in reef ecosystems. *Marine Ecology Progress Series*, 490:11−22

Nelson NB, Carlson CA, Steinberg DK (2004) Production of chromophoric dissolved organic matter by Sargasso Sea microbes. *Marine Chemistry*, 89:273−287

Nelson NB, Siegel DA, Michaels AF (1998) Seasonal dynamics of colored dissolved material in the

Sargasso Sea. *Deep-Sea Research Part I: Oceanographic Research Papers*, 45:931−957

Nightingale PD, Malin G, Law CS, Watson AJ, Liss PS, Liddicoat MI, Boutin J, Upstill-Goddard RC (2000) In situ evaluation of air-sea gas exchange parameterizations using novel conservative and volatile tracers. *Global Biogeochemical Cycles*, 14:373−387

Obernosterer I, Catala P, Lami R, Caparros J, Ras J, Bricaud A, Dupuy C, Wambeke FV, Lebaron P (2008) Biochemical characteristics and bacterial community structure of the sea surface microlayer in the South Pacific Ocean. *Biogeosciences*, 5:693−705

Obernosterer I, Catala P, Reinthaler T, Herndl GJ, Lebaron P (2005) Enhanced heterotrophic activity in the surface microlayer of the Mediterranean Sea. *Aquatic Microbial Ecology*, 39:293−302

Ogawa H, Usui T, Koike I (2003) Distribution of dissolved organic carbon in the East China Sea. *Deep-Sea Research Part II: Topical Studies in Oceanography*, 50:353−366

Ohta K (1997) Diurnal variations of carbon monoxide concentration in the equatorial Pacific upwelling region. *Journal of Oceanography*, 53:173−178

Ohta K, Inomata Y, Sano A, Sugimura K (2000) Photochemical degradation of dissolved organic carbon to carbon monoxide in coastal seawater. In: Handa N, Tanoue E, Hama T (eds) *Dynamics and Characterization of Marine Organic Matter*, Springer, Dordrecht, p 213−229

Ortega-Retuerta E, Passow U, Duarte CM, Reche I (2009) Effects of ultraviolet B radiation on (not so) transparent exopolymer particles. *Biogeosciences*, 6:3071−3080

Parsons TR, Maita Y, Lalli CM (1984) *A Manual of Chemical and Biological Methods for Seawater Analysis*, Pergamon Press, Oxford

Passow U (2000) Formation of transparent exopolymer particles, TEP, from dissolved precursor material. *Marine Ecology Progress Series*, 192:1−11

Passow U (2002) Transparent exopolymer particles (TEP) in aquatic environments. *Progress in*

Oceanography, 55:287−333

Passow U, Alldredge AL (1994) Distribution, size and bacterial colonization of transparent exopolymer particles (TEP) in the ocean. *Marine Ecology Progress Series*, 113:185−198

Passow U, Alldredge AL (1995) A dye-binding assay for the spectrophotometric measurement of transparent exopolymer particles (TEP). *Limnology and Oceanography*, 40:1326−1335

Passow U, Shipe RF, Murray A, Pak DK, Brzezinski MA, Alldredge AL (2001) Origin of transparent exopolymer particles (TEP) and their role in the sedimentation of particulate matter. *Continental Shelf Research*, 21:327−346

Plane JMC, Blough NV, Ehrhardt MG, Waters K, Zepp RG, Zika RG (1997) Report group 3: photochemistry in the sea-surface microlayer. In Liss PS, Duce RA (eds) *The Sea Surface and Global Change*, Cambridge University Press, Cambridge, p 71−92

Ploug H (2008) Cyanobacterial surface blooms formed by *Aphanizomenon* sp. and *Nodularia spumigena* in the Baltic Sea: small-scale fluxes, pH, and oxygen microenvironments. *Limnology and Oceanography*, 53:914–921

Reinthaler T, Sintes E, Herndl GJ (2008) Dissolved organic matter and bacterial production and respiration in the sea-surface microlayer of the open Atlantic and the western Mediterranean Sea. *Limnology and Oceanography*, 53:122−136

Richardson K, Beardall J, Raven JA (1983) Adaptation of unicellular algae to irradiance: an analysis of strategies. *New Phytologist*, 93:157−191

Salter ME, Upstill-Goddard RC, Nightingale PD, Archer SD, Blomquist B, Ho T, Huebert B, Schlosser P, Yang M (2011) Impact of an artificial surfactant release on air-sea gas exchange during DOGEE II. *Journal of Geophysical Research*, 116:C11016

Sasaki H, Miyamura T, Saitoh SI, Ishizaka J (2005) Seasonal variation of absorption by particles and colored dissolved organic matter (CDOM) in Funka Bay, southwestern Hokkaido, Japan. *Estuarine, Coastal and Shelf Science*, 64:447−458

Saunders PM (1967) The temperature at the ocean-air interface. *Journal of the Atmospheric Sciences*, 24:269−273

Schropp SJ, Schwarz JR (1983) Nitrous oxide production by denitrifying microorganisms from the eastern tropical Pacific and the Caribbean Sea. *Geomicrobiology Journal*, 3:17–31

Servais P, Anzil A, Ventresque C (1989) Simple method for determination of biodegradable dissolved organic carbon in water. *Applied Environmental Microbiology*, 55:2732–2734

Sherr EB, Caron DA, Sherr BF (1993) Staining of heterotrophic protists for visualization via epifluorescence microscopy. In: Kemp PF, Sherr BF, Sherr EB, Cole JJ (eds) *Handbook of Methods in Aquatic Microbial Ecology*, Lewis Publishers, London, p 213−228

Shibata A, Goto Y, Saito H, Kikuchi T, Toda T, Taguchi S (2006) Comparison of SYBR Green I and SYBR Gold stains for enumerating bacteria and viruses by epifluorescence microscopy. *Aquatic Microbial Ecology*, 43:221−231

Shimode S, Toda T, Kikuchi T (2006) Spatio-temporal changes in diversity and community structure of planktonic copepods in Sagami Bay, Japan. *Marine Biology*, 148:581–597

Sieburth JM, Willis PJ, Johnson KM, Burney CM, Lavoie DM, Hinga KR, Caron DA, French FW, Johnson PW, Davis PG (1976) Dissolved organic matter and heterotrophic micro-neuston in the surface microlayers of the North Atlantic. *Science*, 194:1415−1418

Soloviev AV, Schlüssel P (1994) Parameterization of the cool skin of the ocean and of the air-ocean gas transfer on the basis of modeling surface renewal. *Journal of Physical Oceanography*, 24:1339−1346

Stolle C, Nagel K, Labrenz M, Jürgens K (2010) Succession of the sea-surface microlayer in the coastal Baltic sea under natural and experimentally induced low-wind conditions. *Biogeosciences*, 7:2975−2988

Stubbins AP (2001) Aspects of aquatic CO photoproduction from CDOM. *Ph. D. Dissertation*, Newcastle University, Newcastle upon Tyne

Stubbins A, Law CS, Uher G, Upstill-Goddard RC (2011) Carbon monoxide apparent quantum yields and photoproduction in the Tyne estuary. *Biogeosciences*, 8:703–713

Stubbins A, Uher G, Kitidis V, Law CS, Upstill-Goddard RC, Woodward EMS (2006a) The open-ocean source of atmospheric carbon monoxide, *Deep-Sea Research Part II: Topical Studies in Oceanography*, 53:1685–1694

Stubbins A, Uher G, Law CS, Mopper K, Robinson C, Upstill-Goddard RC (2006b) Open-ocean carbon monoxide photoproduction. *Deep-Sea Research Part II: Topical Studies in Oceanography*, 53:1695–1705

Sugai Y, Tsuchiya K, Kuwahara VS, Shimode S, Komatsu K, Imai A, Toda T (2016) Bacterial growth rate and the relative abundance of bacteria to heterotrophic nanoflagellates in the euphotic and disphotic layers in temperate coastal waters of Sagami Bay, Japan. *Journal of Oceanography*, 72:577−587

Sugai Y, Tsuchiya K, Shimode S, Toda T (2018) Seasonal variations in microbial abundance and transparent exopolymer particle concentration in the sea surface microlayer of temperate coastal waters. *Aquatic Microbial Ecology*, 81:201–211

Suzuki R, Ishimaru T (1990) An improved method for the determination of phytoplankton chlorophyll using *N*,*N*-dimethylformamide. *Journal of Oceanography*, 46:190−194

Takahashi T, Sutherland SC, Wanninkhof R, Sweeney C, Feely RA, Chipman DW, Hales B, Friederich G, Chavez F, Sabine C, Watson A, Bakker DCE, Schuster U, Metzl N, Yoshikawa-Inoue H, Ishii M, Midorikawa T, Nojiri Y, Körtzinger A, Steinhoff T, Hoppema M, Olafsson J, Arnarson TS, Tilbrook B, Johannessen T, Olsen A, Bellerby R, Wong CS, Delille B, Bates NR, de Baar HJW (2009) Climatological mean and decadal change in surface ocean pCO_2, and net sea–air CO_2 flux over the global oceans. *Deep-Sea Research Part II: Topical Studies in Oceanography*, 56:554–577

Thingstad TF, Zweifel UL, Rassoulzadegan F (1998) P limitation of heterotrophic bacteria and

phytoplankton in the northwest Mediterranean. *Limnology and Oceanography*, 43:88–94

Thompson AM (1992) The oxidizing capacity of the Earth's atmosphere: probable past and future changes. *Science*, 256:1157–1165

Thompson AM, Cicerone RJ (1986) Possible perturbations to atmospheric CO, CH_4, and OH. *Journal of Geophysical Research: Atmosphere*, 91:10853–10864

Tolli JD, Taylor CD (2005) Biological CO oxidation in the Sargasso sea and in vineyard sound, Massachusetts. *Limnology and Oceanography*, 50:1205–1212

Turner RE, Rabalais NN, Zhang ZN (1990) Phytoplankton biomass, production, and growth limitations on the Huanghe (Yellow River) continental shelf. *Continental Shelf Research*, 10:545–571

Turner SM, Liss PS (1989) A cryogenic technique for sampling the sea surface microlayer for trace gases. *Chemical Oceanography*, 10:379–392

Upstill-Goddard RC (2006) Air-sea gas exchange in the coastal zone. *Estuarine Coastal and Shelf Science*, 70:388–404

Upstill-Goddard RC, Frost T, Henry GR, Franklin M, Murrell JC, Owens NJP (2003) Bacterioneuston control of air-water methane exchange determined with a laboratory gas exchange tank. *Global Biogeochemical Cycles*, 17:1108

Valentine RL, Zepp RG (1993) Formation of carbon monoxide from the photodegradation of terrestrial dissolved organic carbon in natural waters. *Environmental Science & Technology*, 27:409−412

Verdugo P, Alldredge AL, Azam F, Kirchman DL, Passow U, Santschi PH (2004) The oceanic gel phase: a bridge in the DOM-POM continuum. *Marine Chemistry*, 92:67−85

Waite AM, Olson RJ, Dam HG, Passow U (1995) Sugar-containing compounds on the cell surfaces of marine diatoms measured using concanavalin A and flow cytometry. *Journal of Phycology*, 31:925–933

Wängberg SÅ, Andreasson KIM, Gustavson K, Reinthaler T, Henriksen P (2008) UV-B effects on microplankton communities in Kongsfjord, Svalbard: a mesocosm experiment. *Journal of Experimental Marine Biology and Ecology*, 365:156−163

Wanninkhof R (1992) Relationship between wind speed and gas exchange over the ocean. *Journal of Geophysical Research: Oceans*, 97:7373−7382

Wanninkhof R, McGillis WR (1999) A cubic relationship between air-sea CO_2 exchange and wind speed. *Geophysical Research Letters*, 26:1889−1892

Welschmeyer NA (1994) Fluorometric analysis of chlorophyll *a* in the presence of chlorophyll *b* and pheopigments. *Limnology and Oceanography*, 39:1985−1992

Wheeler JR (1975) Formation and collapse of surface films. *Limnology and Oceanography*, 20:338–342

Wick GA, Emery WJ, Kantha LH, Schlüssel P (1996) The behavior of the bulk–skin sea surface temperature difference under varying wind speed and heat flux. *Journal of Physical Oceanography*, 26:1969−1988

Wiesenburg DA, Guinasso NL (1979) Equilibrium solubilities of methane, carbon monoxide, and hydrogen in water and sea water. *Journal of Chemical and Engineering Data*, 24:356−360

Wurl O, Holmes M (2008) The gelatinous nature of the sea surface microlayer. *Marine Chemistry*, 110:89−97

Wurl O, Miller L, Röttgers R, Vagle S (2009) The distribution and fate of surface-active substances in the sea-surface microlayer and water column. *Marine Chemistry*, 115:1−9

Wurl O, Miller L, Vagle S (2011b) Production and fate of transparent exopolymer particles in the ocean. *Journal of Geophysical Research*, 116:C00H13

Wurl O, Stolle C, Thuoc CV, Thu PT, Mari X (2016) Biofilm-like properties of the sea surface and predicted effects on air-sea CO_2 exchange. *Progress in Oceanography*, 144:15−24

Wurl O, Wurl E, Miller L, Johnson K, Vagle S (2011a) Formation and global distribution of

sea-surface microlayers. *Biogeosciences*, 8:121–135

Xie H, Andrews SS, Martin WR, Miller J, Ziolkowski L, Taylor CD, Zafiriou OC (2002) Validated methods for sampling and headspace analysis of carbon monoxide in seawater. *Marine Chemistry*, 77:93−108

Xie H, Bélanger S, Demers S, Vincent WF, Papakyriakou TN (2009) Photobiogeochemical cycling of carbon monoxide in the southeastern Beaufort Sea in spring and autumn. *Limnology and Oceanography*, 54:234−249

Xie H, Zafiriou OC, Umile TP, Kieber DJ (2005) Biological consumption of carbon monoxide in Delaware Bay, NW Atlantic and Beaufort Sea. *Marine Ecology Progress Series*, 290:1−14

Yang GP, Ren CY, Lu XL, Liu CY, Ding HB (2011) Distribution, flux, and photoproduction of carbon monoxide in the East China Sea and Yellow Sea in spring. *Journal of Geophysical Research: Oceans*, 116:C02001

Yang GP, Tsunogai S (2005) Biogeochemistry of dimethylsulfide (DMS) and dimethylsulfoniopropionate (DMSP) in the surface microlayer of the western North Pacific. *Deep-Sea Research Part I: Oceanographic Research Papers*, 52:553−567

Yang GP, Tsunogai S, Watanabe S (2005) Biogenic sulfur distribution and cycling in the surface microlayer and subsurface water of Funka Bay and its adjacent area. *Continental Shelf Research*, 25:557−570

Yang GP, Watanabe S, Tsunogai S (2001) Distribution and cycling of dimethylsulfide in surface microlayer and subsurface seawater. *Marine Chemistry*, 76:137−153

Yoshida O, Inoue HY, Watanabe S, Suzuki K, Noriki S (2011) Dissolved methane distribution in the South Pacific and the Southern Ocean in austral summer. *Journal of Geophysical Research: Oceans*, 116:C07008

Zafiriou OC, Andrews SS, Wang W (2003) Concordant estimates of oceanic carbon monoxide source and sink processes in the Pacific yield a balanced global “blue-water” CO budget.

Global Biogeochemical Cycles, 17:1015

Zafiriou OC, Xie H, Nelson NB, Najjar RG, Wang W (2008) Diel carbon monoxide cycling in the upper Sargasso Sea near Bermuda at the onset of spring and in midsummer. *Limnology and Oceanography,* 53:835−850

Zhang J, Liu MG (1994) Observations on nutrient elements and sulphate in atmospheric wet depositions over the northwest Pacific coastal oceans-Yellow Sea. *Marine Chemistry*, 47:173−189

Zhang Y, Xie H, Chen G (2006) Factors affecting the efficiency of carbon monoxide photoproduction in the St. Lawrence estuarine system (Canada). *Environmental Science & Technology*, 40:7771−7777

Zhang ZB, Liu LS, Liu C, Cai W (2003) Studies on the sea surface microlayer: II the layer of sudden change of physical and chemical properties. *Journal of Colloid and Interface Science*, 264:148−159

Zhang ZB, Liu LS, Wu ZJ, Li J, Ding HB (1998) Physicochemical studies of the sea surface microlayer: I thickness of the sea surface microlayer and its experimental determination. *Journal of Colloid and Interface Science*, 204:294−299

Zhou X, Mopper K (1997) Photochemical production of low-molecular-weight carbonyl compounds in seawater and surface microlayer and their air-sea exchange. *Marine Chemistry*, 56:201−213

Zhou J, Mopper K, Passow U (1998) The role of surface-active carbohydrates in the formation of transparent exopolymer particles by bubble adsorption of seawater. *Limnology and Oceanography,* 43:1860−1871

Ziolkowski LA, Miller WL (2007) Variability of the apparent quantum efficiency of CO photoproduction in the Gulf of Maine and Northwest Atlantic. *Marine chemistry*, 105:258−270

Appendix 1. Monthly values of surface water temperature, surface salinity, and mean wind speed during samplings (Sugai et al. 2018)

Month	Temperature (˚C)	Salinity	Wind speed ($m\ s^{-1}$)
Sep 2013	26.1	33.1	1.23
Oct	19.8	30.6	1.23
Nov	18.0	33.9	0.87
Dec	16.3	34.6	2.50
Jan 2014	14.0	34.8	1.50
Feb	13.8	34.0	1.03
Mar	13.0	34.5	2.07
Apr	15.4	34.1	3.80
May	18.4	34.3	4.00
Jun	21.6	32.6	2.30
Jul	24.7	32.3	1.43
Aug	24.8	33.8	1.43
Sep	24.6	34.5	2.07
Oct	22.0	32.4	2.17
Nov	19.0	34.4	1.73
Dec	15.5	34.4	5.37
Jan 2015	15.0	34.0	1.07
Feb	13.8	34.4	1.83
Mar	13.0	34.4	7.27
Apr	14.2	34.1	1.10
May	17.3	33.3	2.77
Jun	20.8	33.0	1.17
Jul	23.9	30.4	3.20
Aug	26.4	33.7	2.47
Sep	25.2	32.0	3.33

Appendix 2. Monthly values of nitrate (NO_3), ammonium (NH_4), phosphate (PO_4), and silicate (SiO_2) in the surface microlayer (SML) and subsurface water (SSW) (Sugai et al. 2018)

Month	NO_3 (µM)		NH_4 (µM)		PO_4 (µM)		SiO_2 (µM)	
	SML	SSW	SML	SSW	SML	SSW	SML	SSW
Sep 2013	1.08	0.14	0.64	0.53	0.02	0.02	5.09	2.69
Oct	14.4	13.2	0.83	0.94	0.46	0.41	31.8	31.5
Nov	3.04	2.78	0.48	0.95	0.15	0.14	6.60	6.23
Dec	4.03	2.27	1.00	0.67	0.19	0.17	12.8	11.7
Jan 2014	7.00	6.53	0.73	0.67	0.43	0.44	23.3	22.6
Feb	6.52	5.76	1.05	0.75	0.41	0.41	23.5	22.5
Mar	3.16	2.73	1.77	0.89	0.25	0.20	14.0	13.2
Apr	0.96	0.04	1.43	0.74	0.61	0.02	3.87	7.48
May	0.87	0.03	1.23	1.14	0.06	0.05	4.94	3.61
Jun	1.23	0.14	1.10	0.86	0.02	0.02	5.15	3.40
Jul	2.08	1.12	1.31	0.88	0.02	0.02	13.9	12.8
Aug	0.45	0.03	0.67	0.79	0.02	0.02	2.56	2.71
Sep	0.91	0.43	0.97	0.95	0.06	0.05	6.60	5.63
Oct	6.34	5.63	1.16	1.89	0.26	0.27	39.6	37.1
Nov	3.50	3.00	0.77	0.67	0.26	0.21	20.5	20.2
Dec	6.48	6.18	0.80	0.67	0.55	0.54	10.9	10.5
Jan 2015	7.64	7.26	1.11	0.96	0.59	0.57	21.1	20.6
Feb	1.66	3.46	1.34	1.39	0.11	0.21	9.52	11.2
Mar	8.70	7.71	1.32	0.84	0.74	0.69	16.7	16.7
Apr	3.84	3.65	2.38	2.72	0.39	0.38	9.81	8.39
May	3.63	0.30	4.69	1.68	0.52	0.05	2.84	1.28
Jun	0.03	0.18	0.88	1.13	0.07	0.02	2.88	1.96
Jul	0.85	0.50	0.46	0.56	0.11	0.04	15.3	15.2
Aug	0.89	0.44	1.10	0.95	0.09	0.04	5.12	4.39
Sep	2.01	0.05	1.19	0.46	0.14	0.03	19.4	22.5

Appendix 3. Monthly values of dissolved organic carbon (DOC), the absorption coefficient of chromophoric dissolved organic matter at 320 nm (a_{CDOM} [320]), particulate organic carbon (POC), and transparent exopolymer particles (TEP) in the surface microlayer (SML) and subsurface water (SSW) (Sugai et al. 2018)

Month	DOC (mgC L^{-1})		a_{CDOM} (320) (m^{-1})		POC (mgC L^{-1})		TEP (mg X_{eq} L^{-1})	
	SML	SSW	SML	SSW	SML	SSW	SML	SSW
Sep 2013	1.53	1.24	0.87	0.79	0.50	0.45	0.43	0.42
Oct	1.33	1.14	0.96	0.94	0.54	0.27	0.45	0.21
Nov	1.01	0.96	0.56	0.55	0.33	0.19	0.31	0.21
Dec	0.92	1.36	0.45	0.37	0.21	0.12	0.29	0.34
Jan 2014	1.04	0.82	0.42	0.35	0.36	0.16	0.37	0.22
Feb	0.88	0.87	0.46	0.63	0.35	0.20	0.22	0.31
Mar	1.09	0.90	0.80	0.56	0.28	0.38	0.38	0.30
Apr	6.60	1.38	2.25	0.73	5.17	0.74	5.44	0.89
May	3.36	1.12	1.35	0.86	0.66	0.37	0.48	0.34
Jun	1.89	1.67	1.22	1.10	0.77	0.54	0.42	0.47
Jul	1.46	1.34	1.26	1.12	0.88	0.52	0.28	0.20
Aug	1.20	1.15	0.83	0.66	0.36	0.22	0.29	0.20
Sep	1.15	1.20	1.29	0.95	0.48	0.27	0.34	0.15
Oct	1.14	0.98	0.93	1.12	0.77	0.27	0.30	0.20
Nov	1.05	0.91	0.89	0.51	0.65	0.22	0.21	0.16
Dec	0.77	0.80	0.53	0.57	0.14	0.09	0.13	0.21
Jan 2015	0.99	0.81	0.57	0.54	0.32	0.09	0.23	0.15
Feb	0.96	0.85	0.37	0.36	0.40	0.33	0.32	0.29
Mar	0.95	0.72	0.38	0.32	0.42	0.13	0.26	0.20
Apr	1.37	1.03	0.74	0.65	0.46	0.19	0.30	0.29
May	6.29	2.18	2.73	1.99	1.98	0.64	2.11	0.71
Jun	1.56	1.17	1.21	1.01	1.60	0.35	0.73	0.37
Jul	1.53	1.25	1.21	1.15	0.83	0.63	0.32	0.26
Aug	1.20	0.84	1.01	0.48	0.67	0.31	0.46	0.20
Sep	1.43	1.11	1.30	1.13	1.11	0.67	0.52	0.52

Appendix 4. Monthly values of chlorophyll (chl.) *a*, autotrophic nanoflagellates (ANF), bacteria, and heterotrophic nanoflagellates (HNF) in the surface microlayer (SML) and subsurface water (SSW) (Sugai et al. 2018)

Month	Chl. *a* (μg L^{-1})		ANF (10^6 cells L^{-1})		Bacteria (10^9 cells L^{-1})		HNF (10^6 cells L^{-1})	
	SML	SSW	SML	SSW	SML	SSW	SML	SSW
Sep 2013	6.07	8.82	4.33	1.29	1.54	1.25	6.70	0.79
Oct	3.67	3.71	5.71	1.86	1.48	0.97	6.10	0.72
Nov	4.15	3.32	1.58	2.14	0.85	0.46	3.15	1.13
Dec	1.76	1.10	0.69	0.79	0.25	0.42	2.26	0.66
Jan 2014	1.93	1.47	2.26	0.63	0.53	0.37	1.87	1.01
Feb	3.87	3.25	3.84	1.35	0.45	0.36	3.84	1.48
Mar	5.33	9.34	3.15	1.20	1.09	0.72	4.33	2.71
Apr	129	17.5	46.3	1.13	16.1	2.07	69.9	1.89
May	8.41	4.09	6.79	1.45	3.74	2.43	12.1	1.95
Jun	8.46	6.05	4.28	2.74	3.84	2.07	6.65	2.74
Jul	7.74	4.58	11.1	5.48	6.56	5.41	11.1	4.73
Aug	0.82	1.03	2.36	0.66	2.69	1.49	6.50	2.55
Sep	2.23	1.80	6.94	4.29	3.61	1.55	14.0	6.05
Oct	3.41	2.21	8.57	1.21	4.02	1.99	10.9	0.92
Nov	1.27	1.15	4.43	0.79	3.52	1.33	2.07	0.91
Dec	0.83	0.91	0.78	1.31	0.96	1.10	0.43	0.22
Jan 2015	0.68	0.56	0.91	0.25	0.80	0.50	0.80	0.13
Feb	6.79	11.8	0.89	0.85	1.94	1.04	0.89	0.28
Mar	2.73	1.92	1.77	0.82	0.80	0.53	2.07	0.77
Apr	1.64	1.03	4.33	2.33	1.73	1.28	6.70	1.83
May	31.4	7.99	25.5	5.48	10.4	1.50	24.0	5.10
Jun	25.9	4.87	17.4	3.33	3.60	2.39	15.9	2.48
Jul	2.00	2.01	12.6	4.06	3.17	1.66	12.0	3.31
Aug	3.06	0.81	5.17	2.27	2.52	1.94	5.17	2.65
Sep	7.78	10.5	21.0	8.51	4.97	2.70	21.6	6.62

Appendix 5. Monthly values of surface water temperature, surface salinity, mean wind speed during samplings, and the integrated solar irradiance during the incubation period

Month	Temperature (˚C)	Salinity	Wind speed ($m\ s^{-1}$)	Irradiance ($kW\ m^{-2}$)
Jun 2017	21.7	33.6	3.23	0.85
Jul	23.4	34.2	3.50	1.38
Aug	26.1	32.4	1.05	1.03
Sep	25.4	34.4	2.70	0.11
Oct	22.2	30.1	1.87	0.20
Nov	19.7	34.2	1.43	0.14
Dec	16.9	34.9	3.38	0.26
Jan 2018	15.0	34.9	1.70	1.05
Feb	13.6	34.8	2.80	1.29
Mar	17.2	34.1	2.85	2.58
Apr	16.2	34.4	4.10	1.98
May	17.9	34.0	3.03	1.46
Jun	22.0	33.6	2.45	1.18

Appendix 6. Monthly values of the absorption coefficient of chromophoric dissolved organic matter at 320 nm (a_{CDOM} [320]), chlorophyll (chl.) *a*, bacteria, and carbon monoxide concentration ([CO]) in the surface microlayer (SML) and subsurface water (SSW)

Month	a_{CDOM} (320) (m^{-1})		Chl. *a* ($\mu g\ L^{-1}$)		Bacteria (10^9 cells L^{-1})		[CO] (nM)	
	SML	SSW	SML	SSW	SML	SSW	SML	SSW
Jun 2017	1.48	0.63	43.39	1.95	3.01	2.05	15.00	7.70
Jul	0.53	0.37	0.65	0.61	2.02	1.32	2.24	3.16
Aug	1.22	0.61	6.41	2.78	6.39	5.71	2.81	2.63
Sep	0.84	0.41	2.68	2.45	3.14	1.54	4.42	5.52
Oct	0.46	0.34	1.90	0.91	0.97	1.06	3.11	2.42
Nov	0.31	0.20	1.27	1.42	1.04	0.63	1.13	2.13
Dec	0.13	0.25	0.40	0.49	0.73	0.74	1.81	1.73
Jan 2018	0.09	0.15	0.35	0.45	0.82	0.94	1.52	0.70
Feb	0.26	0.18	0.25	0.22	0.78	0.63	1.13	1.53
Mar	0.45	0.28	1.88	1.88	2.89	2.56	3.42	3.13
Apr	0.57	0.48	0.77	1.48	3.83	2.94	3.83	9.98
May	0.40	0.18	0.67	0.50	4.25	1.81	1.71	2.75
Jun	0.62	0.41	1.81	1.23	6.22	7.61	3.80	3.23

Appendix 7. Monthly values of the photochemical production rate of carbon monoxide (CO) (CO prod. rate) and biological CO consumption rate constant (k_{CO}) in the surface microlayer (SML) and subsurface water (SSW)

Month	CO prod. rate (nM h^{-1})		k_{CO} (h^{-1})	
	SML	SSW	SML	SSW
Jun 2017	8.95	1.89	0.064	0.094
Jul	3.45	1.24	0.064	0.085
Aug	7.82	2.21	0.074	0.092
Sep	0.38	0.14	0.063	0.081
Oct	1.08	0.39	0.067	0.058
Nov	0.22	0.09	0.042	0.071
Dec	0.31	0.34	0.037	0.031
Jan 2018	0.68	0.48	0.068	0.045
Feb	0.87	0.23	0.043	0.012
Mar	3.15	1.25	0.062	0.018
Apr	2.45	1.25	0.036	0.019
May	3.32	1.32	0.057	0.057
Jun	3.14	1.18	0.048	0.056

Appendix 8. Monthly values of surface water temperature, the integrated solar irradiance during the incubation period, carbon monoxide (CO) concentration ([CO]) in the subsurface water (SSW), [CO] in the surface microlayer (SML), photochemical CO production (prod.) rate, and biological CO consumption rate constant (k_{CO}) during seawater warming experiments. SML samples were incubated at 3°C higher (+ 3°C) and the *in situ* water temperature (control)

Season	Condition	Temperature (°C)	Irradiance (kW m^{-2})	[CO] in SSW (nM)	[CO] in SML (nM)	CO prod. rate (nM h^{-1})	k_{CO} (h^{-1})
AUT	+ 3°C	18.3	0.44	4.37	3.40	0.55	0.028
	Control					0.43	0.021
WTR	+ 3°C	15.5	0.17	5.87	4.73	1.05	0.018
	Control					1.05	0.014
SPR	+ 3°C	20.5	1.77	22.8	4.99	6.18	0.036
	Control					5.83	0.021
SMR	+ 3°C	28.4	2.67	21.9	4.38	15.7	0.047
	Control					16.4	0.052